ASSESSING GRID SIZE EFFECTS ON INUNDATION AND GROUNDWATER USING HYDROLOGICAL MODEL

MR. SUTTHIWAS CHANTALUCK

A THESIS SUBMITTED IN PARTIAL FULFILLMENT OF THE REQUIREMENTS FOR
THE DEGREE OF MASTER OF ENGINEERING (CIVIL ENGINEERING)
FACULTY OF ENGINEERING
KING MONGKUT'S UNIVERSITY OF TECHNOLOGY THONBURI

2014

Assessing Grid Size Effects on Inundation and Groundwater Using Hydrological Model

Mr. Sutthiwas Chantaluck B.Eng. (Civil Engineering)

A Thesis Submitted in Partial Fulfillment of the Requirements for

the Degree of Master of Engineering (Civil Engineering)

Faculty of Engineering

King Mongkut's University of Technolgy Thonburi

2014

Thesis Committee

…… Chairman

(Lect. Duangrudee Kositgittiwong, Ph.D.)

…… Member and Thesis Advisor

(Lect. Chaiwat Ekkawatpanit, Ph.D.)

…… Member and Thesis Co-Advisor

(Asst. Prof. Sanit Wongsa, Ph.D.)

…… Member

(Assoc. Prof. Sacha Sethaputra, Ph.D.)

หัวข้อวิทยานิพนธ์	การประเมินผลกระทบของขนาดกริดต่อปริมาณน้ำท่วมและน้ำใต้ดิน โดยใช้แบบจำลองอุทกวิทยา
หน่วยกิต	12
ผู้เขียน	นายสุทธิวัสส์ ฉันทาลักษณ์
อาจารย์ที่ปรึกษา	ดร.ชัยวัฒน์ เอกวัฒน์พานิชย์
	รศ. ดร.สนิท วงษา
หลักสูตร	วิศวกรรมศาสตรมหาบัณฑิต
สาขาวิชา	วิศวกรรมโยธา
ภาควิชา	วิศวกรรมโยธา
คณะ	วิศวกรรมศาสตร์
ปีการศึกษา	2557

บทคัดย่อ

น้ำท่วมก่อให้เกิดความเสียหายเป็นบริเวณกว้างแต่ในทางกลับกันมันนำไปสู่การเกิดทรัพยากรน้ำใต้ดิน กล่าวคือในฤดูแล้งเมื่อน้ำผิวดินไม่สามารถใช้ได้ น้ำใต้ดินจะถูกนำมาใช้สำหรับดื่ม ชลประทาน อุตสาหกรรมและการใช้งานอื่น ๆ ซึ่งในการศึกษาครั้งนี้ได้ประเมินความสัมพันธ์ระหว่างน้ำท่วมและน้ำใต้ดินโดยใช้แบบจำลองทางคณิตศาสตร์ ในขณะที่ความละเอียดเชิงพื้นที่ที่มีความสำคัญในการศึกษาระหว่างน้ำท่วมและน้ำใต้ดิน ดังนั้นจึงทำศึกษาขั้นต่อไปเพื่อประเมินผลกระทบของขนาดตารางต่อผลการจำลอง การผสมผสานของแบบจำลองทางคณิตศาสตร์แม่น้ำ เช่น แบบจำลองการไหลในแม่น้ำ น้ำผิวดิน และการไหลของน้ำใต้ดินถูกนำมาใช้ในการประเมินผลกระทบขนาดตารางต่อน้ำท่วมและน้ำบาดาลในลุ่มน้ำตอนล่างของแม่น้ำโขงประเทศกัมพูชา แผนที่ความสูงเชิงตัวเลข (ระดับผิวดิน) ถูกขยายโดยใช้ระบบสารสนเทศภูมิศาสตร์ที่มีขนาดเท่ากับ 250, 500 และ 1,000 เมตร ตามลำดับ โดยที่แบบจำลองพารามิเตอร์ของขนาด 90 เมตรถูกใช้เป็นค่าอ้างอิง การคำนวณถูกใช้สำหรับการคำนวณน้ำท่วม การไหลบนดิน และลักษณะการไหลสำหรับเหตุการณ์น้ำท่วมตั้งแต่เดือนมกราคมถึงธันวาคมปี 2543 ผลการทดลองแสดงให้เห็นว่าขนาดของกริด มีผลต่อพื้นที่น้ำท่วมและน้ำใต้ดิน พื้นที่น้ำท่วมและปริมาณน้ำใต้ดินในเดือนกันยายนมีค่า 4,514 ตารางกิโลเมตรและ 59.11 ลูกบาศก์กิโลเมตร, 4,844 ตารางกิโลเมตร และ 61.32 ลูกบาศก์กิโลเมตร และ 6,230 ตารางกิโลเมตร และ 64.79 ลูกบาศก์กิโลเมตร สำหรับ 250, 500 และ 1000 เมตร ตามลำดับ การเปลี่ยนแปลงของขนาดน้ำท่วมมีอิทธิพลต่อทรัพยากรน้ำบาดาลในช่วงเวลาที่น้ำท่วม ความสูงเฉลี่ยของน้ำท่วมและพื้นที่น้ำท่วมเพิ่มขึ้นเมื่อกริดมีขนาดใหญ่ขึ้นพร้อมกับระดับน้ำใต้ดินเฉลี่ยและการจัดเก็บน้ำใต้ดิน

คำสำคัญ : น้ำใต้ดิน / น้ำท่วม / แบบจำลองทางอุทกวิทยา / ลุ่มแม่น้ำโขงตอนล่าง

Thesis Title	Assessing grid size effects on inundation and groundwater using hydrological model
Thesis Credits	12
Candidate	Mr.Sutthiwas Chantaluck
Thesis advisors	Dr. Chaiwat Ekkawatpanit Asst. Prof. Dr. Sanit Wongsa
Program	Master of Engineering
Field of Study	Civil Engineering
Department	Civil Engineering
Faculty	Engineering
Academic Year	2014

Abstract

Flood can cause wide range of destruction. On the other hand, it contributes to groundwater resource. In the dry season, when surface water is not available, groundwater is extracted for drinking, irrigation, industrial and other uses. This study evaluated the relationship between flood and groundwater using a mathematical model. Spatial resolution is important in studying the interaction between flood and groundwater; therefore, this study further evaluated the effect of grid size on simulation results. The coupling of mathematical models, i.e. river routing, overland flow, and groundwater flow model were used to assess the grid size effects on inundation and groundwater in the Lower Mekong River basin, Cambodia. Digital Elevation Map (ground surface level) was extracted by using GIS with grid sizes of 250, 500 and 1000 m, respectively. The model parameters of grid size 90 m was used as a reference value. Calculations were performed for flood, overflow and inundation flows for several flood events from January to December 2000. Results showed that grid size affected inundation area and groundwater storage. The inundation area and groundwater storage in September were estimated as 4514 km^2 and 59.11 km^3, 4844 km^2 and 61.32 km^3; and 6230 km^2 and 64.79 km^3 for 250m, 500m, and 1000m grid resolution, respectively. Changes of flood magnitude influenced groundwater resource during flood period in all simulation regard less of grid sizes. Average inundation depth and area increased as grid and cell-sizes increased along with average groundwater level and groundwater storage.

Keywords: Groundwater/ Hydrological Model/ Inundation/ Lower Mekong river basin

ACKNOWLEDGEMENTS

I would like to thank Department of Civil Engineering and Japan student service organization (JASSO) for providing my to study in the graduate program and financial aid during my study at King Mongkut's University of Technology Thonburi (KMUTT) and Tohoku University, Japan.

I sincerely appreciates help, guidance and advice received from my advisor, Dr. Chaiwat Ekkawatpanit and Asst. Prof. Dr. Sanit Wongsa during this research. Also, thank in extended to my committee members, Dr. Duangrudee Kositgittiwong and Assoc. Prof. Dr. Sacha Sethaputra for their criticisms during the preparation of this thesis.

Special thanks to the Professor Dr. So Kazama, Associate Professor Dr. Daisuke Komori, Ms. Ayako Amano, Mr. Werrayuth Pratoomchai and Kaigan Laboratory, Tohoku University, Japan.

Finally, I wishes to express sincere thanks to the family and friends for their love and continuing support to encourage completing the degree.

CONTENTS

PAGE

LIST OF TABLES

LIST OF FIGURES

FIGURE **PAGE**

LIST OF SYMBLOMS

A	=	Cross-sectional area (m^2)
Q	=	Discharge (m^3/s)
q	=	Inflow per unit area
v	=	Velocity (m/s)
H	=	Water table (m)
n	=	Manning coefficient
g	=	Gravitational acceleration (m^2/s)
h	=	Water depth (m)
Fr	=	Froude number
B	=	Channel Width
Q_a	=	Inflow from tributary
M	=	Discharge flux in x-direction (m^2/s)
N	=	Discharge flux in y-direction (m^2/s)
h_2	=	Water stages from the crest of overflow of a levee
h_1	=	Height of the levee
n_g	=	Specific yield (effective porosity)
h_g	=	Groundwater level (m)
u_g	=	Velocity in east–west (m/s)
v_g	=	Velocity in north–south directions (m/s)
q_g	=	Recharge rate (m/s)
k	=	Hydraulic conductivity (m/s)

CHAPTER 1 INTRODUCTION

1.1 Background and problem

Grid-base model are now widely used in simulating floodplain inundation, rainfall-runoff and other hydrological process which operate by assign single value for each raster cell to represent model parameter and input/output variables. In the development of models, many modelers increase spatial resolution (number of cell) to improved temporal and spatial process. However the spatial resolution affects the solution of the equation and simulation results. The relationship between model space/time resolution and simulation outputs is important to develop hydrological model. A high-resolution model will also be advantage when small scale processes have a significant effect on model prediction, for example where inundation extent is controlled by small topographic features such as dykes, levees and ditches. However reduction of grid size also means considerably more computational time and increase in the work involved in data collection and processing.

Inundation areas are the most important role in the hydrological cycle and water resources in the South East Asia. Although annual floods cause destruction of resources, Some South East Asia countries traditionally used good water from inundation for utilization such as irrigation, fish habitat and natural groundwater recharge. Floodplain areas have been developed for paddy fields that coexist with flooding. Since groundwater resources are recharged from flooding water in large inundation areas during flood period which have dry seasons with severe water resource issues, can store water as groundwater. People can utilize the stored groundwater not only for drinking but also for irrigation, fish culture, industry and other activities in the dry period. Therefore, development of groundwater resources as a potential source of water for dry season will be an important issue in the floodplains.

The Mekong River is one of the largest inundation areas in the South East Asia. The Mekong River is an international river and its basin spreads over six South East Asian countries. Evaluation of groundwater resources in inundation areas during annual flooding and determining the recharge of groundwater resources in flood periods will be important issues in groundwater development activities in the Lower Mekong Basin. Flood and inundation analysis in the Mekong delta have been made with various numerical methods. Most studies focus on the lower part of Mekong River in Vietnam; few studies exist on the Cambodian part of the Mekong due to lack of available data. There are no studies to evaluate the effects and changes of inundation areas on the society and economy in terms of water resources.

1.2 Research Objective

1) Determine the variation of groundwater resources over inundation areas located in Cambodia, in the Lower Mekong river basin
2) Study about effect of grid size (250m, 500m and 1000m) to estimated inundation area and groundwater resource in Lower Mekong river basin.

1.3 Scope of this research work

This research investigates the hydrodynamic in the Lower Mekong River basin and estimated the water level at Phnom Penh to calibration and verification model. This research includes estimate inundation area and groundwater storage in this study area. The study area is Lower Mekong River basin. The duration of simulation covers the largest flood period in Cambodia (January to December 2000).

CHAPTER 2 LITERATURE REVIEWS AND STUDY AREA

2.1 Literature Reviews

2.1.1 Mekong River Basin

The Mekong river basin is one of the largest inundation areas in Southeast Asia.The Mekong river flows through China, Myanmar, Laos, Thailand, Cambodia, and Vietnam into the South China Sea counted for 4,200 kilometers long. As common in international river basins, the development of the Mekong River Basin is highly controversial, and is one of the most prominent components in the discussion about the river and its management. Integrated planning for efficient watershed management is hampered by the difficulties of coordinating between riparian states with diverse and often conflicting needs. This debate occurs in both the academic literature, as well as the media, and is a focus for many activist groups.

Joakim (2000) provided an empirically based study of International River Basin management in order to contribute to the global policy debate on water resources management and the role of water in the development process. The thesis reviews the recent 'water management' debate and a number of theoretical positions on the topic. Three empirical case studies of water management are conducted on regional (including Thailand, Laos, Cambodia and Vietnam), national (Cambodia), and local level (eight villages in Southeast Cambodia) in the Lower Mekong River Basin. The empirical base is researched through a combination of quantitative and qualitative methods, where semi-structured interviews are complemented by local level surveys and reviews of official documents. The thesis proposes that regional cooperation in contrast to statecentrism, and 'alternative' in contrast to 'mainstream' policies, hold greater chances to contribute to development without triggering destructive conflicts in the process. The conclusions reached support that proposition and argue that the 'alternative' approach in combination with a regional perspective represents the best option for contributing to development. However, several qualifications need to be added to the idea of 'alternative' methods if it is to be a viable approach in this context.

Kazama and Sawamoto (2002) studied on the change of inundation area by flood control, and irrigation area estimated from reserved water using a numerical simulation in the lower Mekong. This study show that the decrease of inundation area caused by flood control is much smaller compared with potential irrigation area. Although decrease of inundation area influence agricultural land, that can be made up for by irrigation. However it is hard to prevent inundation of floodplain even if there is large scale water control system.

Evelyn (2004) studied on the regional security implications of resource development on the Lancang Jiang. This study focuses on China's plans for hydropower development on its portion of the upper Mekong basin (Lancang Jiang) and their ecological, political and economic implications for Southeast Asian riparian. It shows that the economic imperative prevails among all riparian states, and that China and other countries tend to confine their cooperation to infrastructural development rather to consultation or management of potential adverse trans boundary impacts of upstream development.

Dushmanta, et al. (2007) studied on A two-dimensional hydrodynamic model for flood inundation simulation (a case study in the lower Mekong river basin) using a modeling system with a one-dimensional river flow model and a two-dimensional surface flow model to simulate flood inundation. The model has incorporated detailed information about urban terrain features like embankments, roads, bridges, culverts, etc. in the simulation. A geographical information system (GIS) - based comprehensive raster database of different spatial data layers is prepared and used in the model development. An explicit solution scheme is used for numerical computation, which considerably reduces the run time and makes the model suitable for use as a flood warning system in a large river basin.

Mira (2008) studied on "Mekong Delta at the Crossroads: More Control or Adaption". He state that agricultural production has developed successfully, and economic growth has been very rapid, but on the other hand, intensifying agriculture and large-scale water-control structures have challenged the environmental sustainability and social equity. The development plans have included a strong belief in the human mastery over the nature and waters of the Mekong Delta. In many cases, water resources planners have underestimated the complexity and integrated nature of the ecology and livelihoods of the Mekong Delta. This study examines cases where development efforts, while successful in some dimensions, have also contributed to create new risks for, especially, the poorest groups. The current situation calls for a more sustainable future route that would require examination of more adaptive measures in relation to the changing water flows of the Mekong River.

Kummu, et al. (2013) presented water balance analysis for the Tonle Sap Lake. The Tonle Sap Lake of Cambodia is the largest freshwater body of Southeast Asia, forming an important part of the Mekong River system. The lake has an extremely productive ecosystem and operates as a natural floodwater reservoir for the lower Mekong Basin, offering flood protection and assuring the dry season flow to the Mekong Delta. In light of the accelerating pace of water resources development within the Mekong Basin and the anticipation of potentially significant hydrological impacts, it is critical to understand the overall hydrological regime of Tonle Sap Lake. We present here a detailed water balance model based on observed data of discharge from the lake's tributaries, discharge between the Mekong and lake was modeled with the EIA 3D hydrodynamic model. We found that majority (53.5%) of the water originates from the Mekong mainstream, but the lake's tributaries also play mainly controlled by the water level in the Mekong mainstream. The Tonle Sap system is hence very vulnerable, from a water quantity point of view, to possible changes in the Mekong mainstream and thus, development activities in the whole Mekong Basin. From a biogeochemical point of view, the possible changes in the lake's own catchment are equally important, together with the changes in the whole Mekong Basin. Based on our findings, we recommend of continuing the monitoring in lake's tributaries and urgently starting of groundwater measurement campaign within the floodplain, and including the groundwater modeling to be part of the hydrodynamic models applied for the lake.

2.1.2 Surface water and groundwater interaction

Despite the fact that water resources and development plans aim to control the annual floods, to reduce inundation areas and to reduce flood damages in the Mekong Delta, those plans have been affected and changed the hydrological balance on the society and economy. In order to discuss the validity of development activities in the region, one must determine both how much water amount can be stored in the upstream dams or reservoirs to control the floods as well as how the control of inundation areas affects the groundwater resources in the area.

Bejranonda, et al. (2001) presented surface water and groundwater dynamic interaction models as guiding tools for optimal conjunctive water use policies in the central plain of Thailand. Many irrigation projects in the central plain of Thailand are not capable of providing sufficient surface water for the cultivation of rice, which is the major cash crop for Thai farmers. To overcome this surface water deficiency, which has been exacerbated in recent years by climate change, groundwater is increasingly being used for irrigation. Thus, large sections of agriculture lands have been converted to conjunctive water use regions. While conjunctive water use may be a suitable option to overcome the temporary water shortage on a short-term basis, it may pose a particular threat to the overall water resources in the long term, if not properly managed. As a remedy, conjunctive water management is basically a toll to optimize productivity, equity, and environmental sustainability through simultaneous management of surface water and groundwater resources. As of now, such a comprehensive approach has been not yet employed in the upper Chao Phraya basin of Thailand, and the present study is one of the first of this kind. The study region is the Plaichumpol Irrigation Project (PIP) where conjunctive water use has become indispensable for meeting the increasing water requirement for farming. To get a first grip on the issue, water demand, supply and actual use in the study area were investigated for the purpose of providing possible guidelines for optimal water exploitation. A numerical groundwater model with a special module for simulating surface-groundwater interaction was applied in the PIP area to understand the impact of the farmer's irrigation behavior on the dominant hydrological processes that determine the seasonal and multi-annual water availability in the irrigation area. A set-up of different agricultural water allocation schemes that depend on the local weather conditions and the regional management rules are examined by the numerical models. The results of the simulation provide adaptation guidelines for the proper management of the conjunctive water resources, namely, optimal water utilization. The numerical results for the surface groundwater in particular indicated that while the irrigation canals recharge water to the aquifer during both dry and wet season, small amounts of discharge from the aquifers to the canals occur only during the wet season. The analysis of the groundwater also showed that the present available groundwater potential is not fully exploited by the farmers, especially during the dry periods of surface water shortage. In contrast, the adoption of an optimal conjunctive management scheme would ensure extra water availability for additional annual rice crops in the region.

Shah (2006) studied on groundwater and human development: challenges and opportunities in livelihoods and environment. Global groundwater use has increased manifold in the past 50 years; and human race has never had to mange groundwater use on such a large scale. Sustaining the massive welfare gains groundwater development

has created without ruining the resource is a key water challenge facing the world today. He offer a typology of 5 groundwater demand systems as groundwater Socio-ecologies, each embodying a unique pattern of interactions between socio-economic and ecological variables, and each facing a distinct groundwater governance challenge. A daunting global groundwater issue today is to apply this knowledge intelligently to by far the more formidable challenge that has arisen in developing regions of Asia and Africa, where groundwater irrigation has evolved into a colossal anarchy supporting billions of livelihoods but threatening the resource itself.

Kazama, et al. (2007) studied on the variation of groundwater resources caused by flooding over inundated areas located in lower part of the Mekong River basin using numerical modeling and field observations. Comparing large, medium and small flood events, they conclude that flood control which reduces the area of inundation, results in a reduction of groundwater resources in the area. In 1993, a 19% reduction in inundation areas resulted in a 31% reduction in groundwater storage. In 1998, a 44% reduction in inundation areas led to a 42% reduction in groundwater storage. Thus, it can be concluded that while flood control activities are vital to reduce negative flood impacts in the Mekong River basin, they also negatively impact groundwater resources in the area.

Rahman, et al. (2009) studied on Arsenic contamination in groundwater in the Southeast Asia region. They present an overview of the arsenic crisis in the Southeast Asian region where groundwater is contaminated with natural occurring arsenic. The study propose that despite investments exceeding many millions of dollars, there are still substantial knowledge gaps about the prevalence and impact of arsenic, notably in its epidemiology, temporal variations, social factors, patient identification, treatment, etc. Arsenic-affected people in the affected regions also face serious social problems.

May, et al. (2009) presented the effects of river on groundwater in Cambodia. The seasonal fluctuation of surface water especially in the wide river significantly contributes to the change of groundwater in the aquifer system. This consequent affects the solute transport and biochemical processes in the system. Therefore, the water interaction is a key to build up the reactive solute transport model in the future study. In order to achieve the above objective, a two dimensional groundwater flow model coupled with a groundwater recharge model was applied in central and southern parts of Cambodia. The variation of river water elevations were taken into account in the modeling process. The model results confirmed the river and groundwater interaction that the Tonle sap River always gain the supply from groundwater at the northwestern mountains region and groundwater elevations raised higher than river in Bassac and Mekong river in dry season and vice verca in rainy season.

May, et al. (2010) applied numerical simulation to highlight the effects of river flooding on groundwater flow. A two-dimensional groundwater flow model coupled with a groundwater recharge model was applied to the research area in central Cambodia. River level variation was included in model processes, and flood areas and periods were assigned. The results showed that during flooding periods, floodwater from the three rivers played an important role in recharging groundwater supply from the northwest, and levels in the Bassac and Mekong River dropped to lower than the groundwater level.

2.1.3 Effect of grid size to hydrological model

Grid-base model are now widely used in simulating floodplain inundation, rainfall-runoff and other hydrological process which operate by assign single value for each raster cell to represent model parameter and input/output variables. In the development of models, many modelers increase spatial resolution (number of cell) to improved temporal and spatial process. However the spatial resolution affects the solution of the equation and simulation results. The relationship between model space/time resolution and simulation outputs is important to develop hydrological model. A high-resolution model will also be advantage when small scale processes have a significant effect on model prediction, for example where inundation extent is controlled by small topographic features such as dykes, levees and ditches. However reduction of grid size also means considerably more computational time and increase in the work involved in data collection and processing.

Bates and De Roo (2000) presented the development of a new model for simulating flood inundation. The model is designed to operate with high-resolution raster Digital Elevation Models, which are becoming increasingly available for many lowland floodplain river and is based on what we hypothesis to be the simplest possible process representation capable of simulating dynamic flood inundation. This consists of a one-dimensional kinematic wave approximation for channel flow solved using an explicit finite difference scheme and a two-dimensional diffusion wave representation of floodplain flow. The model is applied to a 35 km reach of the River Meuse in the Netherlands using only published data sources and used to simulate a large flood event that occurred in January 1995. This event was chosen as air photo and Synthetic Aperture Radar (SAR) data for flood inundation extent are available to enable rigorous validation of the developed model. 100, 50 and 25 m resolution models were constructed and compared to two other inundation prediction techniques: a planar approximation to the free surface and a relatively coarse resolution two-dimensional finite element scheme. The model developed outperforms both the simpler and model complex process representation, with the best fit simulation correctly predicting 81.9% of inundated and non-inundated areas. This compares with 69.5% for the best fit planar surface and 63.8% for the best fit finite element code. However, when applied solely to the 7 km of river below the upstream gauging station at Borgharen the planar model performs almost as well (83.7% correct as the raster model (85.5% correct). This is due the proximity of the gauge, which acts as a control point for construction of the planar surface and the fact that here low-lying areas of the floodplain are hydraulically connected to the channel. Importantly through it is impossible to generalize such application rules and thus we cannot specify a priori where the planar approximation will work. Simulations also indicate that, for this event at least, dynamic effects are relatively unimportant for prediction of peak inundation. Lastly, consideration of errors in typically available gauging station and inundation extent data shows the raster-based model to be close to the current prediction limit for this class of problem.

Horritt and Bates (2001) presented the scaling properties of a simple raster-based flood flow model are investigated. Model of resolution varying from 1000 to 10m are tested and predictions compared with satellite observations of inundated area and ground measurements of flood wave travel times, with a calibration strategy being used to determine channel friction coefficients. The optimum calibration is found to be stable

with respect to changes in scale when the model is calibrated against the observed inundation area, the model reaching maximum performance at a resolution of 100m, after which no improvement is seen with increasing resolution. Projecting predicting water levels onto a high resolution DEM improves performance further, and a resolution of 500m proves adequate for predicting water levels. Predicted flood wave travel time are, however, strongly dependent on model resolution and water storage in low lying floodplain area near the channel is identified as an important mechanism affecting wave propagation velocity. A near channel floodplain storage version of model is shown to be much more stable with respect to changes in scale when the model is calibrated against flood wave travel time, and shown to represent the retardation of the flood wave caused by water storage near the channel. The model cannot be calibrated to give both acceptable travel times and inundated area, and in this respect performance is poor.

Vazquez, et al. (2002) presented discusses the application of the physically based distributed MIKE-SHE code to a medium size catchment using different size to investigate scale effect on the model results. First a 600 m grid-square model was calibrated. This was then subjected to a multi-resolution (MR) validation test by using the effective parameters of the calibrated model in 300 m and a 1200 m grid-square model. The MR test indicated that the models for the resolutions analyzed only differ marginally. Secondly, the effect of grid size on both the calibrated effective model parameters and the model performance was analyzed in the scope of a multi-calibration test in which the calibration and validation processes were kept as unique and standard as possible for every grid size. The model was calibrated and validated for every grid size against both daily catchment discharge measurement and observed water levels using both a split sample procedure and a multi-site validation test. The investigation indicated that the best validation results, in terms of river discharge, were obtained with a 600 m grid-resolution, independent of the stream-flow station. This, together with the exponential increase in computation time when reducing the grid size, indicated that, for the given level of data input and quality, the model type and structure, and the time step, a 600 m grid-resolution is most appropriate for the catchment under study.

Liu, et al. (2005) presented effects of grid size on model parameters and on the performance of a GIS-based hydrological model intended for flood simulation is assesses in this paper. The WetSpa model is used to estimate runoff and flow discharge in the 1176 km2 Alzette river basin, Grand-duchy of Luxembourg. The GIS ArcView and its spatial analyst are used to extract hydrological model parameters from DEMs, soil and land use maps with cell size of 50, 100, 200, 400 and 800m. The value of the model parameter derived from the 50m data is used as the reference value, with estimates of model parameters of coarser resolutions compared against it. Results show that in this integrated model the model the grid size has a considerable effect on runoff and outflow hydrographs. However, coarser grid cell resolutions can be used for runoff simulations as long as parameters are appropriately calibrated.

Schumann, et al. (2013) presented evident in recent literature that hydrodynamic modeling effort have moved to increasing spatial coverage while trying to preserve simulation accuracies at computationally efficient coarse grids (100m to several km). However, it is clear that there is a need to retain fine spatial resolution at large scale wherever possible in order to still retrieve meaningful information from models or indeed observations, such as identifying individual assets at risk from flooding for instance. Since it is currently rather impractical to model hydrodynamic across areas

larger than a couple of thousand km^2 at a fine spatial resolution (finer than 100 m), this paper proposes a method to downscale coarse model simulations (model grid size of 100 m to several km) to a fine spatial resolution. The method is mass conservative and uses a hydraulic 1D approach within the channel and a pseudo region-growing algorithm on the floodplain. Comparison to a high resolution reference model over a domain size much larger than those traditionally modeled showed that downscaling a 600 m grid resolution hydrodynamic LISFLOOD-FP model to 30 m leads to average accuracies greater than 30 cm in water and above 90% in inundation area for a high accuracy digital elevation model (DEM). When employing a SRTM DEM accuracies were still between 0.5 m and 1.5 m for water depth but agreements in inundated area were much lower than 90 m, even a speed-efficient model could take over three years to simulate inundation patterns at that resolution for a one-year hydrograph. However, it is expected that the proposed downscaling method could be used to downscale LISFLOOD-FP model simulation run at a 3 km resolution with reasonably similar accuracies and at only a fraction of computational time required by the 90 m model.

2.2 Precipitation

Subramanya (2009, p.13) describes precipitation as "all forms of water that reach the earth from the atmosphere. The usual forms are rainfall, snowfall, hail, frost and dew. Of all these, only the first two contribute significant amounts of water. Rainfall being the predominant form of precipitation causing stream flow". The main form of precipitation is rain, water drops of sizes larger than 0.5 mm. In term of its intensity, rainfall can be classified as Light rain (trace to 2.5 mm/h), Moderate rain (2.5 mm/h to 7.5 mm/h) and Heavy rain (>7.5 mm/h). Precipitation is expressed in terms of the depth to which rainfall water would stand on an area if all the rain were collected on it. Thus 1 cm of rainfall over a catchment area of 1 km^2 represents a volume of water equal to 10^4 m^3. The precipitation is collected and measured in a rain gauge.

In practice, hydrological analysis requires knowledge of the rainfall over an area, such as over a catchment. To convert the point rainfall values at various stations into an average value over a catchment the following three methods are in use: Arithmetical-mean method, Thiessen-polygon method and Isohyetal method.

2.2.1 Thiessen-polygon method

Thiessen method is a graphical technique assigning weight at each gauge station in proportion to the catchment area that is closest to that gauge. The fraction is figured out based on the relative area of each measurement station in the polygon network. The method of constructing the polygons implies the following steps:

1. Rain gauges are plotted on map of the catchment area of interest.
2. To make network of triangle, adjacent stations are connected with dot lines without any intercept (Figure 2.1a).
3. Perpendicular bisectors of each line are constructed (perpendicular line at the midpoint of each line connecting two stations) (Figure 2.1b).
4. The bisectors are extended and used to form the polygon around each gauge station (Figure 2.1c).

5. Rainfall value for each gauge station is multiplied by the area of each polygon calculated from planimeter or grid graph.
6. All values from step 5 are summed and divided by total basin area. An example of spatial precipitation distribution according to Thiessen method can be appreciated in Figure 2.1d.

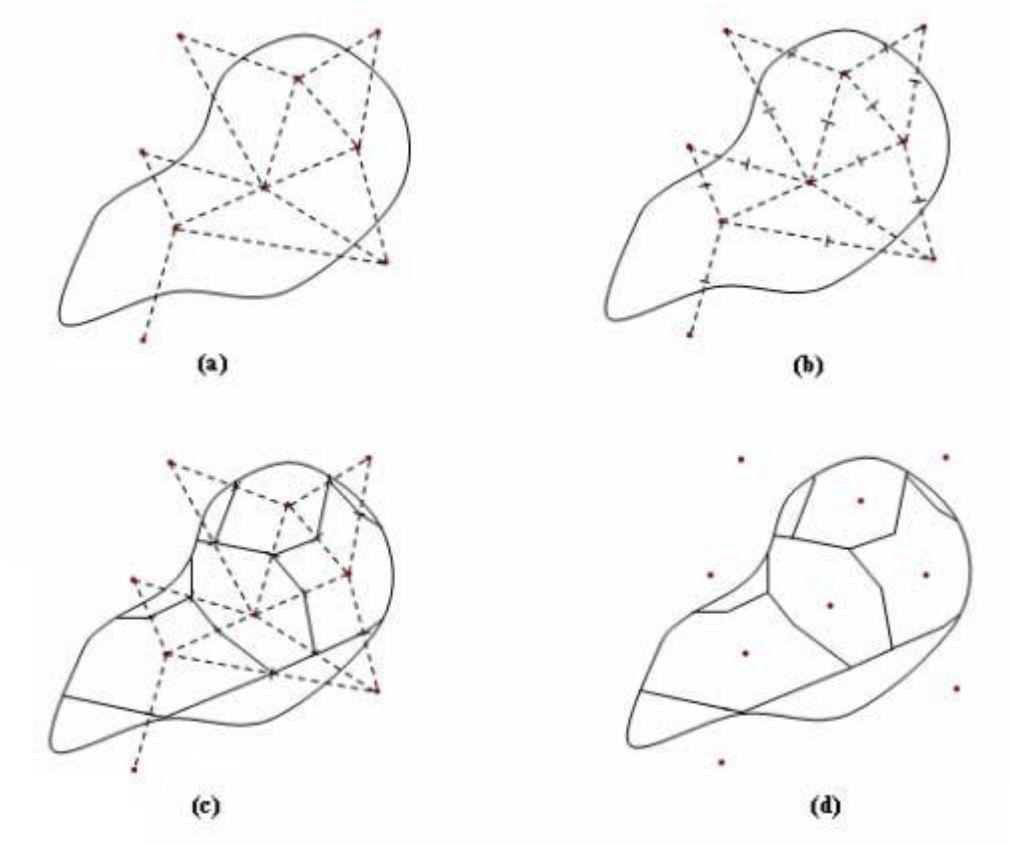

Figure 2.1 Construction of Thiessen polygon
Source: Hamburg University of Technology, 2010

Even though the Thiessen method is better than arithmetical-mean method because of its weighted area, there are several shortcomings should be considered. In wide study area, a little distorted data makes severe impact. Moreover, in mountainous areas, an irregular spatial distribution of precipitation can be formed over small distances, and for such circumstances the Thiessen method can yield erroneous results. Another disadvantage is that the polygon needs to be reconstructed if there is a change in the position of rain gauge.

2.3 Groundwater -Surface Water Interaction

2.3.1 Forms of Subsurface Water

Water beneath earth's surface is called subsurface water and is considered in two principle zones (Figure 2.2) : 1. Saturated zone, and 2. Aeration zone. Saturated zone, also known as groundwater zone, is vital for underground water. This zone can be divided into 3 subzones: soil zone, intermediate zone and the upper part of capillary

fringe. Soil zone, it is accounted for the distance from the surface to 2 meters underground containing roots of trees and having high porosity. Intermediate depth depends on the deep of soil zone and capillary fringe. Capillary fringe is below intermediate zone filled with water due to tension saturation. Zone of Aeration, in this zone the soil pores are only partially saturated with water. The space between the land surface and the water table marks the extent of this zone.

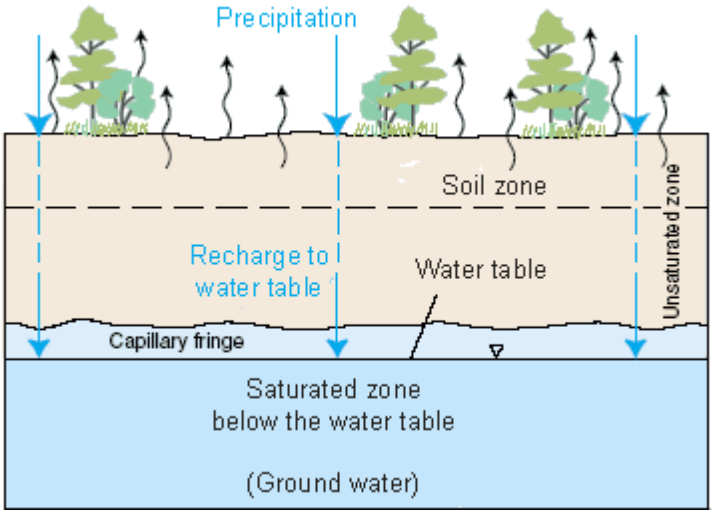

Figure 2.2 Classification of Subsurface Water
Source: USGS., 2014

2.3.2 Groundwater and Streams

The interaction between streams and ground water takes place in two basicways:
gaining streams receive water from the groundwater system and losing streams lose water to the groundwater system. Groundwater discharges into streams when the elevation of the water table above the streambed (Figure 2.3). Usually during dry period, the water table falls below the stream bed. Stream loss water to groundwater (Figure 2.4). Only after rainfall has replenished the groundwater supply does the water table rise sufficiently to intersect the streambed and resume base flow discharge.

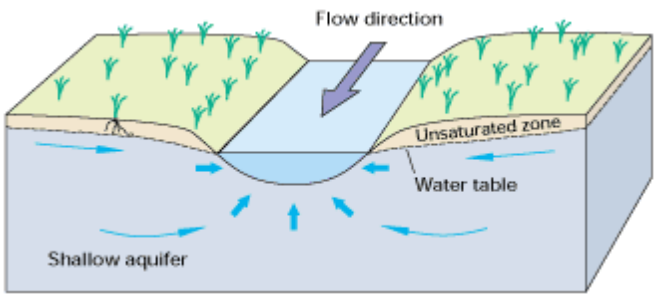

Figure 2.3 Gaining streams receive water from the groundwater system
Source: Environment Canterbury, 2000

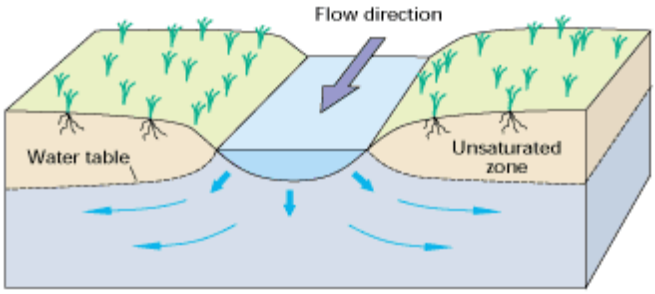

Figure 2.4 Losing streams lose water to the groundwater system
Source: Environment Canterbury, 2000

2.3.4 Interaction of Groundwater and Wetlands

Wetlands are saturated with water either permanently or seasonally; typically occur in areas where ground water discharges to the land surface or in areas where ground conditions impede the drainage of water. They can also be constructed artificially as a water management tool. The interaction between groundwater and wetlands depends largely on the location and changed by precipitation or runoff. For situations where impeded drainage occurs, stream depletion effects are unlikely to be significant because the layer of impeded drainage is also likely to inhibit the upward transmission of any pumping effects. However, in areas where groundwater springs discharge into wetlands, the pumping from underlying aquifers can affect the amount of groundwater discharge.

2.4 Hydrological Model

2.4.1 Introduction

Hydrology is the study of the motion of the earth's waters through the hydrologic cycle including water quality and sustainable use. In order to understand those features, hydrological models are used to simplify systems that represent real elements of the water system, i.e. rivers, lakes, groundwater, soil, snow. Those models can serve as useful tools in the investigation of the impact of natural (e.g. climate change) and environmental impact as a result of human activities (e.g. water withdrawals). In general, the three primary watershed properties governing hydrologic disturbances are soils, land cover and topography. Hermann (2014) said that "hydrological models can be applied on different scales, ranging from local to global, with the degree of complexity usually being dependent on the scale for which they were designed. Some models cover water quality or other ecological aspects". Two major types of hydrologic models are stochastic models and process-based models.

1. Stochastic Models. These models are classified in light of complexities of spatial hydrologic processes (black box systems), used to represent the evolution of some random variables over time. Data are applied with mathematical and statistical concepts to transfer a certain input (for instance rainfall) to the model output (for instance runoff) without considering their internal workings.

2. Process-Based Models. These models enable us to understand the temporal characteristic of physical processes combining multiple and interacting features. Governing equations for the major hydrologic process could be done by these models. Usually, a complex process model consists of interconnected sub models such as surface runoff, subsurface flow, evapotranspiration, and channel flow, but they can be far more complicated than stochastic models.

2.4.2 Model validation

2.4.2.1 Coefficient of determinations (r^2)

The coefficient of determination r^2 is defined as the squared value of the coefficient of the coefficient of correlation according to Bravais-Pearson. It is calculated as:

$$r^2 = \left(\frac{\sum_{i=1}^{n} \left(O_i - \overline{O}\right)\left(P_i - \overline{P}\right)}{\sqrt{\sum_{i=1}^{n} \left(O_i - \overline{O}\right)^2} \sqrt{\sum_{i=1}^{n} \left(P_i - \overline{P}\right)^2}} \right)^2 \tag{2.1}$$

With *O* observed and *P* predicted values

R^2 can also be expressed as the squared ratio between the covariance and the multiplied standard deviations of the observed and predicted value. Therefore it estimated the combined dispersion against the single dispersion of the observed and predicted series. The range of r^2 lies between 0 and 1 which describes how much of the observed dispersion is explained by the prediction. A value of zero means no correlation at all whereas a value of 1 means that dispersion of the prediction is equal to that of the observation. The fact that only the dispersion is quantified is one of the major drawbacks of r^2 if it is considered alone. A model which systematically over or under predicts all the time will still results good r^2 value close to 1.0 even if all predictions were wrong.

2.4.2.2 Root Mean square error (RMSE)

The Root Mean Square Error (RMSE) (also called the root mean square deviation, RMSD) is a frequently used measure of the difference between values predicted by a model and the values actually observed from the environment that is being modelled. These individual differences are also called residuals, and the RMSE serves to aggregate them into a single measure of predictive power.

The RMSE of a model prediction with respect to the estimated variable Xmodel is defined as the square root of the mean squared error:

$$RMSE = \sqrt{\frac{\sum_{i=1}^{n} \left(X_{obs,i} - X_{model,i}\right)^2}{n}} \tag{2.2}$$

Where X_{obs} is observed values and X_{model} is modelled values at time/place i.

The calculated RMSE values will have units, and RMSE for phosphorus concentrations can for this reason not be directly compared to RMSE values for chlorophyll a concentrations etc. However, the RMSE values can be used to distinguish model performance in a calibration period with that of a validation period as well as to compare the individual model performance to that of other predictive models.

2.4.2.3 Nash-Sutcliffe efficiency (Nash)

The efficiency (Nash) proposed by Nash and Sutcliffe (1970) is defined as one minus the sum of the absolute squared differences between the predicted and observed values normalized by the variance of the observed values during the period under investigation. It is calculated as:

$$Nash = 1 - \frac{\sum_{i=1}^{n}\left(O_i - P_i\right)^2}{\sum_{i=1}^{n}\left(O_i - \overline{O}\right)^2} \tag{2.3}$$

The range of Nash lies between 1.0 (perfect fit) and -∞. An efficiency of lower than zero indicates that the mean value of the observed time series would have been a better predictor than the model.

2.4.2.4 Index of agreement (IA)

The index of agreement was proposed by Willmot (1981) to overcome the insensitivity of Nash and r^2 to differences in the observed and predicted means and variances (Legates and McCabe, 1999). The index of agreement represents the ratio of the mean square error and the potential square error (Willmor, 1984) and is defined as:

$$IA = 1 - \frac{\sum_{i=1}^{n}\left(O_i - P_i\right)^2}{\sum_{i=1}^{n}\left(\left|P_i - \overline{O}\right| + \left|O_i - \overline{O}\right|\right)^2} \tag{2.4}$$

The range of IA is similar to that of r^2 and lie between 0 (no correlation) and 1 (perfect fit)

2.5 Study area

The Mekong rivers is estimated length is 4,350 km making it the world's 12th-longest river (Table 2.1).The Mekong starts in the South-eastern Himalayan Mountain and drains the eastern watershed of the Tibetan plateau (Figure 2.5). These rivers fall off the eastern rim of the plateau in a narrow geographic zone characterized by deep gorges and high ridges known as the Three Rivers Area. In this narrow zone the three great rivers flow parallel to one another in a strip of terrain some 100 km wide by 500 km long. Downstream of the Three Rivers Area, the courses of Salween, Mekong, and Yangtze diverge, so that the rivers eventually discharge into the Andaman Sea, South China Sea, and East China Sea respectively.

Table 2.1 The 12 largest rivers of the world ranked by length

Rank	River	Landmass	River Length (km)	Outflow
1	Nile	Africa	6,650	Mediterranean Sea
2	Amazon	South America	6,400	Atlantic Ocean
3	Yangtze	Eurasia	6,300	East China Sea
4	Mississippi	North America	6,275	Gulf of Mexico
5	Yenisei	Eurasia	5,539	Arctic Ocean
6	Yellow River	Eurasia	5,464	Yellow sea
7	Ob'	Eurasia	5,410	Gulf of Ob'
8	Parana	Antarctica	4,880	Tatar Strait
9	Congo (Zaire)	Africa	5,118	Atlantic Ocean
10	Amur	Eurasia	4,909	Sea of Okhotsk
11	Lena	Russia	4,400	Caspian Sea
12	Mekong	Eurasia	4,350	South China Sea

Source: Liu et al. (2009)

The internal drainage patterns within these three basins are unusual when compared to those of other large rivers. Most large-river systems that drain the interiors of continents, such as the Amazon, Congo, and Mississippi have relatively simple tributary networks that resemble a branching tree. Typically, such patterns develop in basins with gentle slopes where the underlying geological structure is fairly stable, no control on river morphology. On the other hand, the tributary networks of the Salween, Yangtze, and particularly the Mekong are complex with different sub basins often exhibiting different, and distinct, drainage patterns. These complex drainage systems have developed in a setting where the basic geological structure is active, and is the major factor controlling the process of rivers and the landscapes they cut out.

Figure 2.5 Major drainage basins of South East Asia
Source: Mekong River Commission 1993-2010

2.5.1 The physiography of the Mekong Basin

The Mekong Basin can be subdivided into seven broad physiographic regions described by topography, drainage patterns, and the geomorphology of river channels (Figure 2.5). The upper three regions (Tibetan Plateau, Three Rivers, and Lancang Basin) make up the Upper Mekong Basin. The Lower Mekong Basin contains four physiographic regions (Northern Highlands, Khorat Plateau, Tonle Sap Basin and the Mekong Delta).

2.5.1.1 Tibetan Plateau

The Guyong-Pudigao creek at 5160 m above sea level near the foot of Mountain Jifu on the Tibetan Plateau is designated as the source of the Mekong. The plateau is the most densely glaciated region on Earth and while nearly half the glaciated area (49,873 km^2) is within China, only 316 km^2 of this area is attributed to the Mekong Basin. The eastern third of the plateau drains into the basins of the Salween, Mekong and Yangtze rivers. On the high plateau the course of the Mekong and its tributary network is influenced strongly by the tectonic fabric of the Tibetan Plateau. Here the mainstream and the major tributaries run more-or-less parallel in a North-west to South-East direction (Figure 2.6).

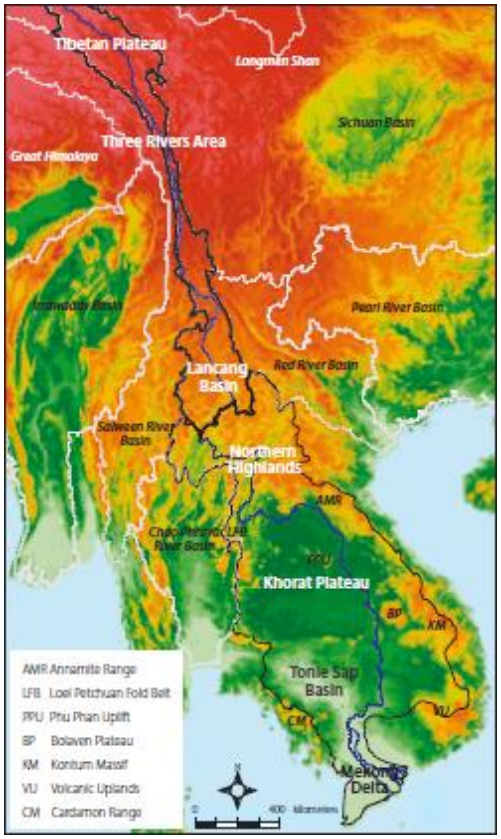

Figure 2.6 Topography and physiographic zones of Mekong Basin
Source: Mekong River Commission 1993-2010

2.5.1.2 The Three Rivers Area

In this area, the Mekong flows for more than 500 km through a deep valley that is cut more than 2500 m in some places (Figure 2.6).In this area where the river has no significant tributaries, the basin is very narrowest is only 20 km wide.

2.5.1.3 Lancang Basin

To the south of the Three Rivers Area the Upper Mekong Basin broadens as the Salween and Yangtze diverge to the west and east respectively (Figure 2.6). This area, known as the Lancang Basin, is still at a high elevation (between 2000 and 3000 m above sea level) compared to the LMB and the river continues to flow down a steep gradient. However, small tributary catchments are now developed on both the right and left banks of the mainstream. Channel morphology is largely bedrock constrained.

2.5.1.4 Northern Highlands

The Northern Highlands forms the upland region of northeast Myanmar, northern Thailand and northern Lao PDR (Figure 2.6). In this region the Mekong is constrained in steep-sided bedrock in channels. The tributary network in this area has large tributaries entering the Mekong's left (Nam Ta, Nam Ou, Nam Soung and Nam Khan) and right (Nam Mae Kok and Nam Mae Ing) banks. These tributary networks mostly flow through steep-sided rock-cut valleys. However, in places the tributaries extend and develop floodplains.

2.5.1.5 Khorat Plateau

The Khorat Plateau is a saucer-shaped basin located at an elevation of about 300 m above sea level. The boundary of the basin is defined by a sharp formed by the highly resistant sandstones of the Khorat Group. The plateau is bound to the west and northwest by the Loei – Petchabun foldbelt, and by the Annamite Mountains to the east and northeast (Figure 2.6). To the south the forms a low edge above the Tonle Sap Basin. The only significant internal topographic feature is a low range of hills (Phu Phan uplift) that cut across the basin trending from the North-West to South-East. This low range divides the Khorat Plateau into two subbasins, the Sakhon Nakhon Savannakhet Basin to the north, and the Mun/Chi Basin to the south. The tributaries on the right bank of the Mekong (Songkhram and Mun), which flow across the low slope central region of the Khorat Plateau, have well developed architecture. In contrast, the tributaries on the left bank of the river (Nam Ca Dinh, Se Bang Fai and Se Bang Hiang) fall steeply from sources high in the Annamites.

2.5.1.6 Tonle Sap Basin

The Tonle Sap Basin is a large dome like structure that has been unroofed through erosion, leaving edge of hills standing above the alluvial plains that fill the center of the basin. The Mekong enters the basin just north of Pakse and flows through a broad valley flanked by the southern rim of the Khorat escarpment to the west and the Boloven Plateau to the east. At the southern end of this stretch the mainstream breaks up into a complex network of branching and reconnecting channels typified by the islands and channels forming the Siphandone (4000 islands) area in southern Lao PDR.

The Mekong drops into the alluvial plain of Cambodia through a series of water fall at Khone Falls. The river then flows southwards along the eastern margin of the basin in a section of branching channels until Kratie. Here, the course of the mainstream takes a right-angled turn westwards as the river is deflected by extensive basaltic lava flows that form the upland area north of Ho Chi Minh City.

The tributary network entering the left bank of the Mekong in this stretch of the river is dominated by the catchments of the Se Song, Se San, and Sre Pok. These fast flowing rivers drain a chain of mountainous terrain that extends from the Boloven Plateau of Lao PDR, though the Kontum Massif, to the volcanic uplands of southern Viet Nam. Downstream of Kratie the mainstream develops a wide alluvial floodplain with associated shifting channel morphologies including meanders.

The western and central part of the Tonle Sap Basin forms a low slope landscape in which locates the Great Lake, its extensive floodplain and the network of tributaries that provide water into the lake. The Tonle Sap River, which links the Mekong and the Great Lake, has hydraulic characteristics rarely found elsewhere in the world. During the dry season, the river behaves as normal tributary draining water off the Cambodian floodplain and its surrounding catchment into the mainstream of the Mekong. However, during the wet season the dramatic increase in the discharge of the mainstream cannot be accommodated by the distributary network of the Mekong Delta, and the level of the Mekong rises higher than the Tonle Sap River. When this happens the flow of the Tonle Sap River reverses direction as water from the Mekong flows upstream overfilling the Great Lake and flooding the surrounding forested lowlands. During this part of the

annual flood-cycle, the area of the Great Lake increases six-fold from 2500 km^2 to 15,000 km^2 and it is volume from 1.5 km^3 to between 60 and 70 km^3. At the end of the wet season the discharge of the Mekong falls, and the flow of the Tonle Sap River reverts to the normal downstream direction, draining excess water off the inundated floodplain surrounding the Great Lake.

2.5.1.7 The Mekong Delta

The top of the Mekong Delta is defined near Phnom Penh where the largest distributary river channel, the Bassac River, splits from the mainstream. South of Phnom Penh, the delta rapidly expands to form a wedge shaped delta plain that covers an area of 62,520 km^2. The modern delta has two major distributary channels, the Mekong and Bassac Rivers which split into a number of smaller channels to form the Nine Dragons as the mouths of the Mekong are known. The sub region of the delta plain can be divided into two parts: an inner delta plain that is dominated by fluvial process and an outer delta plain that is dominated by marine processes. The inner delta plain close to sea level while the outer delta-plain which is built of coastal plain deposits, is fringed seawards by mangrove swamps, beach ridges, sand dunes, spits and tidal flats.

2.5.2 The Rainfall Climate

The distribution of mean annual rainfall over the basin shows a distinct east to west gradient (Figure 2.7). The highest rainfalls of more than 2500 mm/year occur in the western montane regions of Lao PDR and the lowest, less than 1000 mm/year, in the central regions of Thailand within the Mun–Chi Basin. This geographical pattern determines that by far the greatest contributions to stream flows during the summer monsoon season originate within the large left bank tributaries in Lao PDR.

Two characteristics of rainfall climate in Mekong basin, the first being what are known as monsoonal when the conditions linked to rainfall generation weaken and become less active. This typically occurs during July and August and is linked to the reduced formation of tropical monsoonal low pressure systems. The second peak in September and October is partly related to the impact of tropical storms and typhoons moving across the LMB from the Gulf of Tonkin and the South China Sea. Their peak incidence occurs from September to November, although their average track tends to move from north to south as the season progresses.

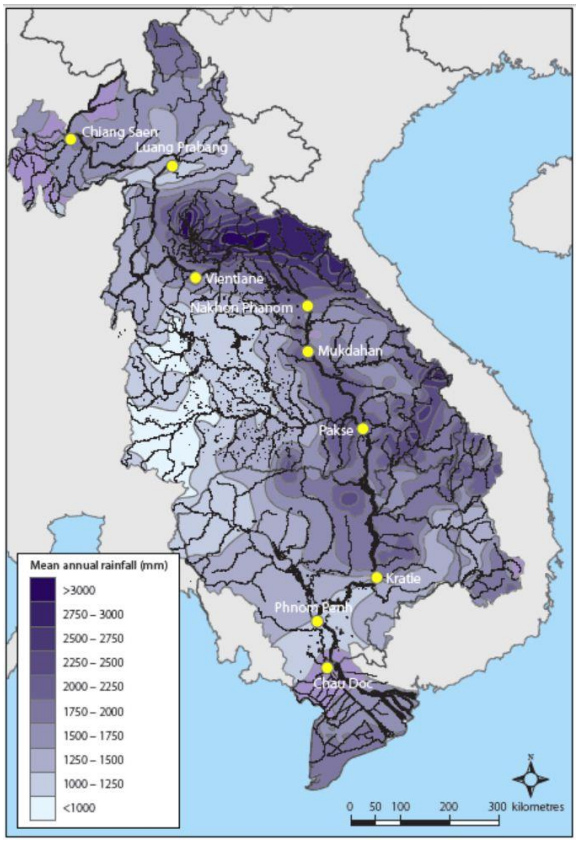

Figure 2.7 Lower Mekong Basin – mean annual rainfall
Source: Mekong River Commission 2010

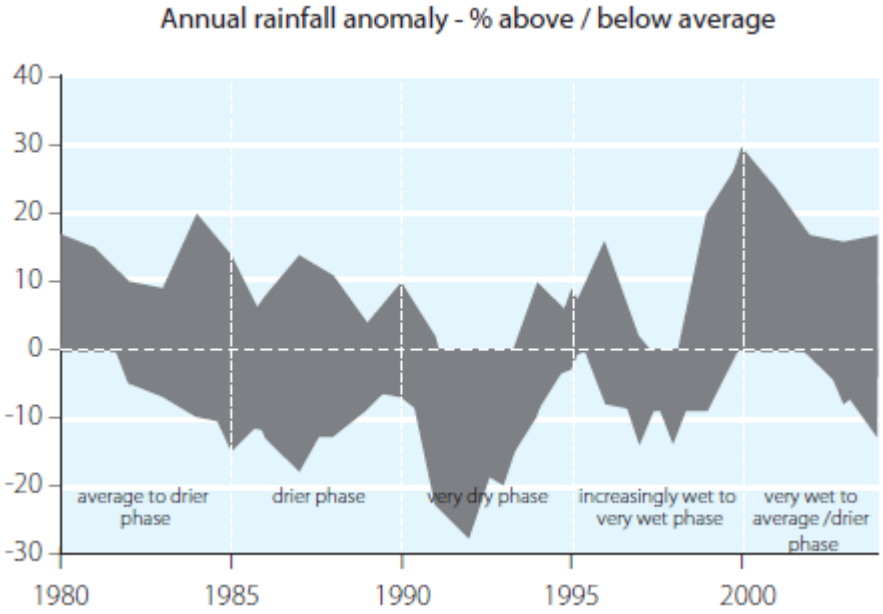

Figure 2.8 Deviations of regional rainfall above and below average over the 25 years between 1980 and 2004, based on pooled data
Source: Mekong River Commission 2010

In most years, the geographic variability of total rainfall over the basin is high since the synoptic conditions that cause major storm rainfall events do not extend to the basin scale. Intense tropical depressions tracking from east to west typically affect only part of the region while distribution of rainfall associated with these depressions also depends on how rapidly they move towards the west. Convective cells typical of the monsoon are even more localized in their impacts. Such storm episodes provide most of the annual rainfall and their local frequency in any given year determines whether the year is particularly wet.

Despite the high spatial variability of tropical monsoon rainfall, it is possible to obtain a general regional overview of the conditions over recent years by pooling the annual time series expressed as deviations above and below the mean annual rainfall for the 25 years from 1980 to 2004 (Figure 2.8). The period began with average to drier conditions which intensified post 1985 and then became much more severe during the early 1990s when almost all sites recorded a run of several years of much reduced rainfall. After 1995, general regional rainfall moved back to normal levels and then into a distinctly wetter phase between 1999 and 2002, after which it decreased to average and below.

2.5.3 Hydrology

The annual hydrological regime of the Mekong (Figure 2.9) is determined by two major influences. Climate and the response to the south-west monsoon between June and October. This results in an annual flood pulse and therefore a distinct seasonality in the annual hydrological cycle between a flood season and a low-flow season.

On the mainstream and within its larger tributaries the wide areas of drainage systems result in runoff responses to individual storm events caused by monsoonal depressions that tend to connect and therefore accumulate into a single seasonal flood flow regime. This means it is not generally possible to divide the runoff response to individual events unless the cyclonic storm system is very intense and regional in scale. Tropical typhoon incursions into the basin from the South China Sea are the weather systems most responsible for generating distinct individual peaks to the monsoonal flow. These generally occur during September and October when the seasonal discharge is already high and tend to generate a second significant peak to the annual flow. Historically these events have been responsible for many of the most extreme flood discharges and water levels that have been observed.

Figure 2.9 Major Mekong mainstream gauging station
Source: Mekong River Commission 2010

2.5.3.1 Region runoff and stream flow

The hydrological geography of the lower Mekong is to some extent affected by upstream conditions but most water is contributed from within the LMB (Table 2.2). The upper Mekong in China contributes 16 percent of the total flow in an average year, while 55 percent comes from the large left bank tributaries in Lao PDR along with the Se Kong, Se San and Sre Pok river system. This is reflected in regional distribution of annual runoff (Figure 2.10). Although the Mun/Chi tributary complex drains 20 percent of the lower basin area, average annual runoff is only 250 mm, which is considerably less than half of the regional average figure of 600 mm, with the result that this wide area of northeast Thailand contributes less than 6 percent to the mean annual Mekong flow.

Table 2.2 Proportional contributions to total Mekong mean annual flow by river reach, distinguishing those made by the left and right bank tributary system

River Reach	Left bank (%)	Right bank(%)	Total (%)
China	16		16
China – Chiang Sean	1	3	4
Chuang Sean – Luang Prabang	6	2	8
Luang Prabang – Vientiane	1	2	3
Vientiane – Nakhon Phanom	18	4	22
Nakhon Phanom - Mukdahan	3	1	4
Mukdahan – Pakse	4	6	10
Pakse – Kraite	22	2	24
Tonle Sap			9
Total	55	20	100

Source: Mekong River Commission 1993-2010

The estimated mean annual flow of the basin as a whole is almost 460 km^3 (Table 2.3). Of the total annual flow, in an average year about 75 percent occurs within just four months between July and October (Table 2.3). The minimum flow occurred in 1992 and the maximum of almost 630 km^3 was associated with the disastrous flooding in Cambodia and Viet Nam in 2000.

Table 2.3 Distributions of annual flow volumes

Mainstream site	Catchment area (km^3)	Mean annual flow as			As % total Mekong
		Discharge m^3/sec	Volume km^3	Runoff mm	
Chiang Saen	189,000	2,700	85	450	19
Vientiane	299,000	4,400	139	460	30
Pakse	545,000	9,700	306	560	67
Kratie	646,000	13,200	416	640	91
Total	760,000	14,500	457	600	100

Source: Mekong River Commission 1993-2010

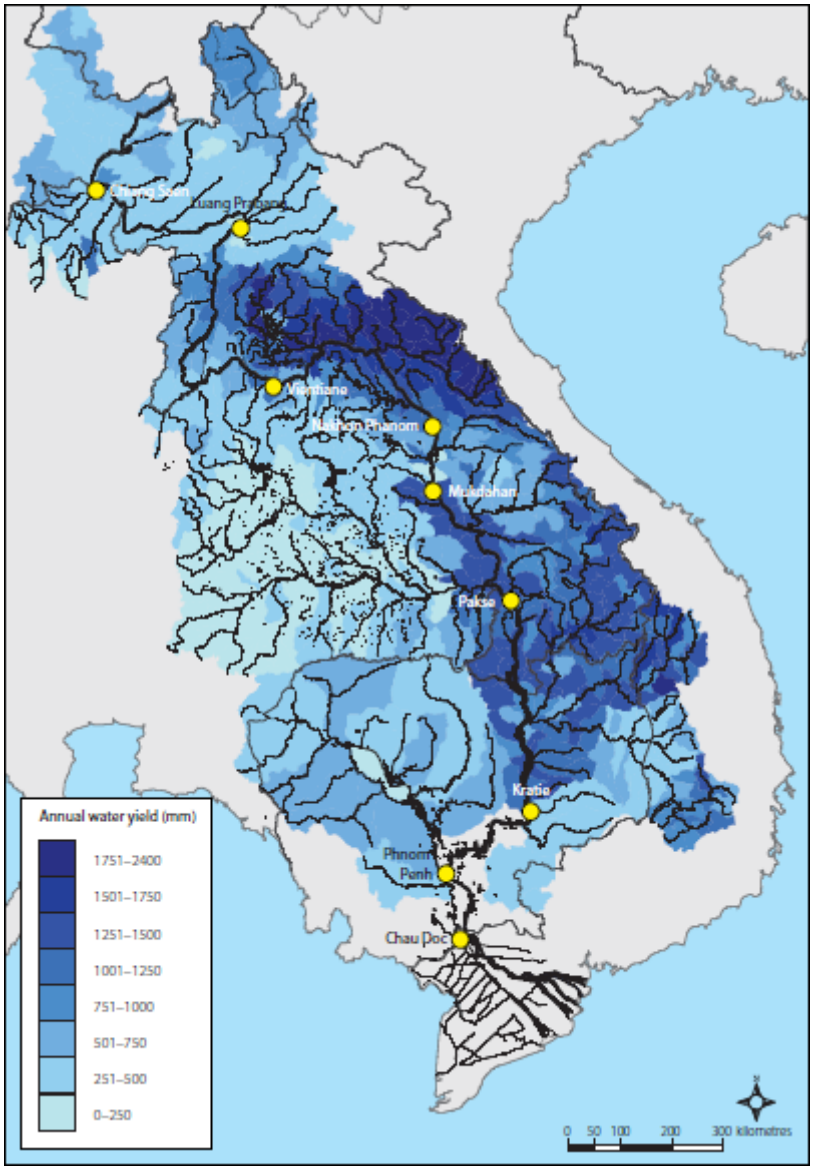

Figure 2.10 Mean annual runoff (mm) in the Lower Mekong Basin
Source: Mekong River Commission 1993-2010

CHAPTER 3 METHODOLOGY

3.1 Mathematical model

A mathematical model is a description of a system using mathematical concepts and language. To estimate the effects of flood on groundwater resources, numerical processes based on finite difference techniques were able to successfully solve governing non-linear partial differential equations and couple each parameter.

To analyze the impacts on the overland flow, a flood model of 110 km by 160 km developed by Kazama et al., (2007) was applied. The model is constructed using finite difference techniques to numerically model flood flow, inundation depth and overflow by solving the basic governing equations (Figure 3.1). Two data sets were required so as to simulate this model. First, input data and boundary condition necessitate hydro-meteorological data - rainfall, evaporation, river discharge and water level. Second, as we considered the surface water, soil properties play a vital role in this study as shown in Figure 3.2 The model parameters such as manning roughness reported by Kazama et al.,(2007) were adopted for this study.

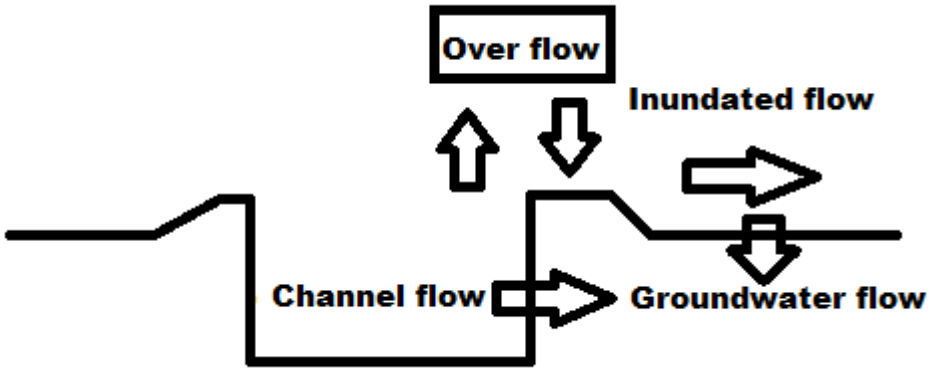

Figure 3.1 Integration of channel flow, inundated flow, overflow and groundwater flow

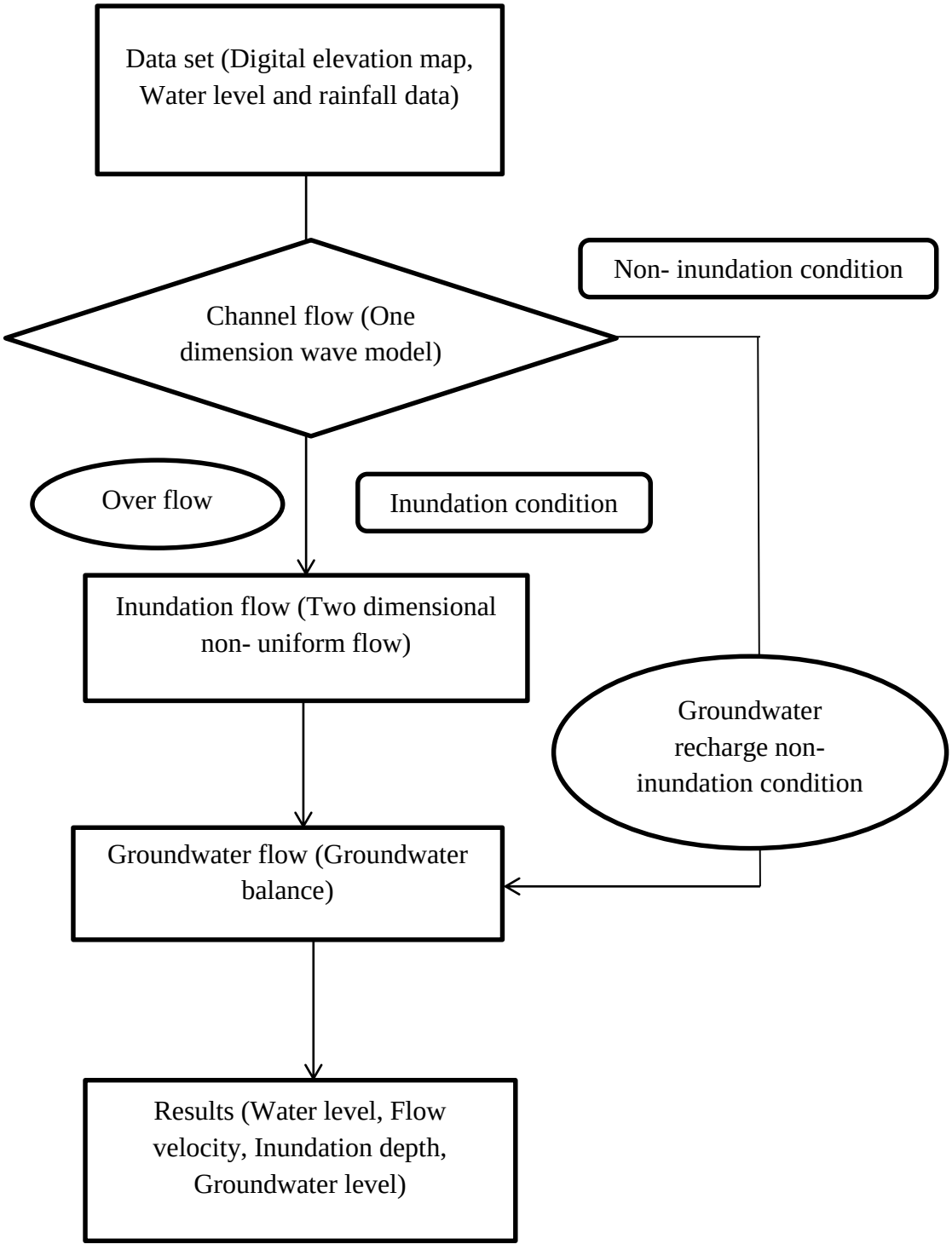

Figure 3.2 Flow chart of Numerical model

3.1.1 Channel flow calculation

Governing equation in flood flow is a non-linear partial differential equation. It has been solved using a finite difference by set the control volume of one-dimensional flow. We used the dynamic wave model as a numerical calculation model which consists of a continuity equation and a momentum equation as follow:

$$\frac{1}{g}\left(\frac{\partial v}{\partial t}\right)+\frac{1}{g}\frac{\partial}{\partial x}\left(\frac{v^2}{2}\right)+S+\frac{\partial h}{\partial x}+\frac{n^2|v|v}{h^{4/3}}=0 \tag{3.1}$$

$$\frac{\partial A}{\partial t}+\frac{\partial Q}{\partial x}-q=0 \tag{3.2}$$

Where A is the cross-sectional area (m^2); Q is discharge (m^3/s) and g is gravitational acceleration (m^2/s). v represent the velocity (m/s), S represent the river bed elevation, h represents the river water depth (m), n represent the Manning coefficient and q refers to the inflow per unit area such as tributary inflow or rainfall.

When performing finite difference calculation, water levels in the channels have been solved by equation 3.5 and 3.8 . Both equation show calculation flow rate from momentum equation and water level determined from continuous equation. Momentum Equation of the flood calculations for river channel is shown in 3.1 formula is shown in 3.3 as a differential equation around a point time t = n, the number of space x = i for this sections.

$$\frac{\partial v}{\partial t}=\frac{{}_{n+1}v_i-{}_{n-1}v_i}{\Delta t} \tag{3.3a}$$

$$\frac{\partial v^2}{\partial x}=\frac{{}_{n-1}v_{i+2}^2-{}_{n-1}v_{i-2}^2}{2\Delta x} \tag{3.3b}$$

$$\frac{\partial h}{\partial x}=\frac{{}_{n}h_{i+1}-{}_{n}h_{i-1}}{\Delta x} \tag{3.3c}$$

$$S=\frac{z_{i+1}-z_{i-1}}{\Delta x} \tag{3.3d}$$

$$\frac{\partial H}{\partial x}=\frac{{}_{n}H_{i+1}-{}_{n}H_{i-1}}{\Delta x}=\frac{\partial h}{\partial x}+S=\frac{\left({}_{n}h_{i+1}+z_{i+1}\right)-\left({}_{n}h_{i-1}+z_{i-1}\right)}{\Delta x} \tag{3.3e}$$

$$h=\frac{{}_{n}h_{i+1}+{}_{n}h_{i-1}}{2} \tag{3.3f}$$

$$v=\frac{{}_{n+1}v_i+{}_{n-1}v_i}{2} \tag{3.3g}$$

$$|v|=\left|{}_{n-1}v_i\right| \tag{3.3h}$$

Where z = river bed elevation

$$\frac{1}{g}\frac{{}_{n+1}v_i-{}_{n-1}v_i}{\Delta t}+\frac{1}{2g}\frac{{}_{n-1}v_{i+2}^2-{}_{n-1}v_{i-2}^2}{2\Delta x}+\frac{{}_nH_{i+1}-{}_nH_{i-1}}{\Delta x}+\frac{n^2\left|{}_{n-1}v_i\right|}{h^{4/3}}\frac{{}_{n+1}v_i+{}_{n-1}v_i}{2} \tag{3.4}$$

$$\frac{1}{g}\frac{{}_{n+1}v_i-{}_{n-1}v_i}{\Delta t}+\frac{1}{2g}\frac{{}_{n-1}v_{i+2}^2-{}_{n-1}v_{i-2}^2}{2\Delta x}+\frac{{}_nH_{i+1}-{}_nH_{i-1}}{\Delta x}+\frac{n^2\left|{}_{n-1}v_i\right|}{h^{4/3}}\frac{{}_{n+1}v_i+{}_{n-1}v_i}{2}=0$$

$$\Leftrightarrow {}_{n+1}v_i-{}_{n-1}v_i+\frac{\Delta t}{4\Delta x}\left({}_{n-1}v_{i+2}^2-{}_{n-1}v_{i-2}^2\right)+g\frac{\Delta t}{\Delta x}\left({}_nH_{i+1}-{}_nH_{i-1}\right)+\frac{g\Delta tn^2\left|{}_nv_i\right|}{2h^{4/3}}{}_{n+1}v_i$$

$$+\frac{g\Delta tn^2\left|{}_nv_i\right|}{2h^{4/3}}{}_{n-1}v_i$$

where $fr=\dfrac{gn^2\left|{}_{n-1}v_i\right|}{2h^{4/3}}\Delta t$

$$\Leftrightarrow \frac{\Delta t}{4\Delta x}\left({}_{n-1}v_{i+2}^2-{}_{n-1}v_{i-2}^2\right)+g\frac{\Delta t}{\Delta x}\left({}_nH_{i+1}-{}_nH_{i-1}\right)+\left(1+fr\right){}_{n+1}v_i-\left(1-fr\right){}_{n-1}v_i=0$$

$$\Leftrightarrow \left(1+fr\right){}_{n+1}v_i={}_{n-1}v_i\left(1-fr\right)-\frac{\Delta t}{4\Delta x}\left({}_{n-1}v_{i+2}^2-{}_{n-1}v_{i-2}^2\right)-g\frac{\Delta t}{\Delta x}\left({}_nH_{i+1}-{}_nH_{i-1}\right)$$

$$\therefore {}_{n+1}v_i=\left\{{}_{n+1}v_i\left(1-fr\right)-\frac{\Delta t}{4\Delta x}\left({}_{n-1}v_{i+2}^2-{}_{n-1}v_{i-2}^2\right)-g\frac{\Delta t}{\Delta x}\left({}_nH_{i+1}-{}_nH_{i-1}\right)\Big/\left(1+fr\right)\right\} \tag{3.5}$$

Similar to the momentum equation and perform central finite difference as time t=n and space x=i with continuity equation. River channel is rectangular cross section of width, thus cross section area $A= Bh$, as the discharge $Q= vBh$. The continuity equation shown in equation 3.2 and solve by finite different equation shown in 3.8

$$\frac{\partial Bh}{\partial t}+\frac{\partial vBh}{\partial x}-q=0 \tag{3.6}$$

$$B\frac{{}_{n+1}h_i-{}_{n-1}h_i}{\Delta t}+\frac{B}{\Delta x}\left(\frac{{}_{n-1}h_i+{}_{n-1}h_i}{2}{}_nv_{i+1}-\frac{{}_{n-1}h_{i-2}+{}_{n-1}h_i}{2}{}_nv_{i-1}\right)-q=0 \tag{3.7}$$

$$\Leftrightarrow {}_{n+1}h_i-{}_{n-1}h_i+\frac{\Delta t}{\Delta x}\left(\frac{{}_{n-1}h_i+{}_{n-1}h_i}{2}{}_nv_{i+1}-\frac{{}_{n-1}h_{i-2}+{}_{n-1}h_i}{2}{}_nv_{i-1}\right)-\frac{\Delta t}{B}q=0$$

$$\therefore {}_{n+1}h_i={}_{n-1}h_i-\frac{\Delta t}{\Delta x}\left(\frac{{}_{n-1}h_i+{}_{n-1}h_i}{2}{}_nv_{i+1}-\frac{{}_{n-1}h_{i-2}+{}_{n-1}h_i}{2}{}_nv_{i-1}\right)+\frac{\Delta t}{B}q \tag{3.8}$$

Flood calculation in river channel are performed by one-dimensional flow but the Mekong river joins the Tonle sap river in Phnom Penh and diverted to Bassac river in same place at Phnom Penh. In the point of confluence and diversion from tributaries using equation 3.1 by neglect term of velocity head $\frac{1}{g}\frac{\partial}{\partial x}\left(\frac{v^2}{2}\right)$. Equation 3.9 shown concept of the partial confluence calculation by difference between water depth of the Mekong river meeting at point b ($_n h_b$) and water depth of the Tonle Sap river meeting at point a ($_n h_a$) at time t=n. When t=n+1 at point ab velocity $_{n+1}v_{ab}$ have been calculated and solved by finite difference method as shown in equation 3.11

$$\frac{1}{g}\left(\frac{\partial v}{\partial t}\right)+\frac{\partial H}{\partial x}+\frac{n^2|v|v}{h^{4/3}}=0 \tag{3.9}$$

$$\frac{\partial v}{\partial t}=\frac{{}_{n+1}v_{ab}-{}_{n-1}v_{ab}}{\Delta t} \tag{3.10a}$$

$$\frac{\partial H}{\partial x}=\frac{{}_n H_a-{}_n H_b}{\Delta x}=\frac{\partial h}{\partial x}+S=\frac{{}_n h_a-{}_n h_b}{\Delta x} \tag{3.10b}$$

$$h=\frac{{}_n h_a+{}_n h_b}{2} \tag{3.10c}$$

$$v=\frac{{}_{n+1}v_{ab}+{}_{n-1}v_{ab}}{2} \tag{3.10d}$$

$$|v|=\left|{}_{n-1}v_{ab}\right| \tag{3.10e}$$

where $fr=\dfrac{gn^2\left|{}_{n-1}v_{ab}\right|}{2\left(\frac{{}_n h_a+{}_n h_b}{2}\right)^{4/3}}\Delta t$

$$ {}_{n+1}v_{ab}=\left\{ {}_{n-1}v_{ab}(1-fr)-g\frac{\Delta t}{\Delta x}\left({}_n h_b-{}_n h_a\right)\Big/(1+fr)\right\} \tag{3.11}$$

${}_{n+1}v_{ab}$ can be obtained from equation 3.11. Lateral flow q_{ab} can be obtained by equation 3.12

$$q_{ab}=\frac{B_2\left(h_a+h_b\right)}{B_1}{}_{n+1}v_{ab} \tag{3.12}$$

Where B_1 present about river width in the Mekong river (1200m), B_2 present river width in the Bassac river and Tonle sap river.

3.1.2 Inundated flow

The following two-dimensional non-uniform flows are used for water distribution in inundation area as shown in the following equation. This inundation flow consists of continuity equation and momentum equation in two directions, which are applied to the flood plain

Momentum equation

X-direction

$$\frac{\partial M}{\partial t}+\frac{\partial(uM)}{\partial X}+\frac{\partial(vM)}{\partial Y}=-gh\frac{\partial H}{\partial X}-\frac{\tau_{xb}}{\rho} \tag{3.13}$$

Y-direction

$$\frac{\partial N}{\partial t}+\frac{\partial(uN)}{\partial X}+\frac{\partial(vN)}{\partial Y}=-gh\frac{\partial H}{\partial Y}-\frac{\tau_{yb}}{\rho} \tag{3.14}$$

Continuity equation

$$\frac{\partial h}{\partial t}+\frac{\partial M}{\partial X}+\frac{\partial N}{\partial Y}=f_{in} \tag{3.15}$$

Where *h*: water depth, *M(=uh)* : discharge flux in x-direction (m^2/s), *N(=vh)*: discharge flux in y-direction(m^2/s), u: flow rate in x-direction (m/s), v: flow rate in y-direction(m/s), τ_{xb}: shear force in x-direction (N/m^2), τ_{yb}: shear force in y-direction(N/m^2), ρ: density(kg/m^3), H: water level from the reference plane in the flood plain. f_{in}: rainfall, evaporation and infiltration (m/s).In term of $\frac{\partial(ux)}{\partial X},\frac{\partial(ux)}{\partial Y}$ in two-dimensional flow that very small effect to flood calculation. We neglect them to avoid complex calculation. Momentum equation in x-direction and y-direction as shown in equation 3.16 and equation 3.17 respectively.

X-direction

$$\frac{\partial M}{\partial t}=-gh\frac{\partial H}{\partial X}-\frac{\tau_{xb}}{\rho} \tag{3.16}$$

Y-direction

$$\frac{\partial N}{\partial t}=-gh\frac{\partial H}{\partial Y}-\frac{\tau_{yb}}{\rho} \tag{3.17}$$

From equation 3.16 and equation 3.17, we used central finite difference to solved this equation to find velocity in x-direction and y-direction at time t=n, space Y=i, X=j.

$$\frac{\partial M}{\partial t} = \frac{{}_{n+1}M_{i,j} - {}_{n-1}M_{i,j}}{\Delta t} \tag{3.18a}$$

$$\frac{\partial M}{\partial X} = \frac{{}_{n}M_{i,j+1} - {}_{n}M_{i,j-1}}{\Delta X} = 0 \tag{3.18b}$$

$$\frac{\partial N}{\partial t} = \frac{{}_{n+1}N_{i,j} - {}_{n-1}N_{i,j}}{\Delta t} \tag{3.18c}$$

$$\frac{\partial N}{\partial Y} = \frac{{}_{n}N_{i+1,j} - {}_{n}N_{i-1,j}}{\Delta Y} = 0 \tag{3.18d}$$

$$\frac{\partial H}{\partial X} = \frac{{}_{n}H_{i,j+1} - {}_{n}H_{i,j-1}}{\Delta X} \tag{3.18e}$$

$$\frac{\partial H}{\partial Y} = \frac{{}_{n}H_{i+1,j} - {}_{n}H_{i-1,j}}{\Delta Y} \tag{3.18f}$$

$$M = \frac{{}_{n+1}M_{i,j} + {}_{n-1}M_{i,j}}{2} \tag{3.18g}$$

$$N = \frac{{}_{n+1}N_{i,j} + {}_{n-1}N_{i,j}}{2} \tag{3.18h}$$

where $\tau_{xb} = \dfrac{\rho g n^2 u\sqrt{u^2+v^2}}{h^{1/3}}$ substituting in equation 3.16

$$\frac{\partial M}{\partial t} = -gh\frac{\partial H}{\partial X} - \frac{gn^2 M\sqrt{M^2+N^2}}{h^{7/3}} \tag{3.19}$$

We substitute all of equation 3.18 to equation 3.19 to calculation discharge in x-direction and y-direction at time t=n, space Y=i, X=j

$$\frac{{}_{n+1}M_{i,j} - {}_{n-1}M_{i,j}}{\Delta t} = -gh\frac{{}_{n}H_{i,j+1} - {}_{n}H_{i,j-1}}{\Delta X} - \frac{gn^2}{h^{7/3}}\left(\frac{{}_{n+1}M_{i,j} + {}_{n-1}M_{i,j}}{2}\right)\sqrt{{}_{n-1}M_{i,j}^2 + \overline{N}^2} \tag{3.20}$$

where $\overline{N} = \dfrac{{}_{n-1}N_{i-1,j-1} + {}_{n-1}N_{i-1,j-1} + {}_{n-1}N_{i+1,j-1} + {}_{n-1}N_{i+1,j+1}}{4}$

$$F_M = \frac{gn^2\Delta t}{2h^{7/3}}\sqrt{{}_{n-1}M_{i,j}^2} + \overline{N}^2$$

$${}_{n+1}M_{i,j} = \frac{\left(1 - F_M\right)_{n-1}M_{i,j} - gh\dfrac{\Delta t}{\Delta X}\left({}_{n}H_{i,j+1} - {}_{n}H_{i,j-1}\right)}{1 + F_M} \tag{3.21}$$

Y-direction

Where $\tau_{yb} = \dfrac{\rho g n^2 v\sqrt{u^2+v^2}}{h^{1/3}}$ substituting in equation 3.19

$$\frac{{}_{n+1}N_{i,j} - {}_{n-1}N_{i,j}}{\Delta t} = -gh\frac{{}_{n}H_{i+1,j} - {}_{n}H_{i-1,j}}{\Delta Y} - \frac{gn^2}{h^{7/3}}\left(\frac{{}_{n+1}N_{i.j} + {}_{n-1}N_{i,j}}{2}\right)\sqrt{\overline{M}^2 + {}_{n-1}N_{i,j}^2} \tag{3.22}$$

where $\overline{M}^2 = \dfrac{{}_{n-1}M_{i-1,j-1} + {}_{n-1}M_{i-1,j+1} + {}_{n-1}M_{i+1,j-1} + {}_{n-1}M_{i+1,j+1}}{4}$

$$F_N = \frac{gn^2\Delta t}{2h^{7/3}}\sqrt{\overline{M}^2 + {}_{n-1}N_{i,j}^2}$$

$${}_{n+1}N_{i,j} = \frac{(1-F_N)_{n-1}N_{i,j} - gh\dfrac{\Delta t}{\Delta Y}\left({}_{n}H_{i,j+1} - {}_{n}H_{i,j-1}\right)}{1+F_N} \tag{3.23}$$

From continuity equation in equation 3.15 We can solve this equation by finite difference by substitute equation 3.20 and find water level in inundation flow calculation at time=n , space Y=i, X=j

$$\frac{{}_{n+1}h_{i,j} - {}_{n-1}h_{i,j}}{\Delta t} + \frac{{}_{n}M_{i,j} + {}_{1-n}M_{i,j-1}}{\Delta X} + \frac{{}_{n}N_{i+1,j} - {}_{n}N_{i-1,j}}{\Delta Y} = f_{in}$$

$$\therefore {}_{n+1}hi = {}_{n-1}h_i - \frac{\Delta t}{\Delta x}\left({}_{n}M_{i,j+1} - {}_{n}M_{i,j-1}\right) - \frac{\Delta t}{\Delta x}\left({}_{n}N_{i+1,j} - {}_{n}N_{i-1,j}\right) + f_{in} \tag{3.24}$$

3.1.3 Overflow

Overflow equation which combines river flow and the floodplain flow. It generates complete over flow and submerge overflow under supercritical and subcritical flow, respectively. When flood water flows to dry lands through the colmatage cut, a complete overflow occurs there and when flood water flows to wet area through the colmatage cut, a sub-merged overflow occurs (Figure 3.3). The complete overflow (Q_c) is given by:

$$Q = 0.35Bh_1\sqrt{2gh_1} \tag{3.25}$$

Whereas the submerged overflow Q_s is given by:

$$Q = 0.91Bh_2\sqrt{2g(h_1 - h_2)} \tag{3.26}$$

Where Q: overflow discharge (m^3/s), B: width of overflow (=10m), h_1,h_2: water level in the overflow from the surface.

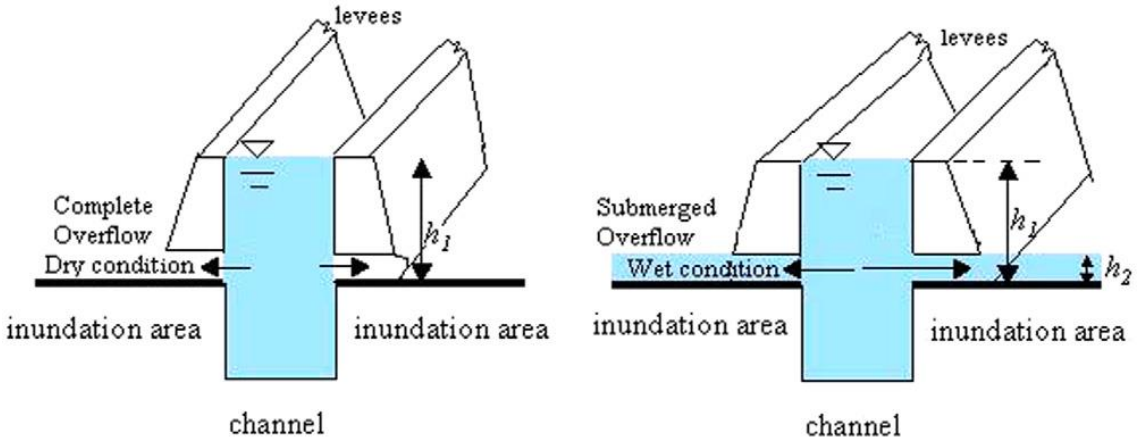

Figure 3.3 Schematic diagrams of complete overflow and submerged flow

3.1.4 Groundwater and Evaporation

Groundwater balance is calculated from the following conservation equation and Darcy's law. We neglect water movement of unsaturated zones and assumed a uniform soil structure and uniform aquifer properties over the selected flood plain area. Groundwater level was estimated assuming a saturated soil layer because groundwater movement is inactive compared to surface water.

We have calculated every 1 hour time interval to find increase or decrease in the groundwater calculation, evaporation and rainfall in this present study. If floodwater depth is zero, Groundwater level impact from evaporation and porosity. On the other hand if floodwater depth is not zero, Groundwater level determine by infiltration rate, evaporation and porosity over this area.

Basic equation on the water balance of the saturated zone as shown in equation 3.27 as considering porosity of the soil, groundwater recharge and evaporation.

$$\theta \frac{\partial h_{GW}}{\partial t} + \frac{\partial (u_{GW} h_{GW})}{\partial X} + \frac{\partial (v_{GW} h_{GW})}{\partial Y} = f \tag{3.27}$$

Where θ: Specific yield (=effective porosity), h_{GW}: groundwater level(m), u_{GW}: velocity in x-direction(m/s), v_{GW}: velocity in y-direction(m/s), f: recharge rate (m/s)

$$u_{GW} = -k \frac{\partial h_{GW}}{\partial X} \tag{3.28a}$$

$$v_{GW} = -k \frac{\partial h_{GW}}{\partial Y} \tag{3.28b}$$

$$\theta \frac{\partial h_{GW}}{\partial t} - k\left(\frac{\partial h_{GW}}{\partial X}\right)^2 - k h_{GW} \frac{\partial^2 h_{GW}}{\partial X^2} - k\left(\frac{\partial h_{GW}}{\partial Y}\right)^2 - k h_{GW} \frac{\partial^2 h_{GW}}{\partial Y^2} = f \tag{3.29}$$

Where k: hydraulic conductivity (m/s) Equation 3.30 obtained by finite difference method from equation 3.29

$$ {}_{n+1}h_{GWi,j} = {}_{n-1}h_{GWi,j} + \frac{k\Delta t}{\theta}\left(\frac{{}_{n-1}h_{GWi,j+1} - {}_{n-1}h_{GWi,j-1}}{2\Delta x} \right) $$

$$ + \frac{k\Delta t}{\theta}{}_{n-1}h_{GWi,j} \frac{{}_{n-1}h_{GWi,j+1} - 2{}_{n-1}h_{GWi,j} + {}_{n-1}h_{GWi,j-1}}{(\Delta X)^2} + \frac{k\Delta t}{\theta}\left(\frac{{}_{n-1}h_{GWi+1} - {}_{n-1}h_{GWi-1,j}}{2\Delta Y} \right) $$

$$ + \frac{k\Delta t}{\theta}{}_{n-1}h_{GWi,j} \frac{{}_{n-1}h_{GWi+1,j} - 2{}_{n-1}h_{GWi,j} + {}_{n-1}h_{GWi-1,j}}{(\Delta Y)^2} + \frac{f\Delta t}{\theta} \quad (3.30) $$

Stability in finite difference scheme

$$ \Delta t < \frac{\Delta x}{|v_{max}| + \sqrt{g h_{max}}} \quad (3.31) $$

Where h_{max}: Highest water level in boundary condition and v_{max}: Maximum velocity of the Mekong River. It was estimated by using average velocity by Manning equation.

$$ v = \frac{1}{n_{river}} h^{2/3} I^{1/2} \quad (3.32) $$

Where n: roughness coefficient along the river, h: water level in the channel, I: channel slope.

3.2 Model set-up (run scenarios)

3.2.1 Precipitation Data

The relationship between precipitation, river flow, inundation flow and groundwater is illustrative of the complexity and changing nature of the water cycle. The duration and intensity of the precipitation, soil porosity, the slope of the ground, infiltration rate and evapotranspiration emerge as some of the potential factors in the interaction. In the model, rainfall data were added to water level all over the area (IH=IH + Rain) then the water level is the factor to determine groundwater level. There are 4 cases to determine groundwater level as follow.

1. Water level is less than 0

$$GW = GW - \frac{eva}{poro} \tag{3.35}$$

2. Water level is less than evaporation rate

$$GW = GW - \frac{(eva - IH)}{poro} \tag{3.36}$$

$$IH = 0 \tag{3.37}$$

3. Water level is less than evaporation rate and penetration rate

$$GW = GW + \frac{(IH - eva)}{poro} \tag{3.38}$$

4. Water level is greater than evaporation rate and penetration rate

$$GW = GW + \frac{fc}{poro} \tag{3.39}$$

$$IH = IH - (eva + fc) \tag{3.40}$$

Where GW = Groundwater Level (m)
eva = Evaporation Rate (m/month)
$poro$ = Porosity
IH =Water Level (m)
fc = Penetration Rate (m/hour)

3.2.1.1 Thiessen - Mean Method for Precipitation Data

In this method, the rainfall recorded at each station is given a weightage on the basis of an area closest to the station 7 hydrological stations (Kompong Tralach (Zone 1), Oudong (Zone 2), Batheay (Zone3), Thnal Tetung (Zone 4),Peam Chikang (Zone 5), Samroong (Zone 6) and Chau Doc (Zone 7)) provided weighted area using Thiessen Polygons (Figure 3.4). Table 3.1 shows the fraction of total area, multiplying the fraction to rainfall data from 7 observed stations provide mean precipitation over a study area.

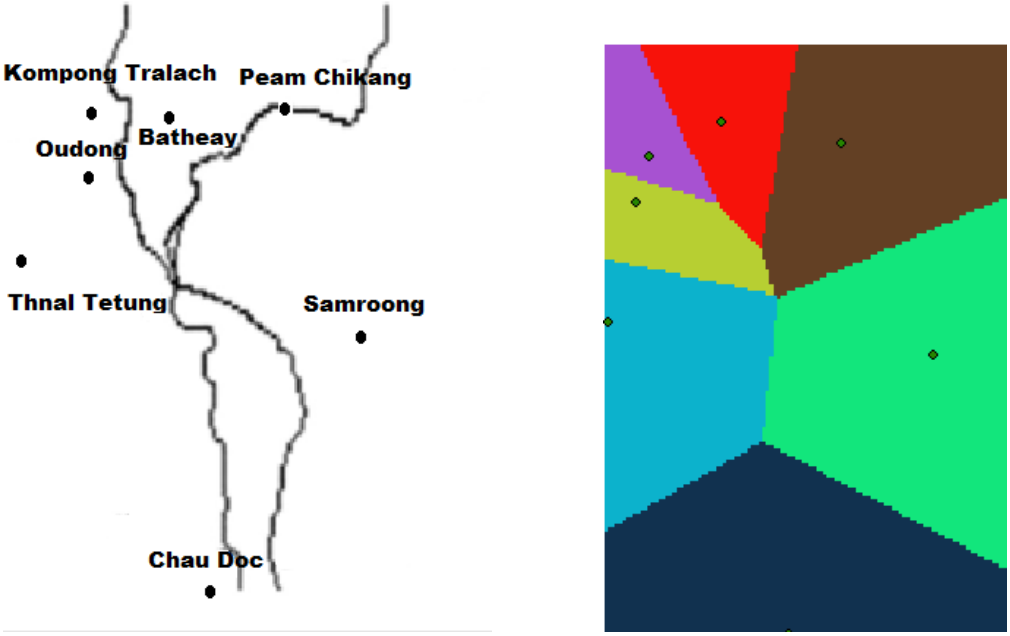

Figure 3.4 Thesisen Polygon Method

Table 3.1 Fraction of total area using Thiessen Polygons for mean Preciptation

Station	Area (km^2)	Fraction of total area
Kompong Tralach	727.2648	0.0413
Oudong	933.2753	0.0530
Batheay	1,345.296	0.0764
Thnal Tetung	2,570.819	0.1461
Peam Chikang	3,467.683	0.1970
Samroong	4,548.519	0.2584
Chau Doc	4,007.143	0.2277
Total	17,600	1

3.2.2 Boundary Condition

Water levels used as the boundary conditions for flood simulation model (Kampong Cham upstream of the Mekong River ; Tan chau downstream of the Mekong river ; Chan Doc station of Bassac River and Prek Kdam station of Tone Sap River) were periodically obtained from the measurement of the Mekong river Commission (MRC, 1993-2001). Water Level data at Phnom Penh, Where Tonle Sap and Bassac tributaries meet the Mekong River, are used for the validation of the developed numerical models (Fig 3.5)

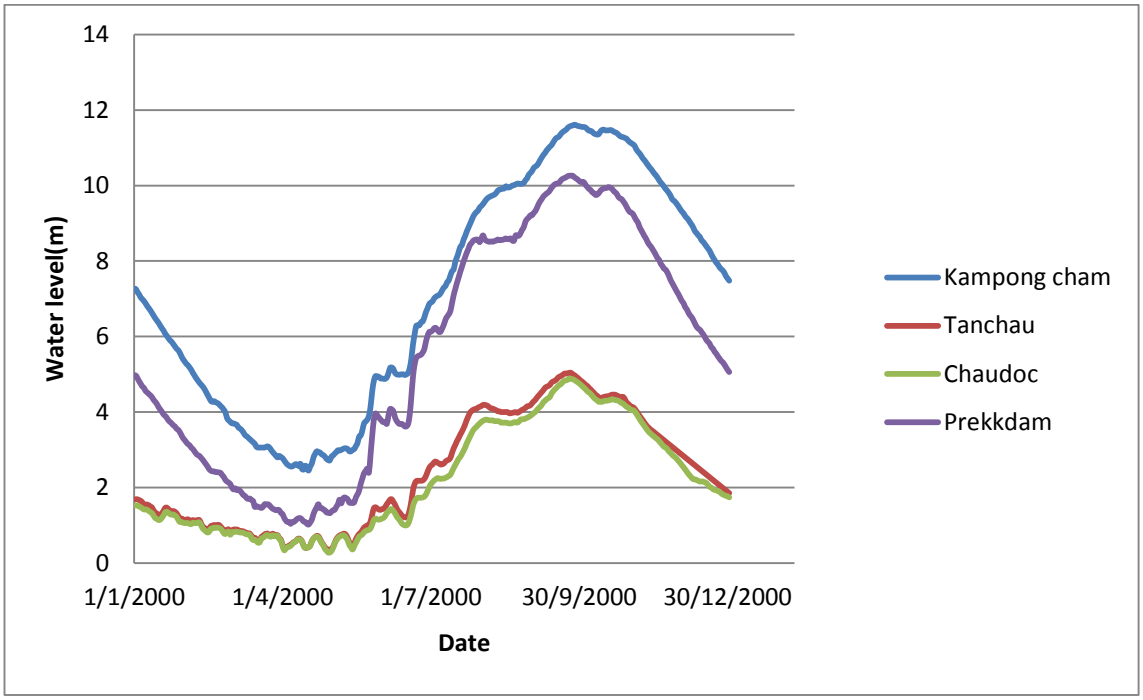

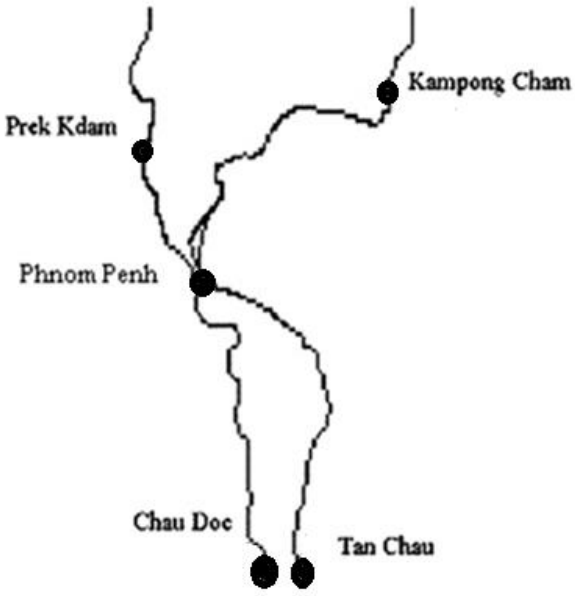

Figure 3.5 Water levels for the boundary conditions

3.2.3 Digital elevation map (DEM)

In this area, we used digital elevation map (DEM) by download from the first release of Shuttle Radar Topography Mission (SRTM). The SRTM digital elevation data, produced by NASA originally, is a major breakthrough in digital mapping of the world, and provides a major advance in the accessibility of high quality elevation data for large portions of the tropics and other areas of the developing world. The NASA Shuttle Radar Topographic Mission (SRTM) has provided digital elevation data (DEMs) for over 80% of the globe. This data is currently distributed free of charge by USGS and is available for download from the National Map Seamless Data Distribution System, or the USGS ftp site. The SRTM data is available as 3 arc second (approx. 90m resolution). In this study we resample about 90m to 250m, 500m and 1000m to simulation in hydrological model.

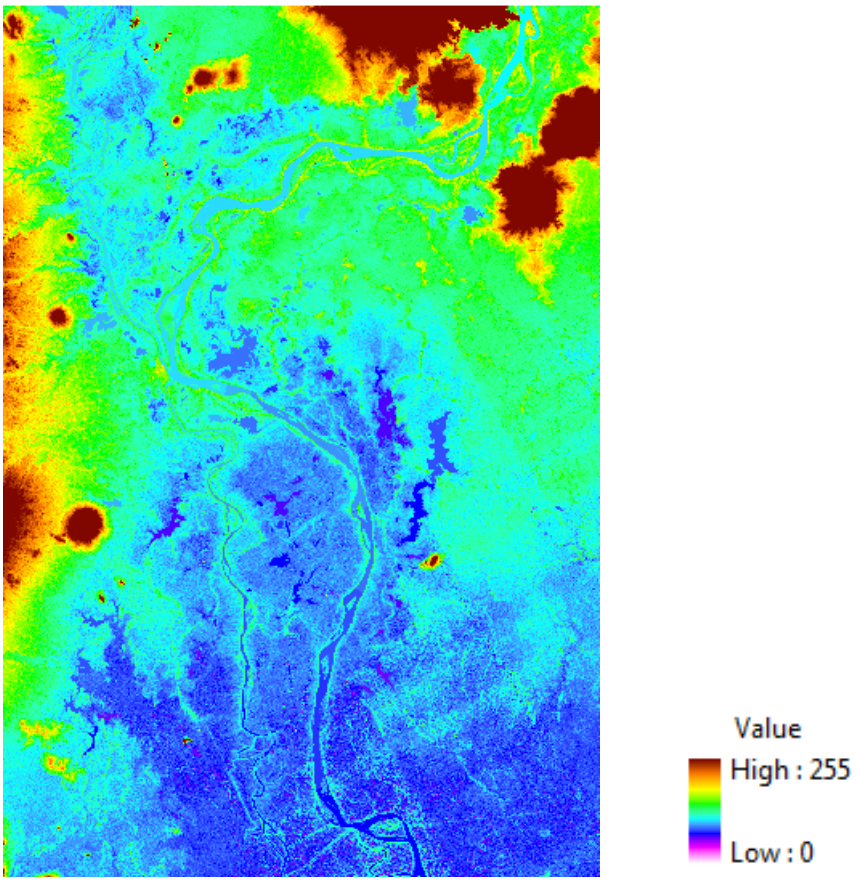

Figure 3.6 Digital elevation maps in study area (90m resolution)

3.2.3.1 Resample analysis

Resampling is the process of interpolating the pixel values while transforming your raster dataset. This is used when the input and output do not line up exactly, when the pixel size changes, when the data is shifted, or a combination of these reasons. In this study Original digital elevation maps is 90m from resolution and then we used ArcGis program to resample about 90m resolution to 250m, 500m and 1000m to use in this model. There are three options for the resampling technique; nearest, bilinear

interpolation and cubic convolution. In this study we used cubic convolution to find elevation of 250m, 500m and 1000m from resolution.

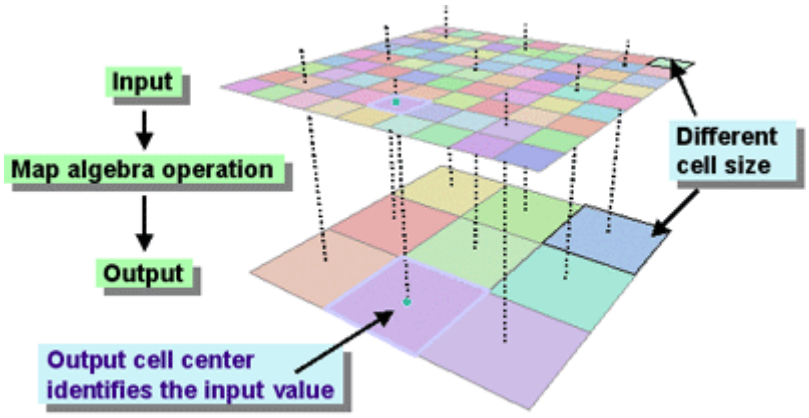

Figure 3.7 Process of resample technique in ArcGis
Source: ArcGIS help

3.2.3.2 Fill sinks analysis

Fills sinks in a surface raster to remove small imperfections in the data. It used to sink a cell that undefined drainage direction. When we resample about elevation some of cell have pour point in the boundary cell with the lowest elevation. If the sink were filled with water, this is the point where water would pour out.

3.2.4 Evaporation, Infiltration, Hydraulic conductivity

A sensitivity analysis has been performed to understand the sensitivity of hydraulic conductivity, potential infiltration rate, and Manning coefficient by comparing the charge in groundwater when changing the each parameter. Since silt is the main soil type of this area and the hydraulic conductivity is around 0.1 m/s, hydraulic conductivity has been used as 0.1 m/s for the groundwater model. (Kazama, et al. 2007)

Groundwater recharge rate were divided into non-inundation and inundation, it is estimated by the potential infiltration rate as 10 mm/h and 0.1 m/s respectively. Evapotranspiration flux is assumed as 150 mm/month for the whole season (Nawarathna and Kazama, 1999). The specific yield has been estimated as 0.4 based on lab experimental results (Kazama, et al., 2007).

3.2.5 Position of river node

In this model we need to set up about position of river by create .txt file. It selects the position of river by digital elevation map in this area. When elevation is very low, it means that that is position of river or low land. We can check about position of river by

compare between the position of river and digital elevation map. Other thing when we change about resolution in this model. Position of river must change at the same time.

3.3 Model Validation

Simulation models are increasingly being used to solve problems and to aid in decision-making. The developers and users of these models, the decision makers using information obtained from the results of these models, and the individuals affected by decisions based on such models are all rightly concerned with whether a model and its results are correct. In this model three sets of data are required to show accuracy of simulated surface flow and groundwater levels.

3.3.1 Water Level data

Water level data observed from hydrological station in Phnom Penh is used to compare with calculated result. Just above Phnom Penh is the confluence with the Tonle Sap, the main Cambodian tributary. Below Phnom Penh, it divides into Bassac and the Mekong River. Since, Phnom Penh is the capital and largest city of Cambodia developed to a nation's center of economic and industrial activities, as well as the center of security, politics, cultural heritage, and diplomacy of Cambodia.

Figure 3.8 Water level observation points at Phnom Penh

3.3.2 Groundwater Level data

While the variation of groundwater levels is lower than the propagation of inundation depth and inundation areas, the long-term change of groundwater levels in the area was taken into account to verify the simulation of the variation of groundwater levels. Simulated groundwater levels were compared with those observed at three observation well stations close to the Mekong River, located between Tan Chau and Phnom Penh. These three observation wells are marked as P24 is located at 40 km from the Mekong River bank (Figure 3.9).

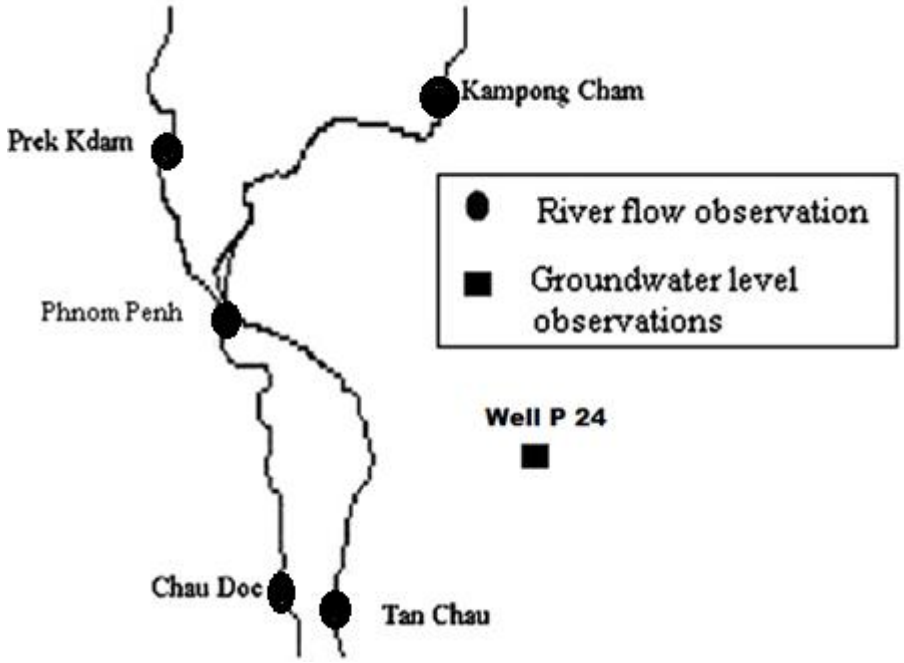

Figure 3.9 Ground water level observation points

3.3.3 Satellite map

Hatfield Consultants Company limited from Canada make final report to Mekong river commission to analysis flood area and flood volume by RADARSAT images (2003). The report relied on a series of radar imagery collected by the Canadian RADARSAT-1 satelite image the Lowe Mekong River basin in Cambodia during years 1999 to 2002. RADARSAT-1 synthetic-aperture radar (SAR) was the primary source of image data used and represent a unique techology that has been applied in Cambodia and other countries of the LMB since 1998. Techquies for derinving reliable flooding estimated are sufficiently development to contribute greatly to visualization and quantification of flood events. This report estimation flood inundation area and presentation of results and maps in the Lower Mekong Basin. In this study we used flood map from this report to calibration about hydrological model in year 2000.

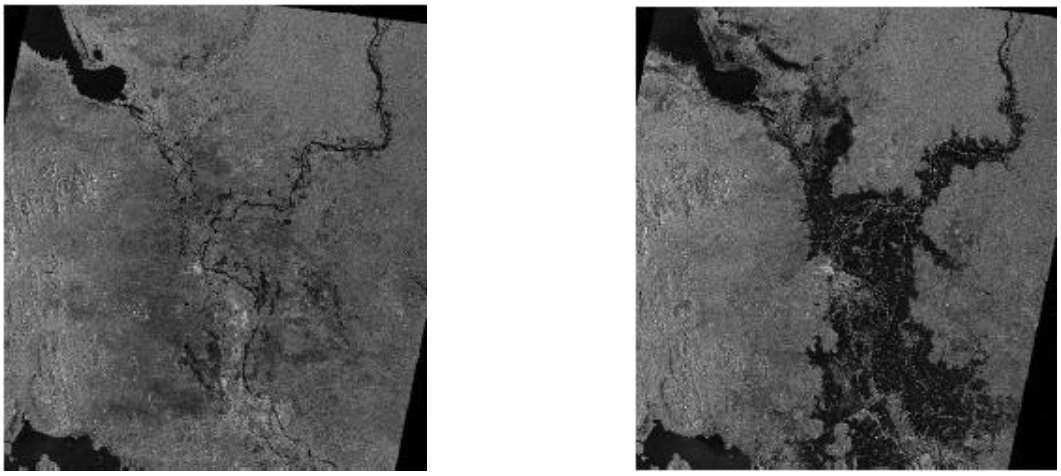

Figure 3.10 Progression of flooding in the Lower Mekong Basin shown by RADARSAT-1
Source: Mekong river commission secretariat (2003)

3.4 Analyzing Groundwater and Inundation Area

In this study, all of the results were analyzed into monthly data in order to show monthly fluctuation of groundwater and inundation area, to make suitable comparison of 2 difference grid size from inundation and groundwater level in year 2000.

3.4.1 Groundwater storage calculation

The temporal and spatial distribution of groundwater levels in year 2000. This result was used to estimate the groundwater storage in each month. Maximum groundwater storage in the area was calculated by the integration of the difference between highest and lowest groundwater levels in the area as follows:

$$\text{Groundwater storage} = \int \left(GWL_h - GWL_l\right) dA x n_g \qquad (3.4)$$

Where GWL_h is the highest groundwater level and GWL_l is the lowest groundwater level.

3.4.2 Graphical and Motional Distribution

In order to analyze complexity data sets from a mathematical model and functional code (C Language Programming) were used to display graphical and motional distribution. The processes to manage those data are shown in Figure 3.10. Sources from the main code provided water level indicating inundation depth and groundwater level (Figure 3.10a). Functional code (Figure 3.10b) was adept to read those data and show colors classifying by their level (Figure 3.10c). The interval of inundation level is between 0 and 10 meter whereas 0 to 10 meter for groundwater level.

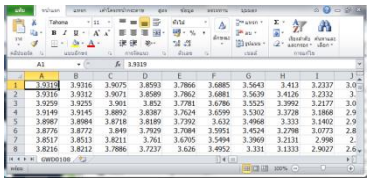

```
#include<stdio.h>
#include<stdlib.h>

void main(void){
    int i,j,t;
    int a;
    double H1[160][109];

    char name2[15]="IHD0001.txt";
    FILE *fin,*fout;

    for(t=1;t<=365;t++){


    name2[3]='0'+t/1000;
    name2[4]='0'+(t/100)%10;
    name2[5]='0'+(t/10)%10;
    name2[6]='0'+t%10;
```

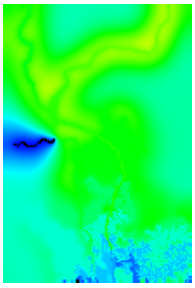

(a) (b) (c)

Figure 3.11 Processes showing how to change numerical data into graphical and motional distribution

3.4.3 Animation

In order to analyze data from graphical image from mathematical model were used to Giam program to create about motional distribution of inundation and groundwater level. Giam was used to create animation or movement of inundation and groundwater level by daily.

CHAPTER 4 RESULTS AND DISCUSSION

4.1 Analysis of Water level at Phnom Penh

Using the numerical solution of each governing equations, calculations were performed for flood, overflow and inundated flows for several flood events in the Lower Mekong river basin. In the year 2000, the Mekong delta was affected with a record-breaking flood. Therefore, we used the year 2000 flood data mainly for comparison with field observations and model verification. Simulation of the year 2000 flood was carried out for the period of July 7 to November 10, 2000. Figure 4.1 shows the comparison of calculated and observed water levels during this period at Phnom Penh, the model estimated water levels are in good agreement with the observed water levels at Phnom Penh in Table 4.1

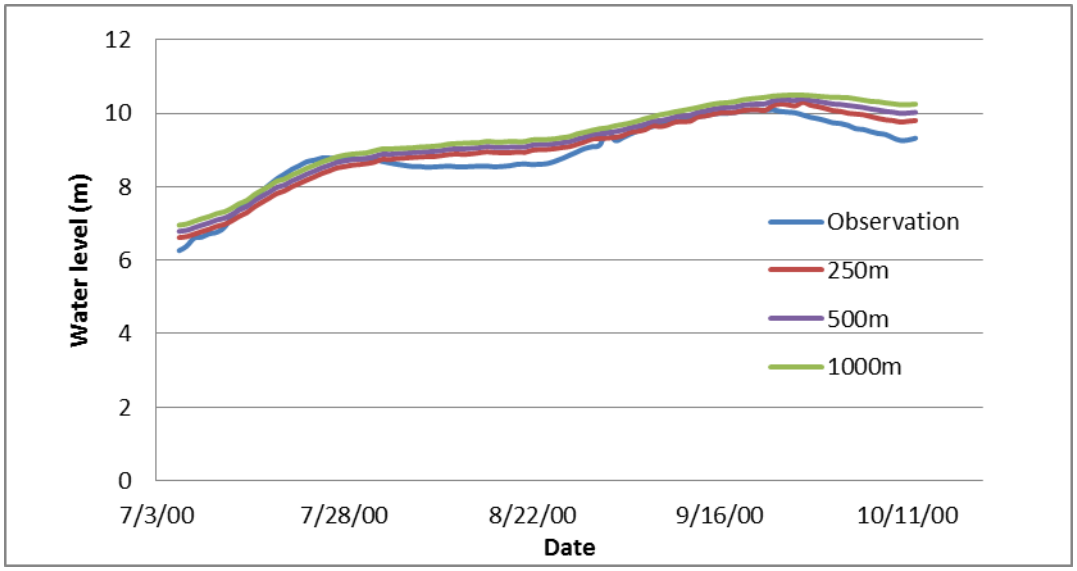

Figure 4.1 Comparison of calculated and observed water level at Phnom Penh

Table 4.1 Calibration of the water level at Phnom Penh with different grid size

DEM resolution	r^2	Nash	IA	RMSE
250m	0.962	0.830	0.791	1.345
500m	0.950	0.795	0.825	1.452
1000m	0.948	0.755	0.812	1.545

Table 4.1 presents the Coefficient of determination (r^2), Nash- Sutcliffe's coefficients (Nash), Index of agreement (IA) and Root mean square error (RMSE) of the simulation water level in comparison with the observed water level at Phnom Penh by different grid size. The highest value of Nash and r^2 were 0.830 and 0.962 with 250 m resolution. From Index of agreement (IA) 500m is the best of value. However three of grid size resolutions show good results from water level at Phnom Penh.

4.2 Comparison between observation and calculation of inundation area

Figure 4.2 and Figure 4.3 shows the comparison of calculated inundation areas and satellite image outputs on September 23, 2000 and October 22 2000. It shows a good agreement between estimated inundation areas and the satellite image of three grid sizes. First of interesting in calibration of calculation inundation from model simulation and satellite map that in upstream in this study area because of the boundary condition in this simulation water move out in the east of Mekong River and different grid size that effect to infiltration rate. Almost inundation that cause in downstream because it is low land area then inundation spread to the upstream, west side of Bassac River and east side of Mekong River and the other thing in the upstream in this study area have Tonle Sap Lake. In the dry season Tonle Sap Lake recharge water from upstream to downstream. On the other hand in the wet period the water in downstream move from the downstream to go to upstream (Tonle Sap Lake).

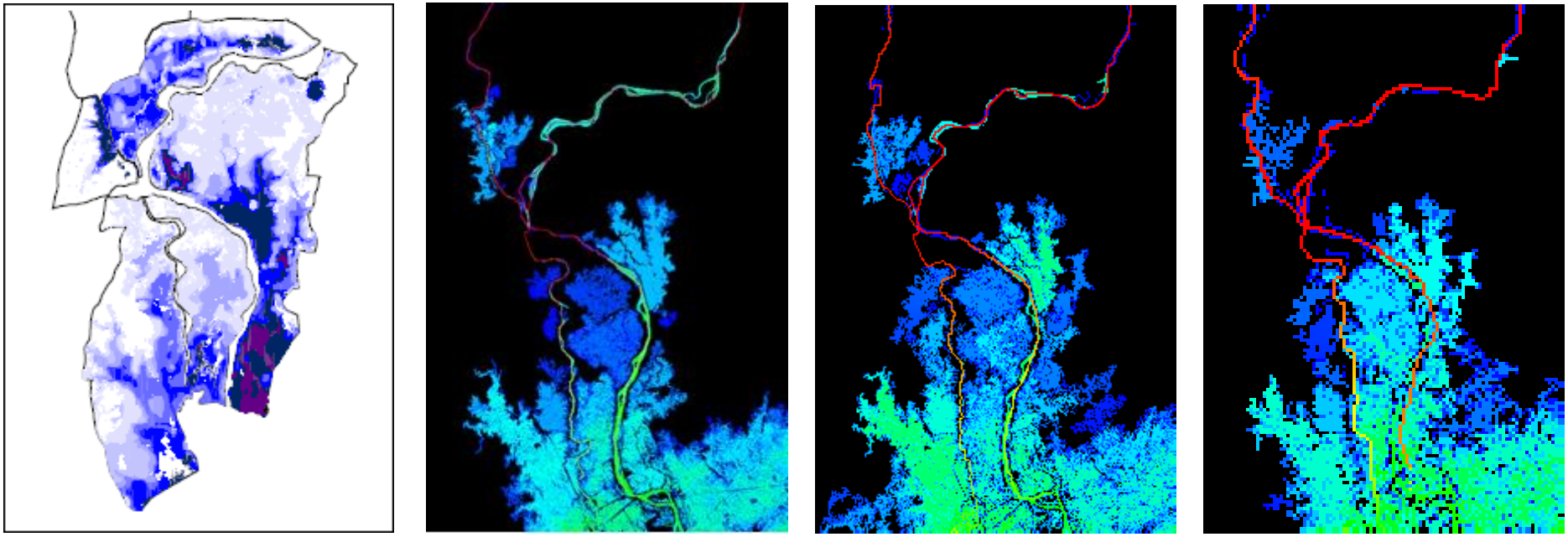

Source: Mekong river commission secretariat (2003)

22 October 2000

Figure 4.2 Comparison of inundation with observation on 22 October 2000

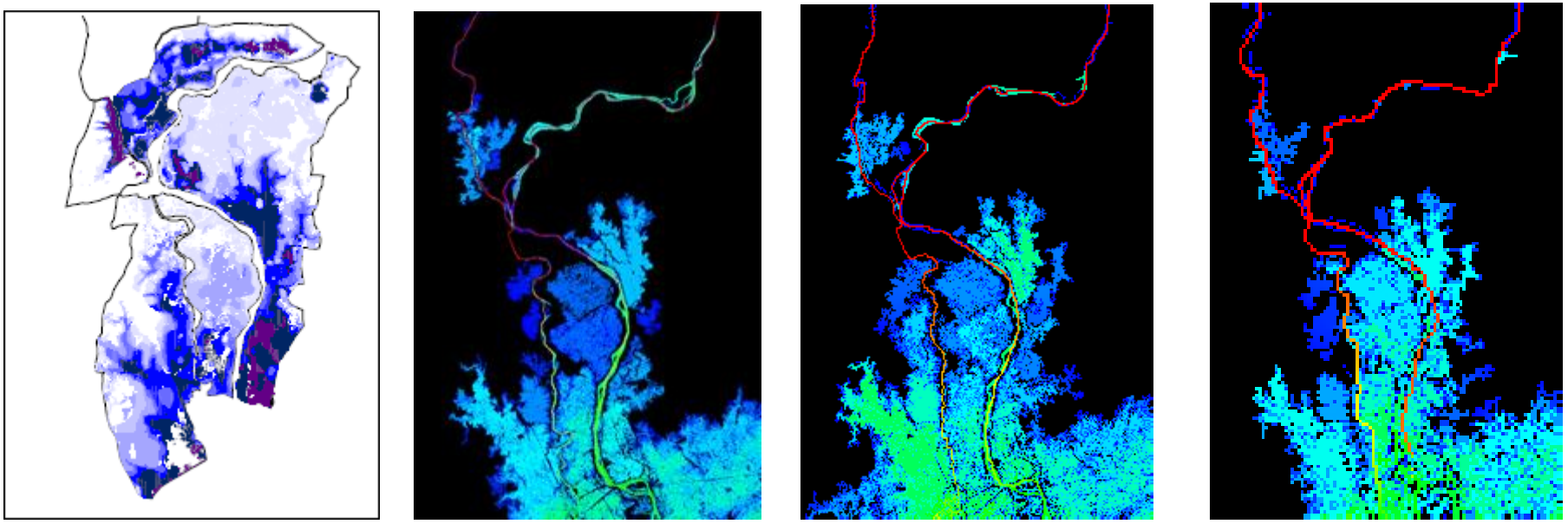

Source: Mekong river commission secretariat (2003)

Figure 4.3 Comparison of inundation with observation on 23 September 2000

4.3 Observation of groundwater levels

Since the variation of groundwater levels is lower than the propagation of inundation depth and inundation areas, the long term change of groundwater levels in the area was taken into account to verify the simulation of the variation of groundwater levels. Simulated groundwater levels were compared with those observed at observation well stations close to the Mekong River, located between Tan Chau and Phnom Penh. Observation wells are marked as Well P 24 is located at 40km from the Mekong River bank (Figure 4.4). Observed groundwater levels in 2000 were compared with simulation groundwater levels over the same period. Comparison of the observed and simulated groundwater levels for the observation point is depicted in Figure 4.5. It shows that good agreement in the three grid sizes.

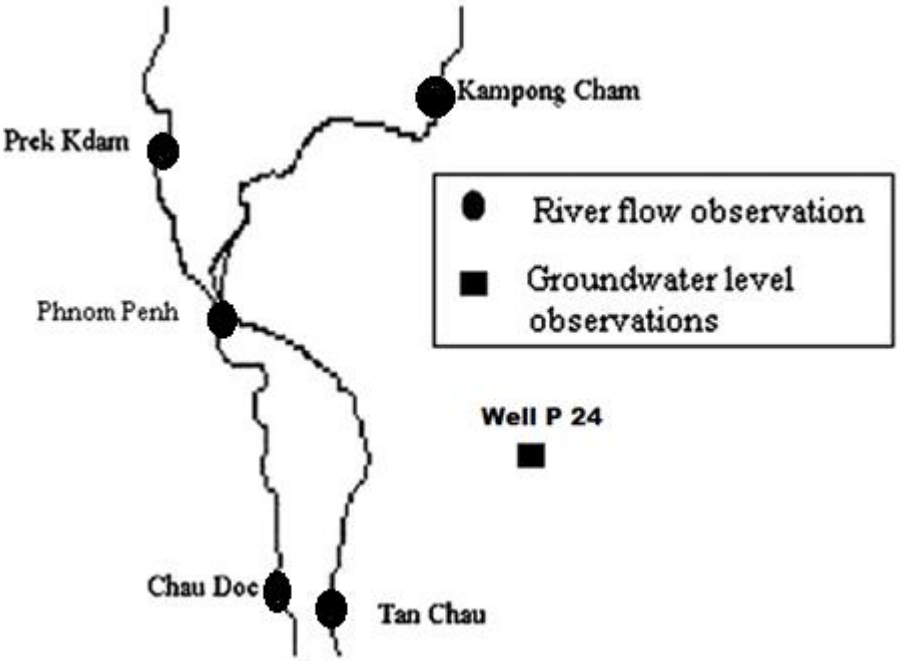

Figure 4.4 Ground water level observation points

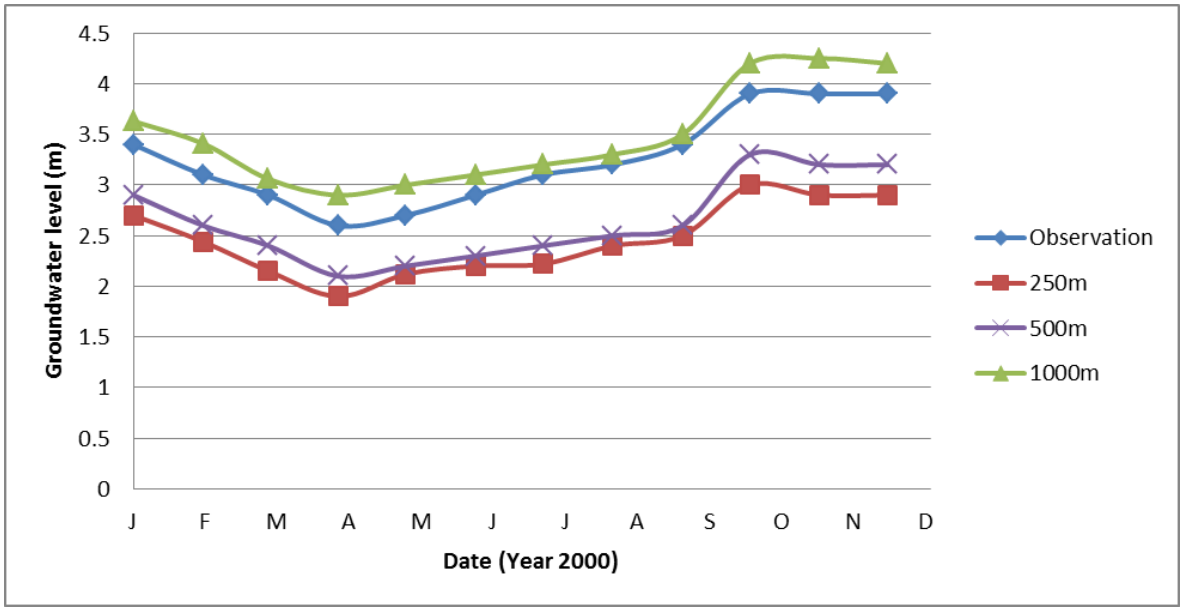

Figure 4.5 Comparison of ground water level between observed and calculated value with different grid size

Figure 4.5 shows the comparison of groundwater level between observed and calculated with different grid size. First of all three grid size show good trend from groundwater level and 1000m from resolution groundwater level is larger than observations and 250m and 500m are less than observation in the groundwater level. It means that 1000m is overestimated in the groundwater level.

4.4 Maximum monthly analysis of inundation area (250m, 500m 1000m)

Due to change of precipitation in the Mekong upstream and along the Mekong delta, the expansion of the inundation also changes with time. To observe the propagation and temporal distribution of inundation area, the simulation results from the distribution of inundation area, the simulation results from the distribution of inundation from July 2000 to December 2000 were considered. The estimated temporal and spatial variation within inundation areas is presented in Figure 4.6 (250m), Figure 4.7 (500m) and Fig 4.8 (1000m). In the beginning, inundation areas is generated in the low land at downstream, located in the lower part of Mekong basin. Then, inundation areas spread to the east side of the Mekong and the west side of the Bassac River and the upper part of the Mekong basin. Normally, the largest flooding period in the Mekong region is from September to October and flood water retreats to downstream areas after November. The simulation also accurately reproduced this process and completely agrees with the regular flooding pattern in these areas. Therefore, we can conclude that this simulation can express the inundation mechanism in the Mekong river basin.

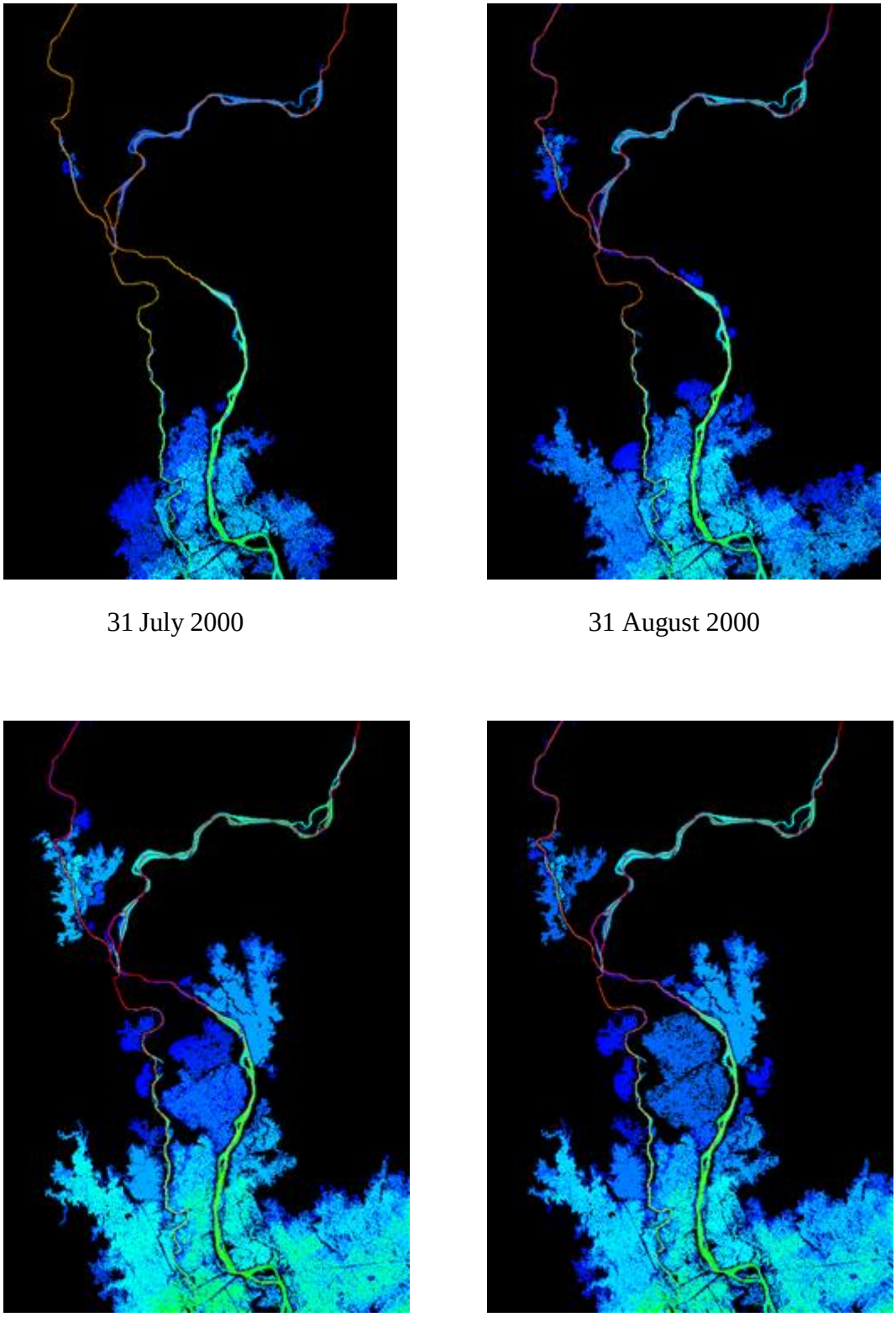

Figure 4.6 Temporal and spatial distribution of inundation area (250 m)

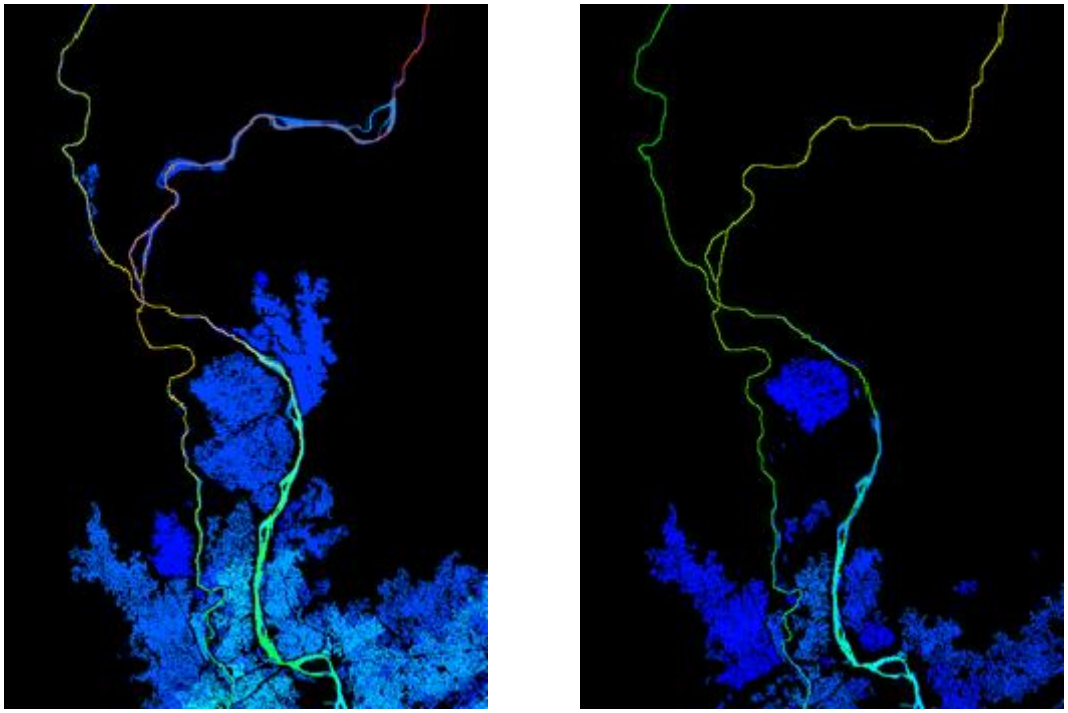

30 November 2000 31 December 2000

Figure 4.6 Temporal and spatial distribution of inundation area (250 m) (Cont.)

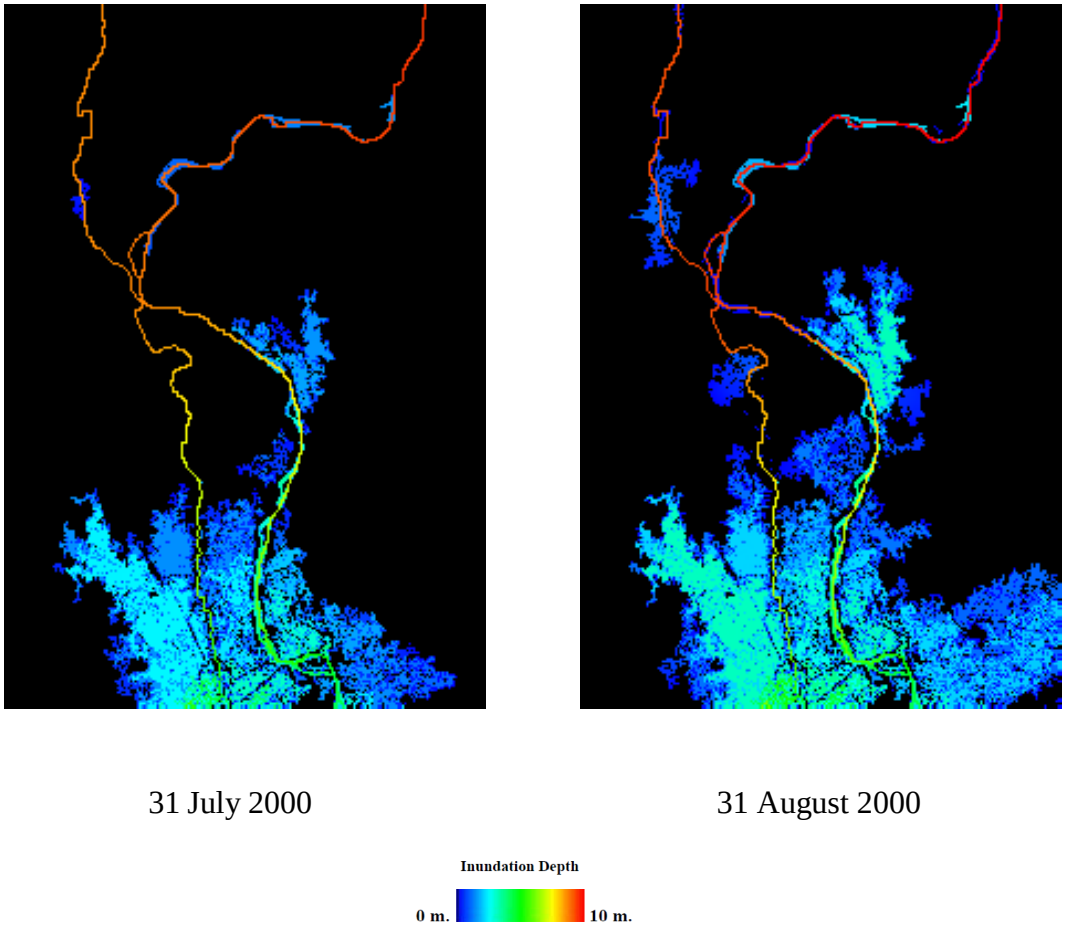

31 July 2000 31 August 2000

Figure 4.7 Temporal and spatial distribution of inundation area (500 m)

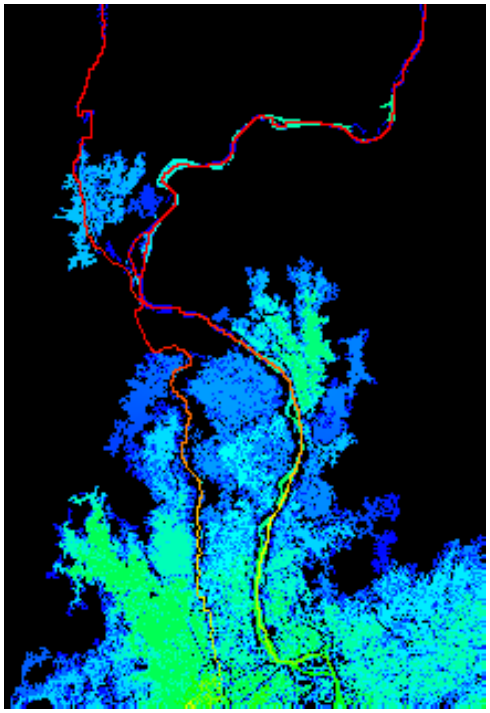

30 September 2000

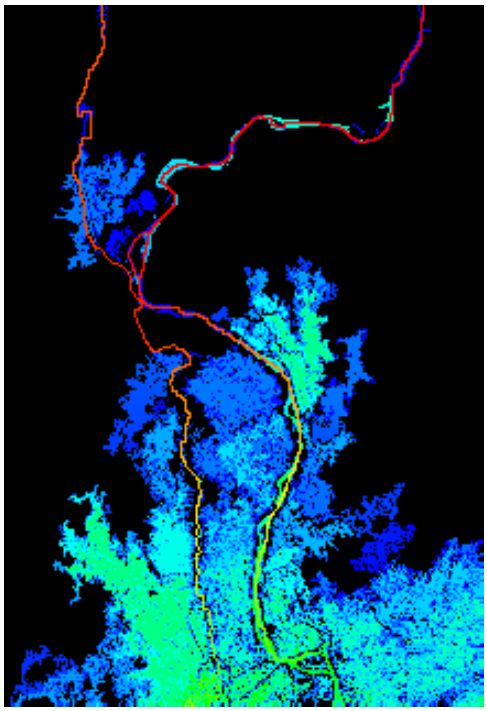

31 October 2000

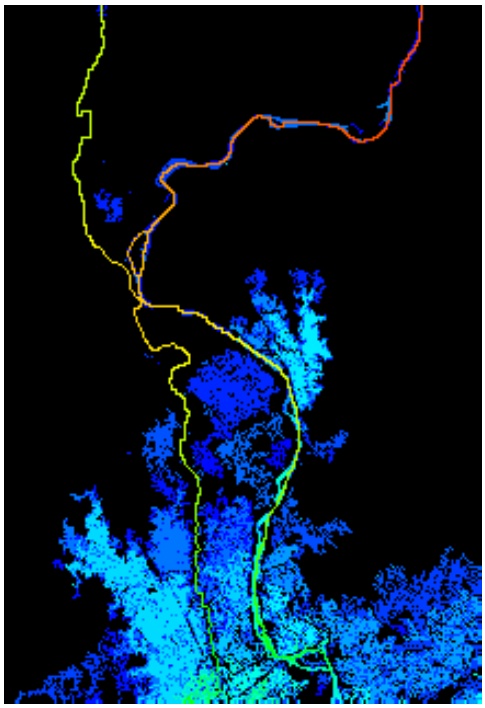

30 November 2000

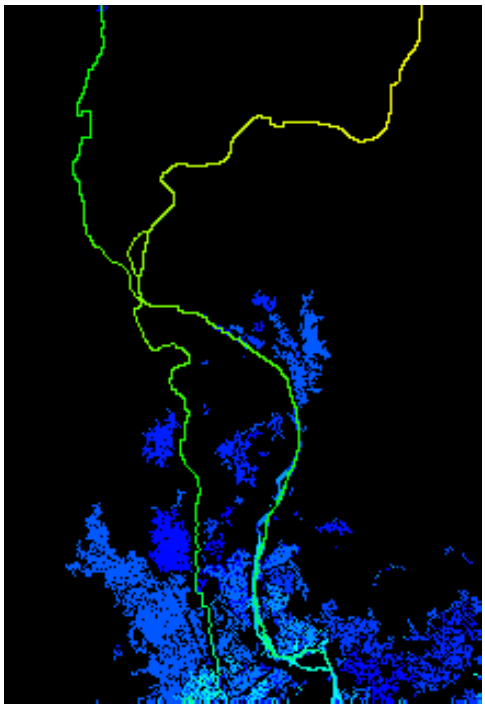

31 December 2000

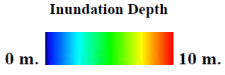

Figure 4.7 Temporal and spatial distribution of inundation area (500 m) (Cont.)

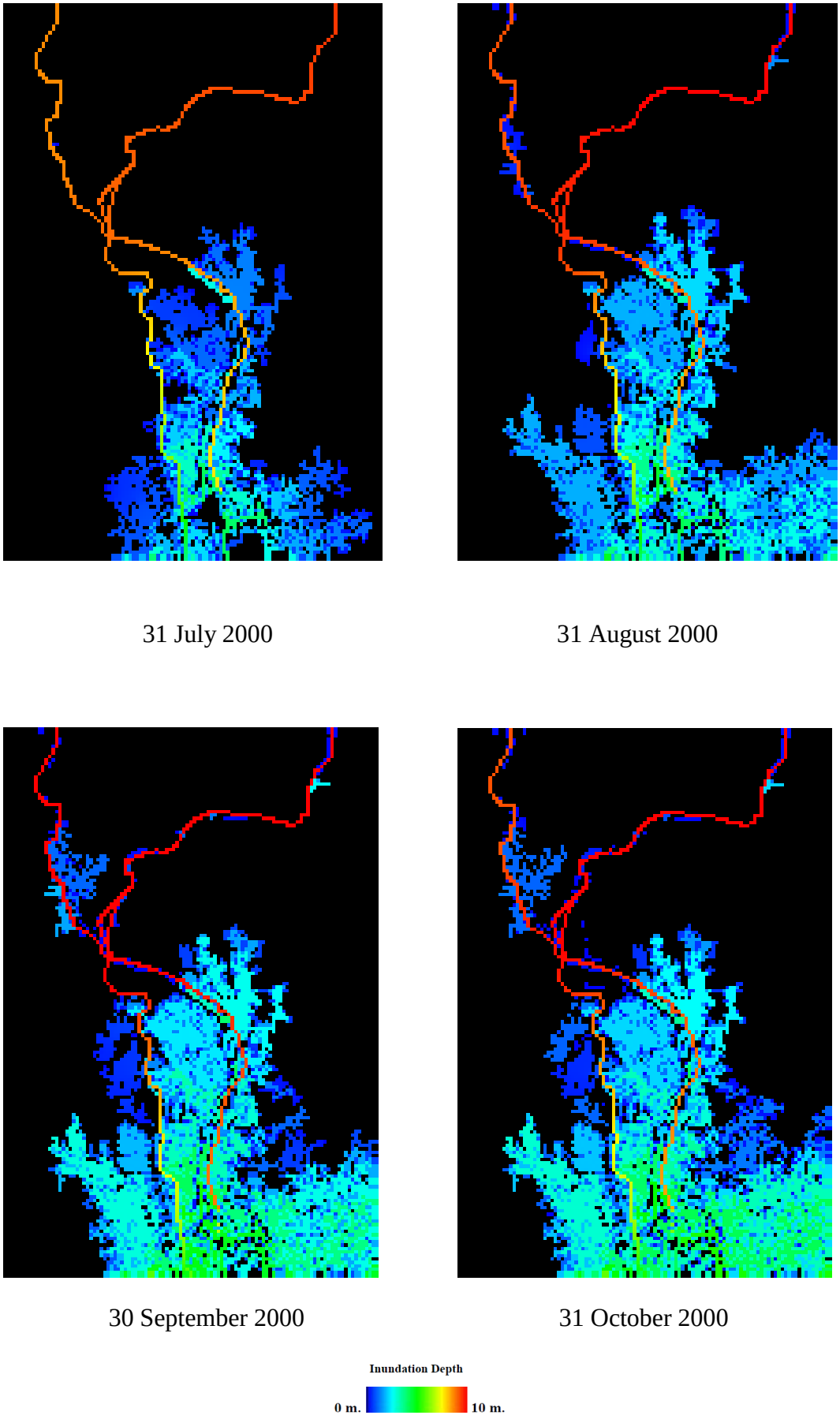

Figure 4.8 Temporal and spatial distribution of inundation level (1000m)

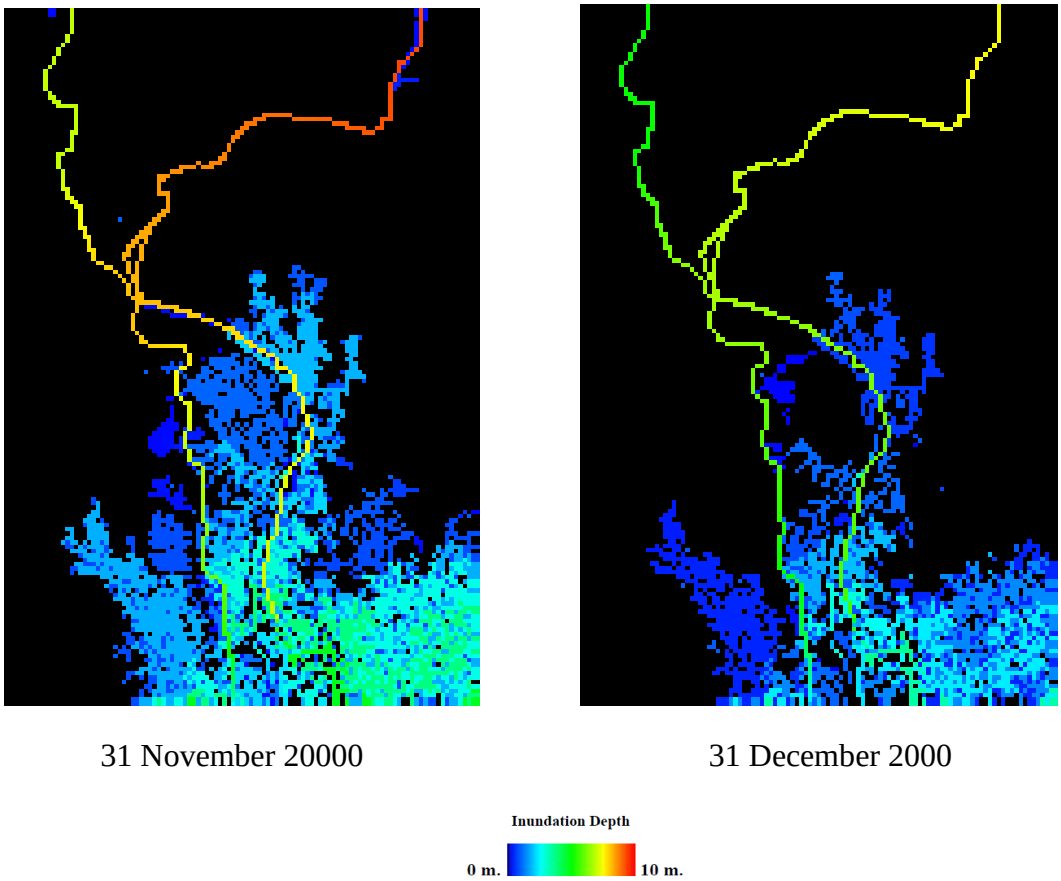

Figure 4.8 Temporal and spatial distribution of inundation level (1000m) (Cont.)

4.5 Comparison inundation areas by grid sizes

First of all initial condition of inundation we simulation in January to December in year 1999. The end of this year used to initial condition in year 2000. Figure 4.9 present the comparison between grid size of inundation area by spatial and temporal distribution. January and February are inundation area in downstream because it affected from reduction of flood area by end of year 1999 in initial condition. After that In July inundation area of three grid sizes cause from the low land area in the downstream. Inundation area (250m) is less than 500m and 1000m as shown in July 2000 (Figure 4.9). Three month later (August, September, October) both grid size extend inundation area from the downstream to east, west, upper of Mekong River. One of interesting three grid sizes that peak flood flow in October look similar from inundation area. After October three grid sizes inundation are quietly decrease.

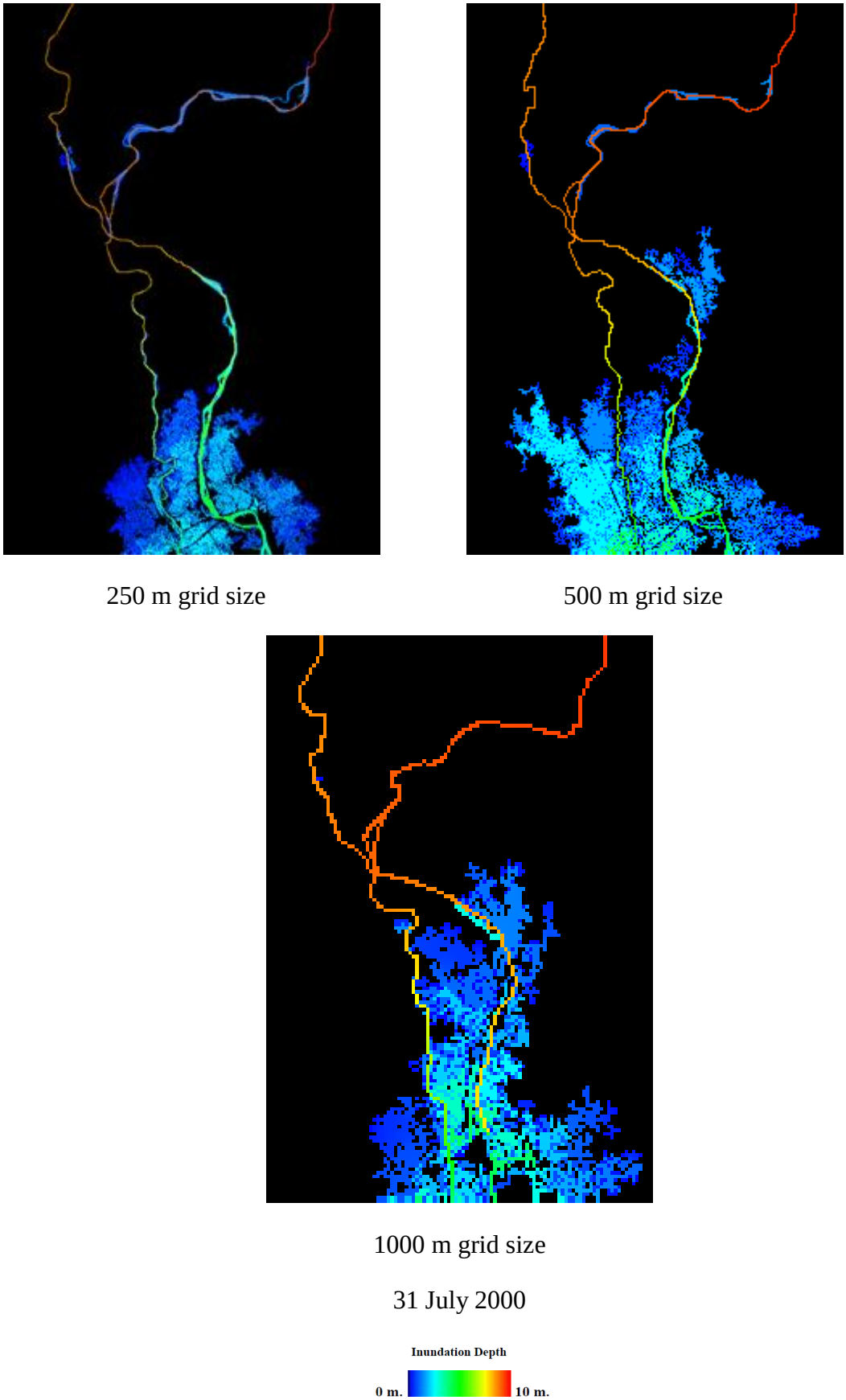

Figure 4.9 Comparison between three grid sizes by inundation level

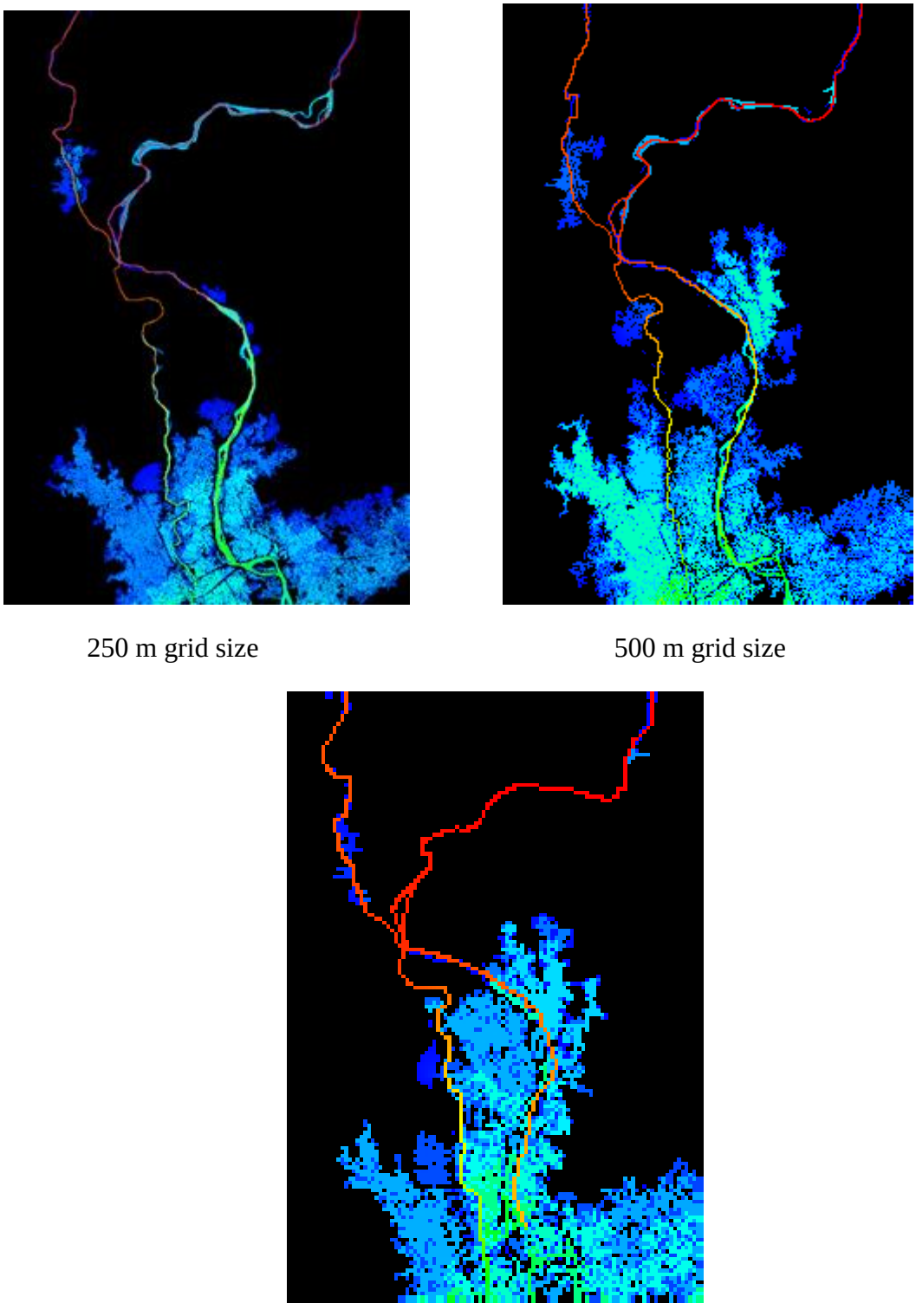

Figure 4.9 Comparison between three grid sizes by inundation level (Cont.)

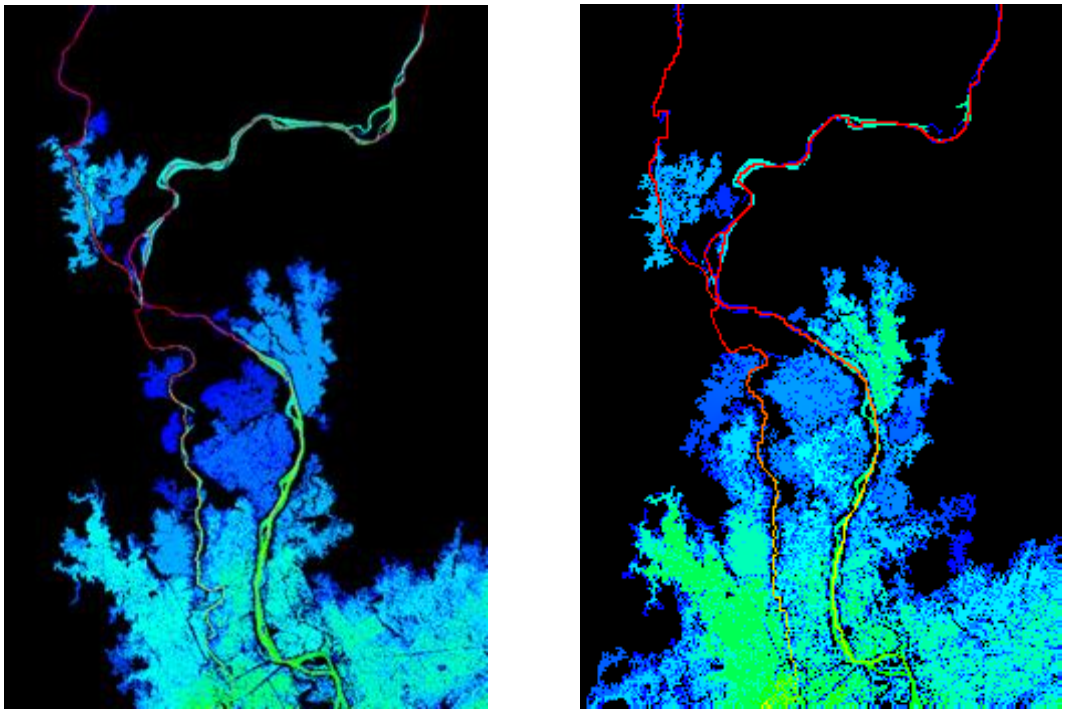

250 m grid size

500 m grid size

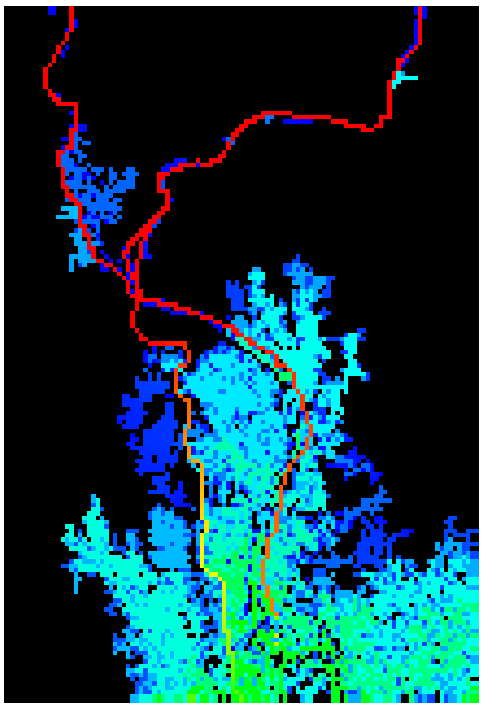

1000 m grid size

30 September 2000

Figure 4.9 Comparison between three grid sizes by inundation level (Cont.)

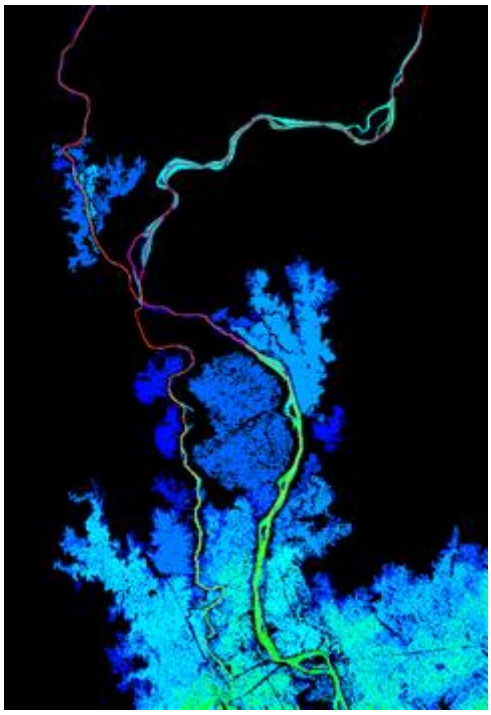

250 m grid size

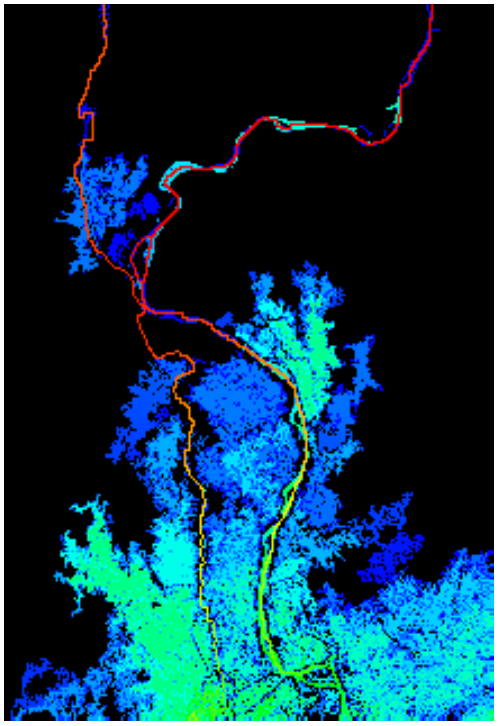

500 m grid size

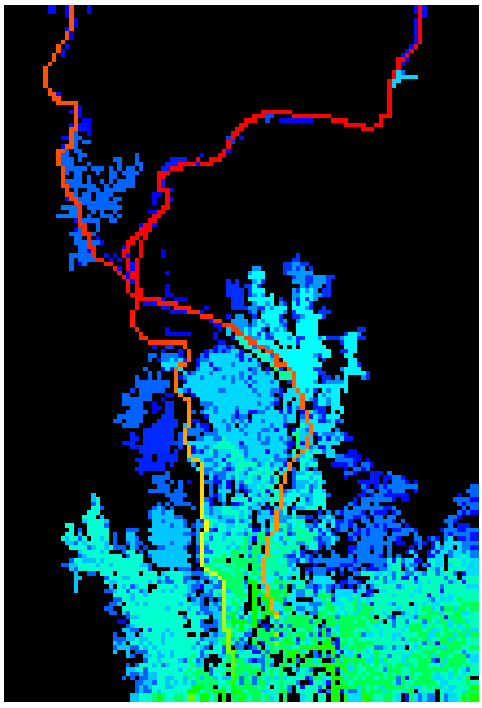

1000 m grid size

31 October 2000

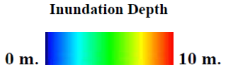

Figure 4.9 Comparison between three grid sizes by inundation level (Cont.)

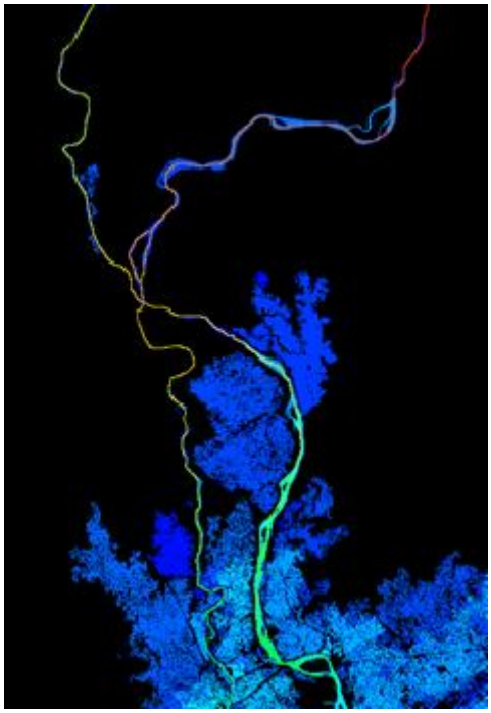

250 m grid size

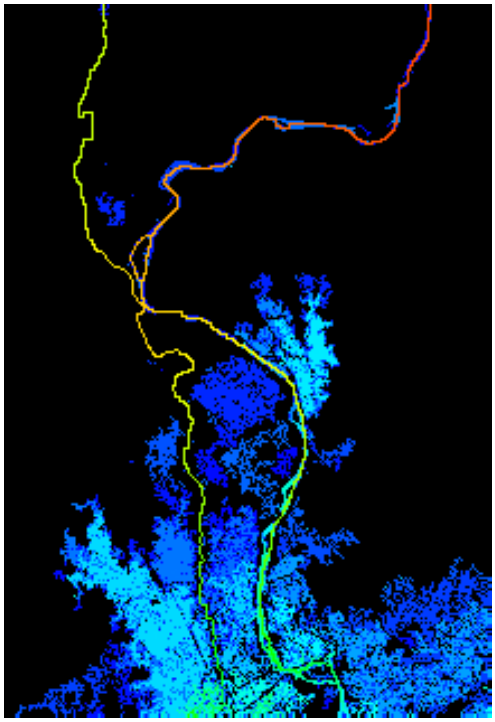

500 m grid size

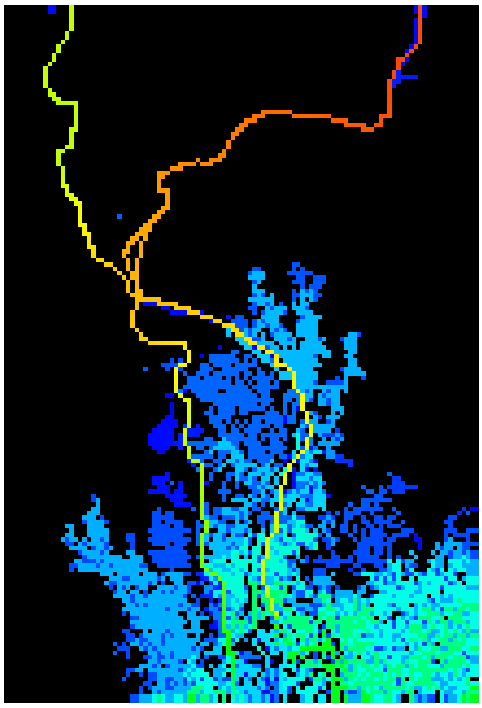

1000 m grid size

30 November 2000

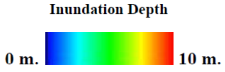

Figure 4.9 Comparison between three grid sizes by inundation level (Cont.)

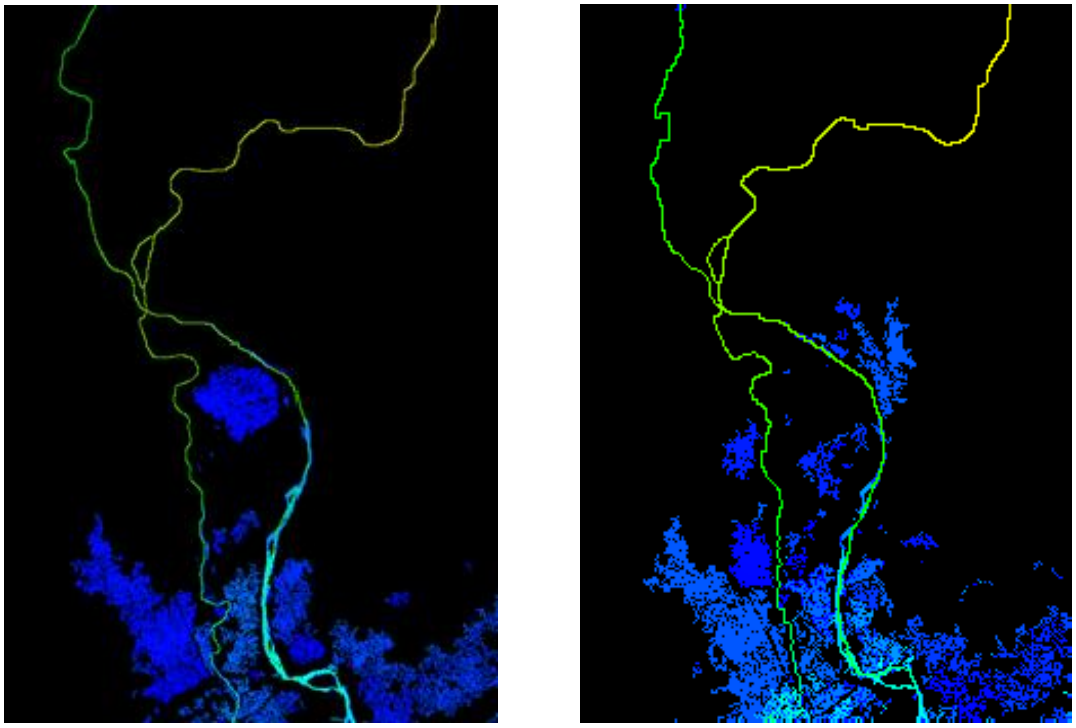

250 m grid size

500 m grid size

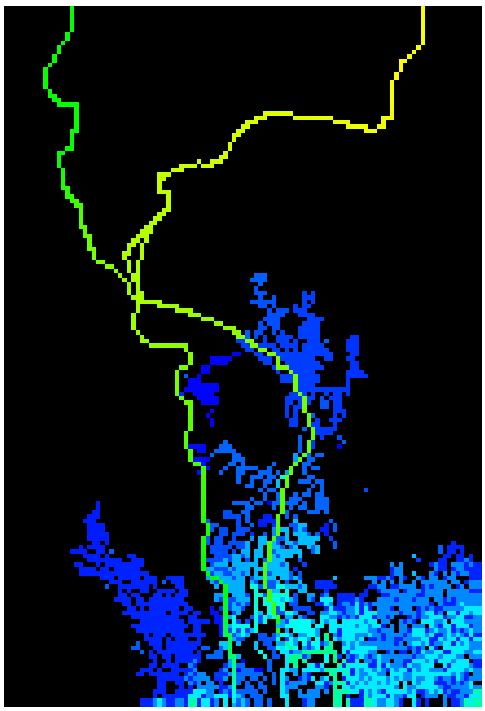

1000 m grid size

31 December 2000

Figure 4.9 Comparison between three grid sizes by inundation level (Cont.)

4.6 Monthly analysis distribution groundwater (250m, 500m and 1000m)

Figure 4.10 (250m), Figure 4.11 (500m) and Figure 4.12 (1000m) expresses the distribution of groundwater levels in dry and wet seasons in 2000. Both groundwater levels in the dry season (January- July) are almost similar but those in the flooding period (August-October) show differences of several meters. In the dry season groundwater level in channel is less than groundwater in left blank and right blank, so groundwater level in left and right blank recharge to river channel. On the other hand in wet season, groundwater level in river channel is more than water level in left and right blank because it causes inundation area in river channel. It means that groundwater level in channel recharge to left and right blank. This means that changes of flood magnitude influences groundwater resources during flood seasons and do not strongly influence groundwater resource in dry season.

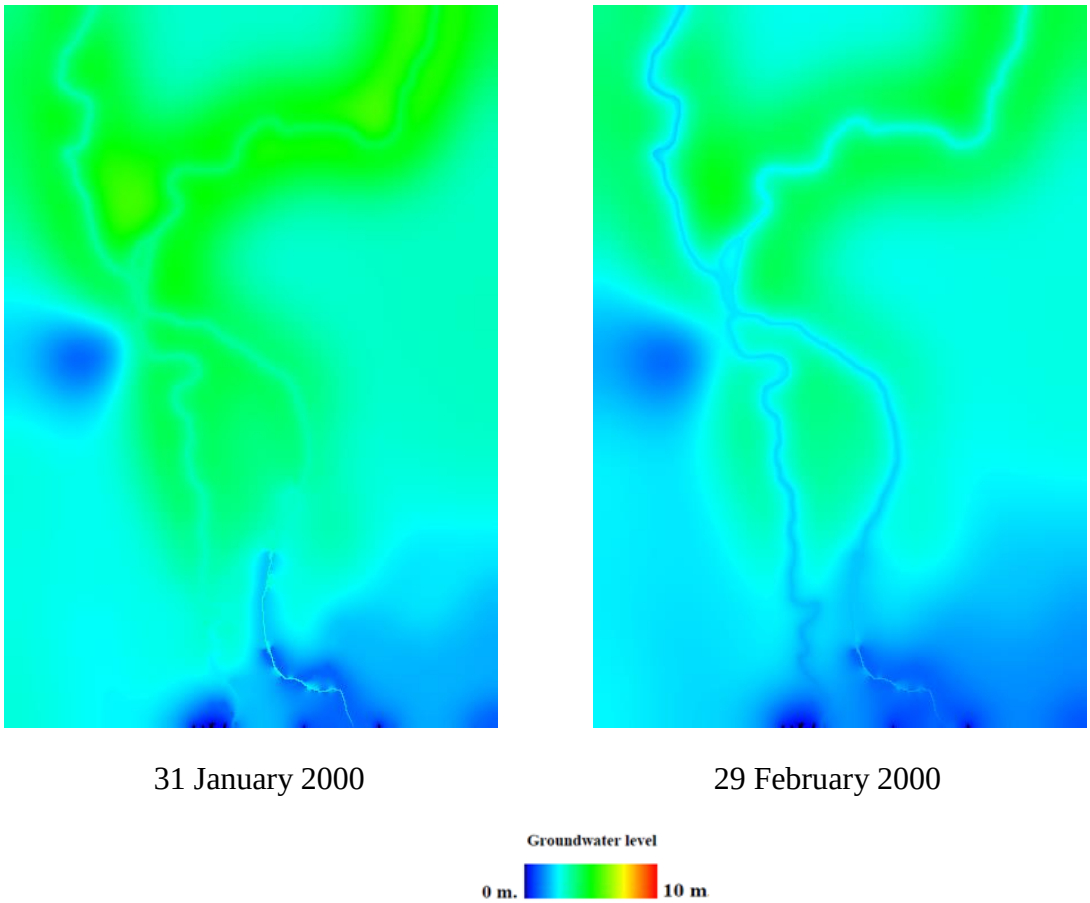

Figure 4.10 Temporal and spatial distribution of ground water level (250m)

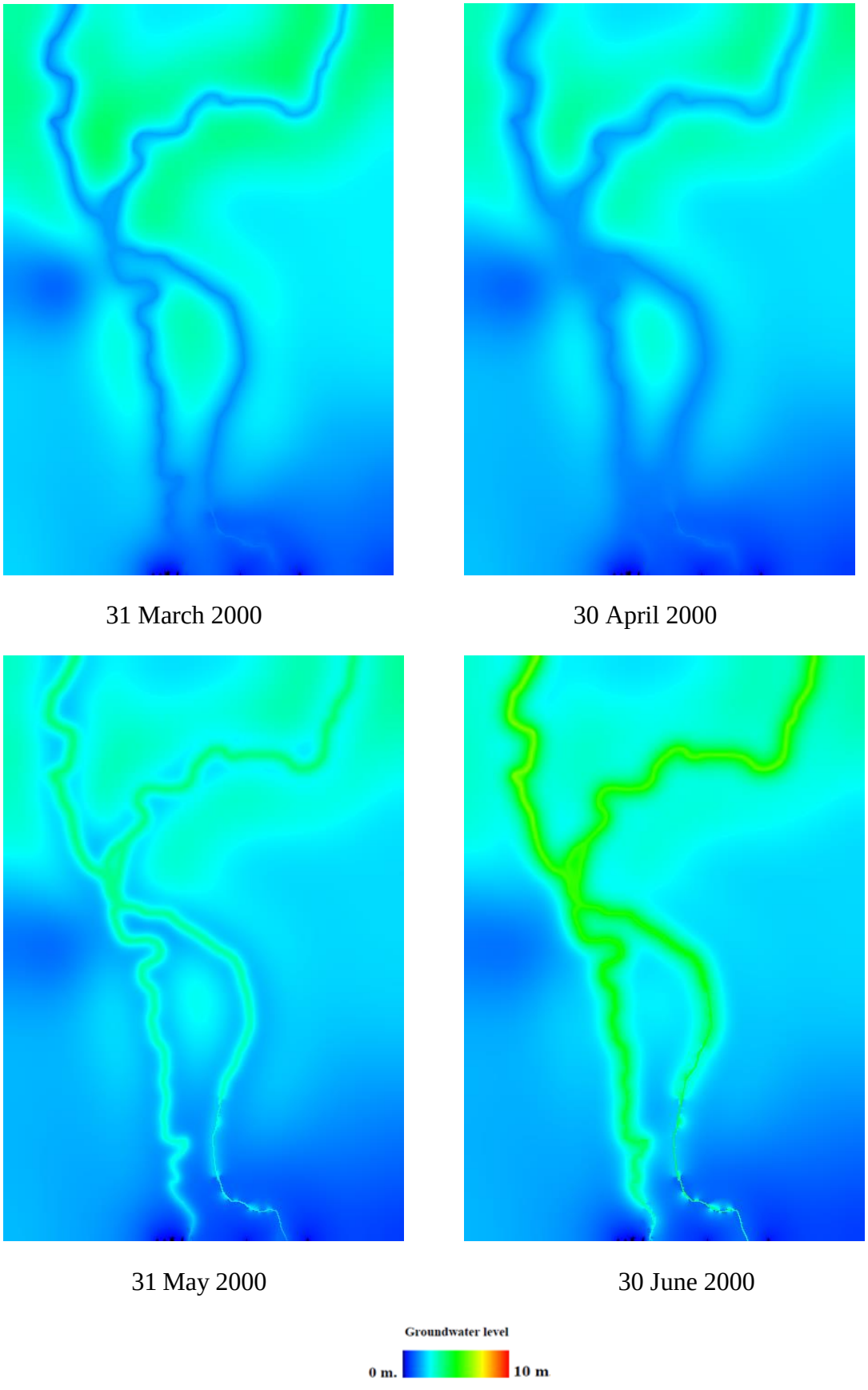

Figure 4.10 Temporal and spatial distribution of ground water level (250m) (Cont.)

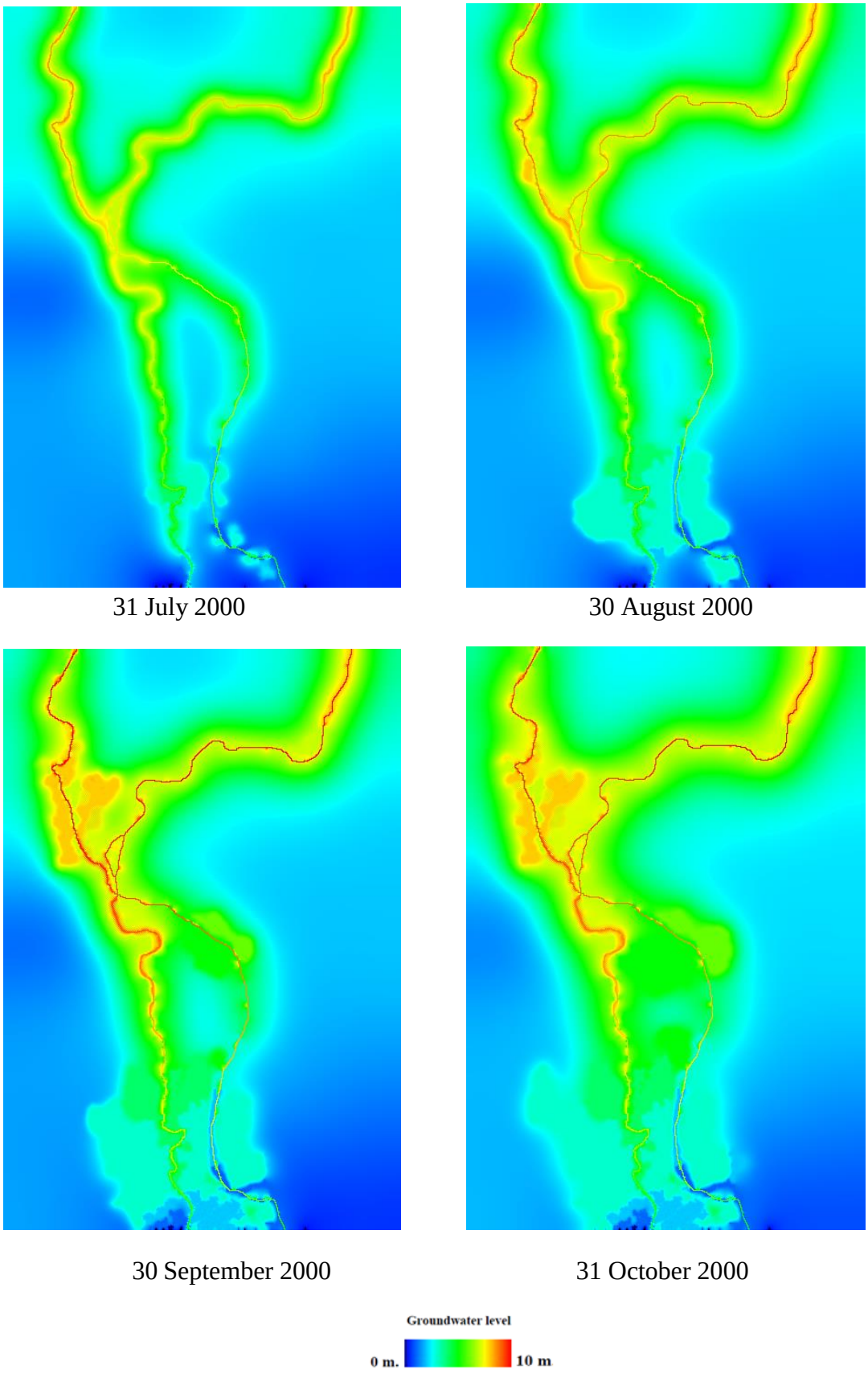

Figure 4.10 Temporal and spatial distribution of ground water level (250m) (Cont.)

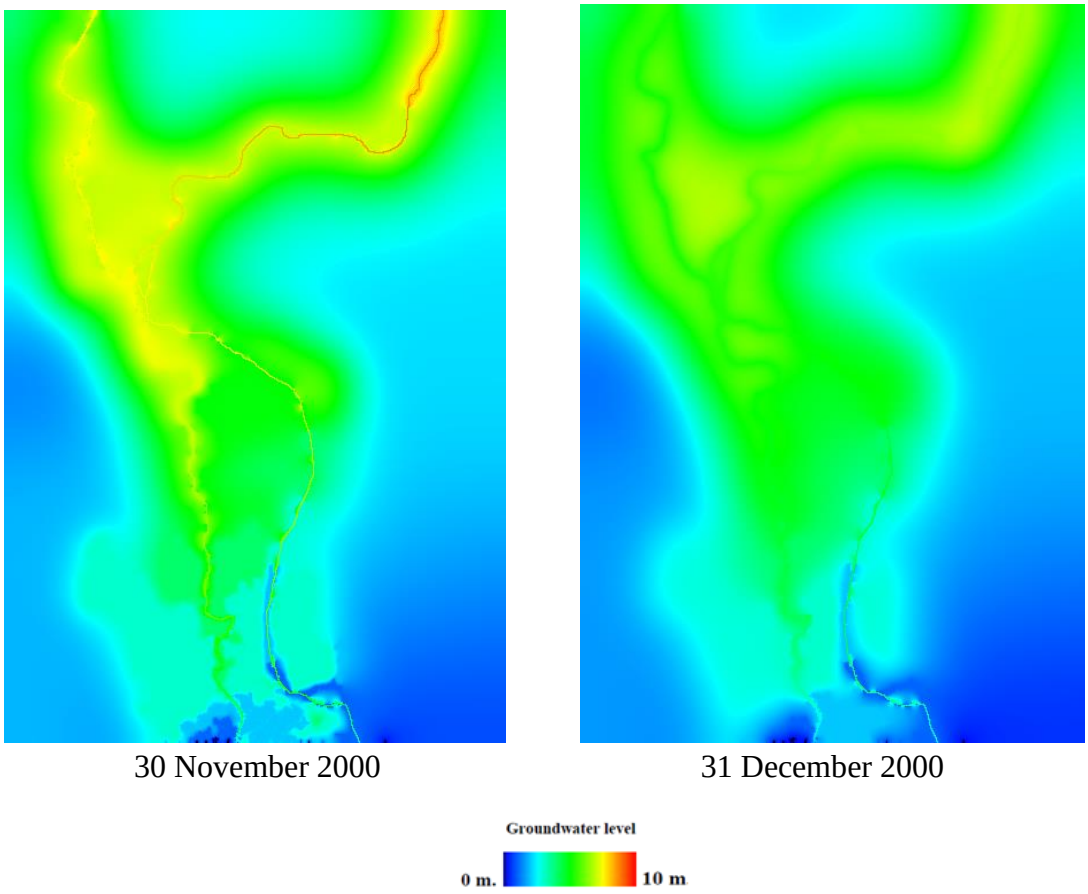

30 November 2000 31 December 2000

Figure 4.10 Temporal and spatial distribution of ground water level (250m) (Cont.)

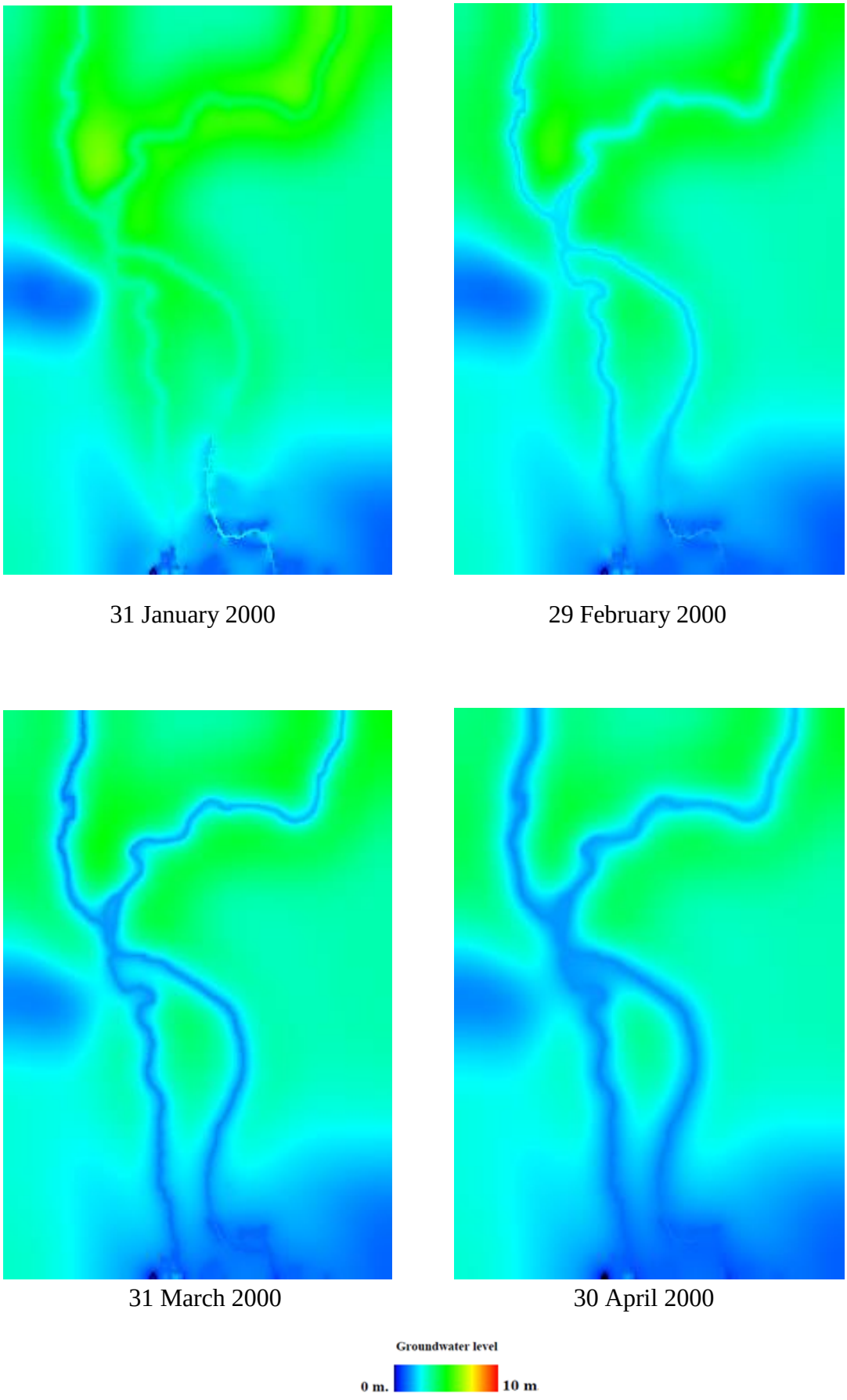

Figure 4.11 Temporal and spatial distribution of ground water level (500m) (Cont.)

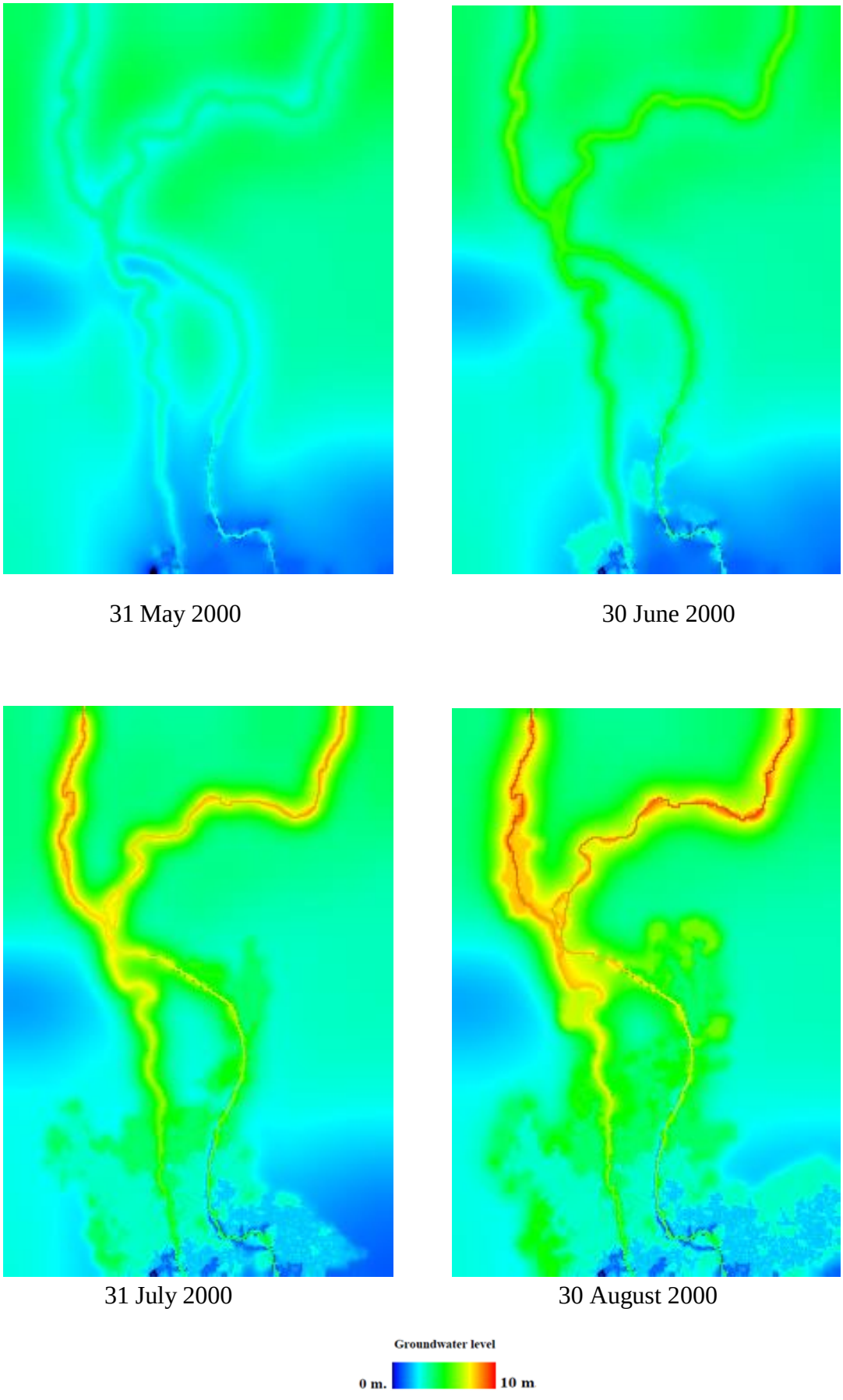

Figure 4.11 Temporal and spatial distribution of ground water level (500m) (Cont.)

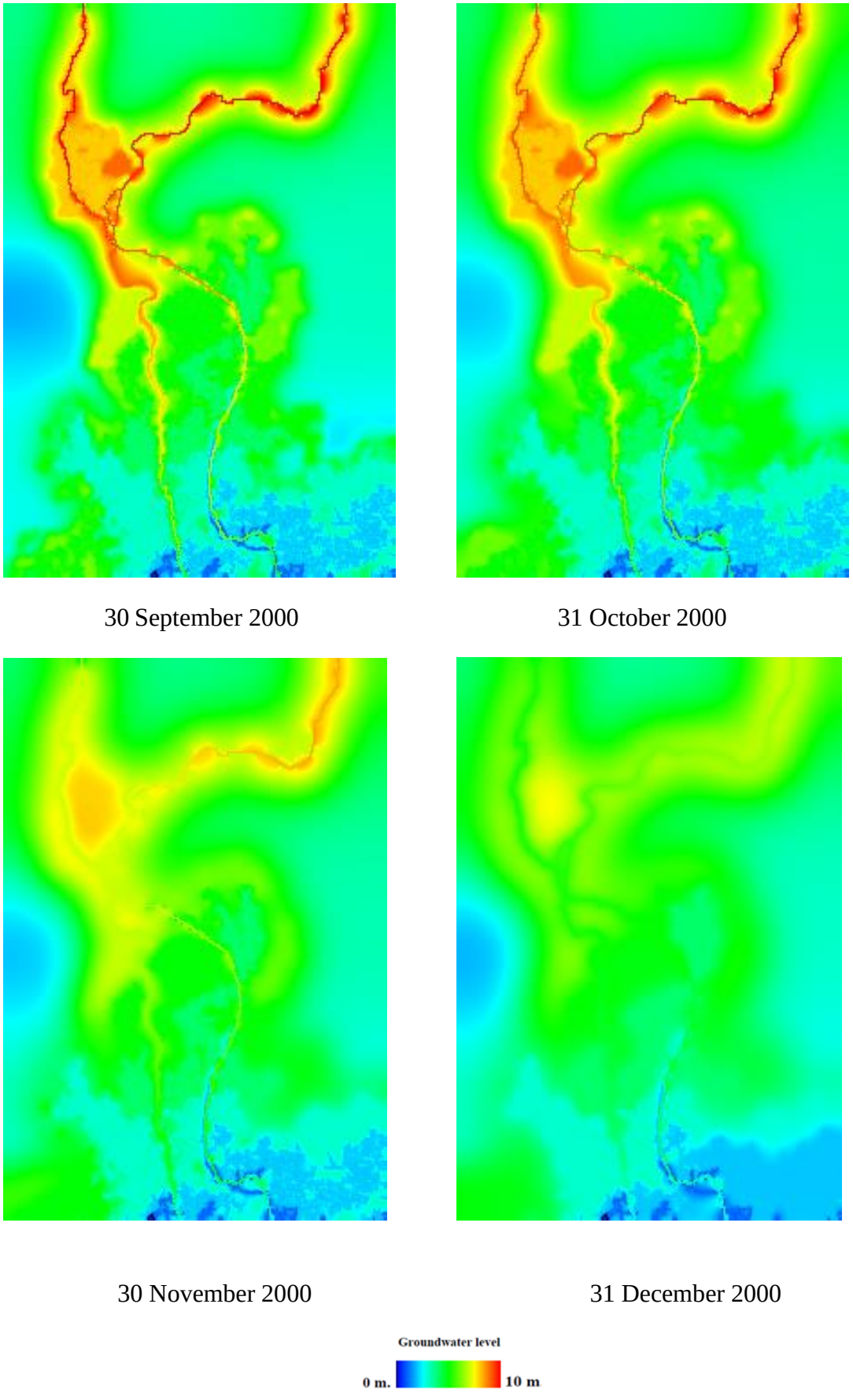

Figure 4.11 Temporal and spatial distribution of ground water level (500m) (Cont.)

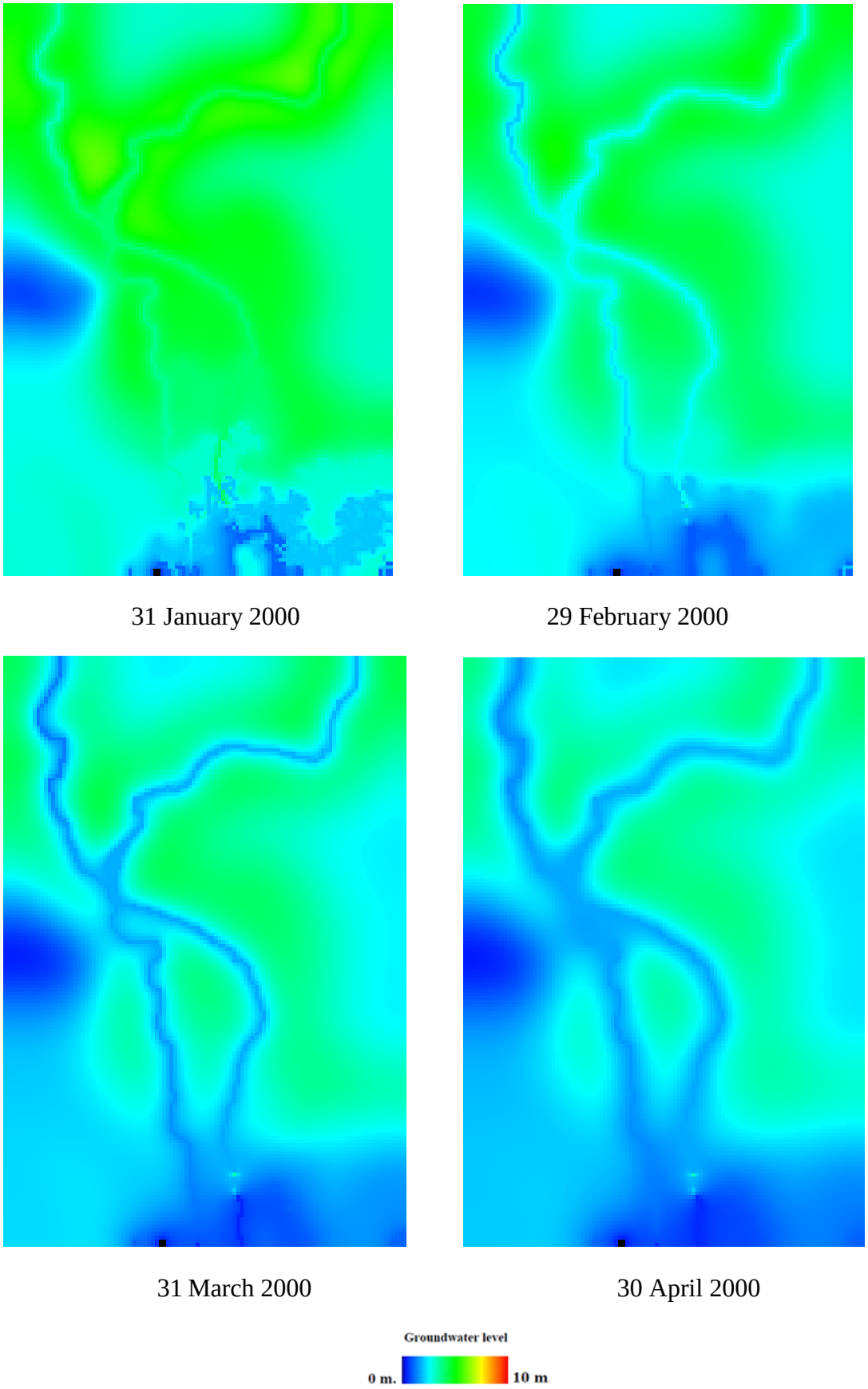

Figure 4.12 Temporal and spatial distribution of ground water level (1000m)

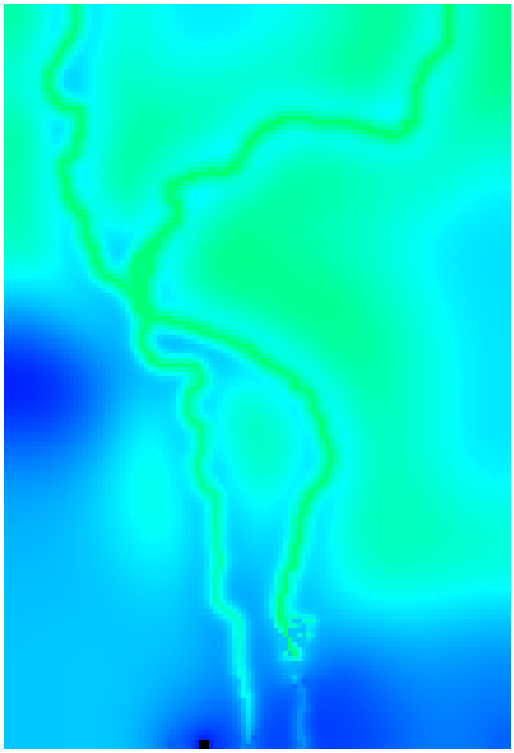

31 May 2000

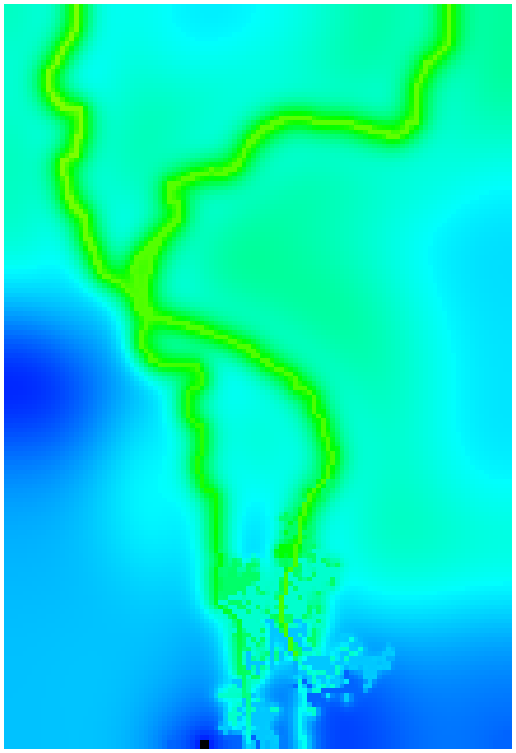

30 June 2000

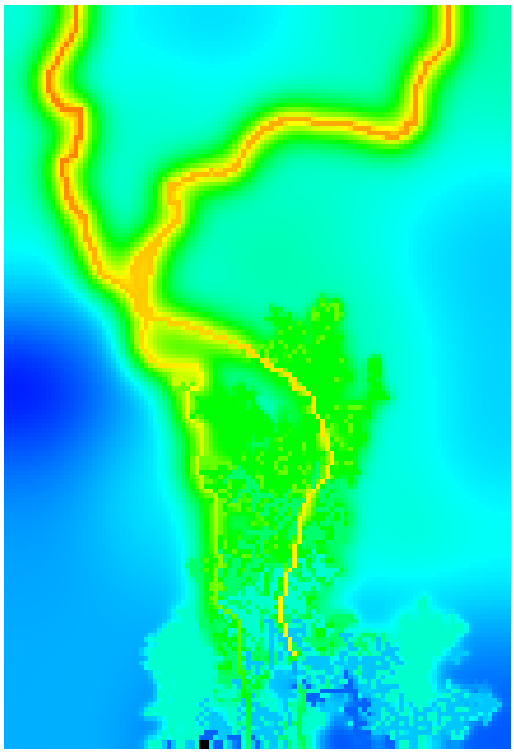

31 July 2000

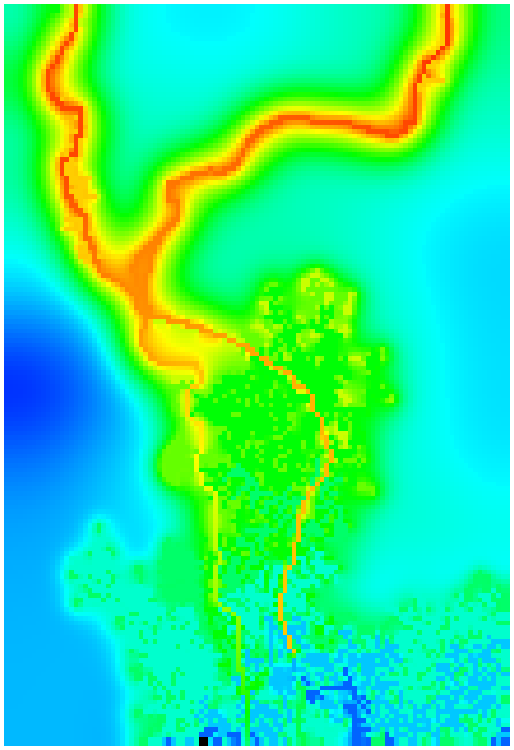

30 August 2000

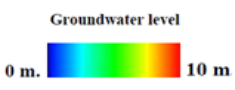

Figure 4.12 Temporal and spatial distribution of ground water level (1000m) (Cont.)

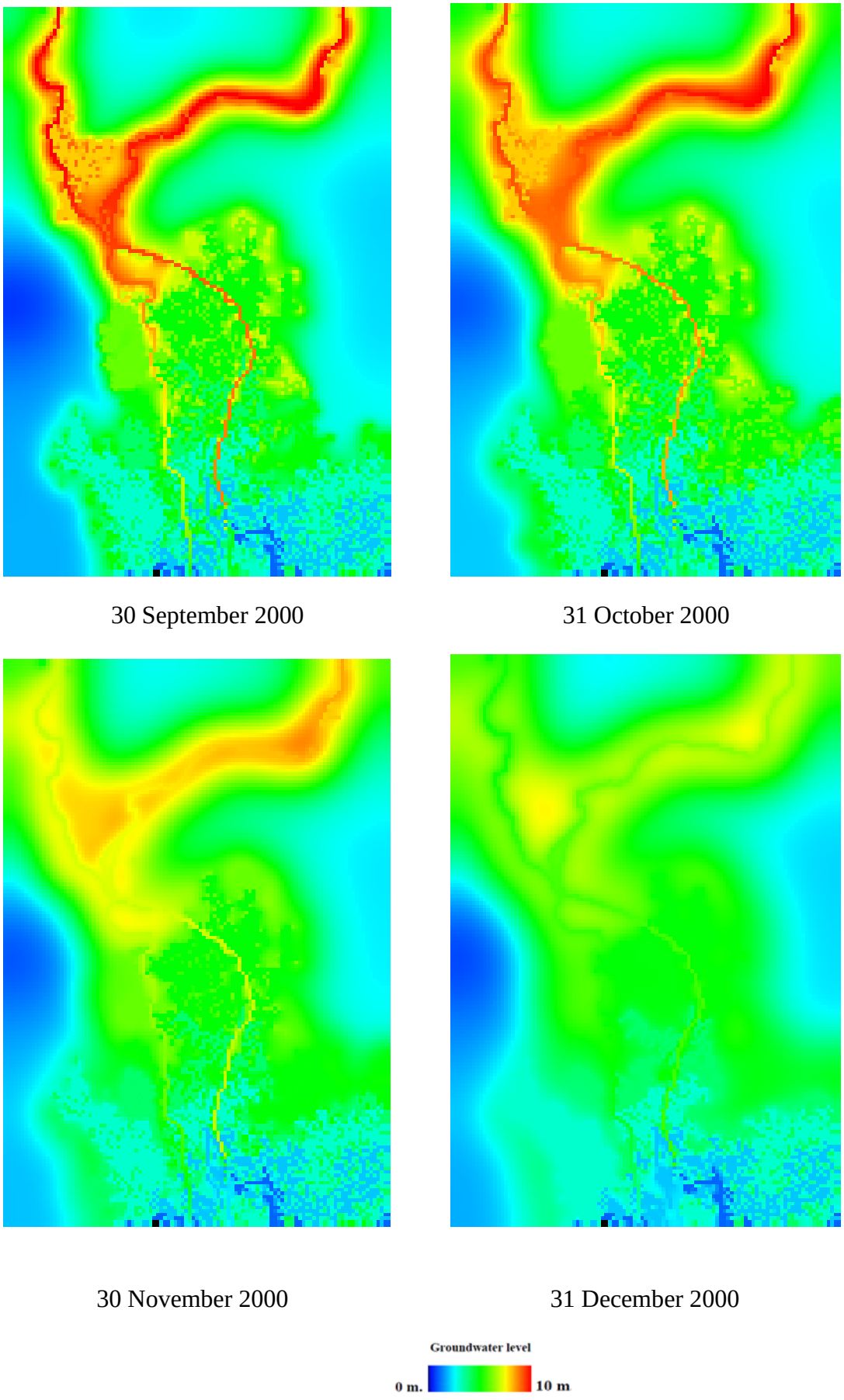

Figure 4.12 Temporal and spatial distribution of ground water level (1000m) (Cont.)

4.7 Groundwater storage

The temporal and spatial distribution of groundwater levels in year 2000. This result was used to estimate the groundwater storage in each month. Maximum groundwater storage in the area was calculated by the integration of the difference between highest and lowest groundwater levels in the area as follows:

$$\text{Groundwater storage} = \int \left(GWL_h - GWL_l\right) dA x n_g \qquad (4.7)$$

Where GWL_h is the highest groundwater level and GWL_l is the lowest groundwater level and n_g is specific yield.

Using this equation, the average groundwater storage in the study area has been estimated as 55 km^3 (55 billion m^3) from 250m resolution and 59.41 km^3 (59.41 billion m^3) from 1000m resolution. When this groundwater volume is divided 3.9m as the average this groundwater amount in almost double the average rainfall of the area. It is well known that Tonle Sap Lake is a big reservoir functioning in the lower Mekong. This lake has inflow from the Mekong River in dry season. It has reported that the storage of the lake was almost 76.1 km^3 in year 2000 (M. kummu, et al. 2013). It is clear that groundwater storage in the study area is almost similar to the capacity of the Tonle Sap Lake. Therefore, groundwater resource can be considered as a large potential water source in the lower Mekong region. These two big reservoirs contribute to the base flow of the Mekong River and give natural blessings to the downstream region during dry season.

4.8 Relationship between inundation area and groundwater resources

Table 4.13 Summarizes the inundation area and groundwater storage in 2000

Duration	Inundation area (km^2)			Groundwater storage (km^3)		
	250m	500m	1000m	250m	500m	1000m
July	1575	1602	3675	54.73	55.23	58.02
August	2750	3243	5068	58.24	59.73	62.02
September	4554	4925	6256	59.92	61.45	65.23
October	4806	5310	6602	62.5	64.52	68.42
November	3545	3768	5385	62.1	63.95	67.54
December	2650	3320	3864	60.23	61.94	64.52

The relationship between inundation areas and groundwater storage were carried out for the period of July 2000 to December 2000 show in Table 4.13.It summarizes that inundation areas and groundwater storage with different grid sizes. First of all Inundation area and groundwater storage are decrease by changes slope of digital elevation map. Other thing is groundwater storage in both three grid size are similar by trend of groundwater. In the wet season when flow rate in channel exceeds the capacity

of the river channel and inundates the adjoining area. Some of water moves out by infiltration in the soil. It increases about groundwater levels in wet season. Figure 4.14 shows about summarize inundation and groundwater storage in both three grid size (250m, 500m and 1000m). It shows that trend of inundation and groundwater level increase in the same time.

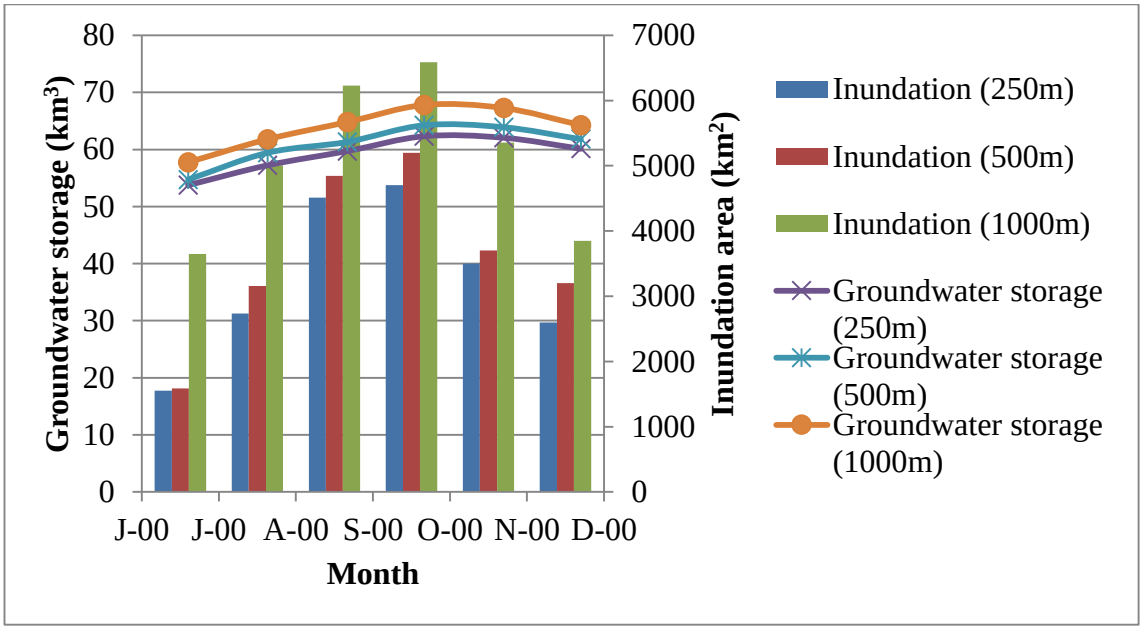

Figure 4.14 Summarizes the inundation area and groundwater storage in 2000

4.9 Impact of grid size resolution on simulated flood inundation and groundwater

The model was further applied to carry out simulations with three sets of DEMs of different resolution: 250, 500 and 1000m for the 2000 flood event to analyze the impacts of grid resolution in simulated inundation and groundwater level outputs. The results were compared in terms of average flood height, maximum flooded areas, groundwater storage and average groundwater level.

Table 4.15 summarizes the variations of inundation and groundwater level characteristics with different grid DEM resolution and the outcomes demonstrate that flood depths and extents are highly influenced by the DEM resolution: the average flood heights decreases with the decrease of DEM resolution. At the same time from groundwater storage and average groundwater level increase with the increase of DEM resolution.

Table 4.15 Comparison inundation and groundwater for different grid size

DEM Resolution (m)	Average flood depth (m)	Maximum flood area (km^2)	Groundwater storage (km^3)	Average groundwater level (m)	Average elevation (m)
250	0.55	4806	62.5	3.92	11.93
500	0.59	5310	64.52	4.06	11.88
1000	0.93	6602	68.42	4.8	11.86

As a result of grid resampling, simulate average groundwater level and groundwater storage increased as grid cell sizes increased (Fig 4.16) Inundation area decreased with decreasing grid cell size because change of elevation in this area it cause inundation area are decreasing too. (Fig 4.17)

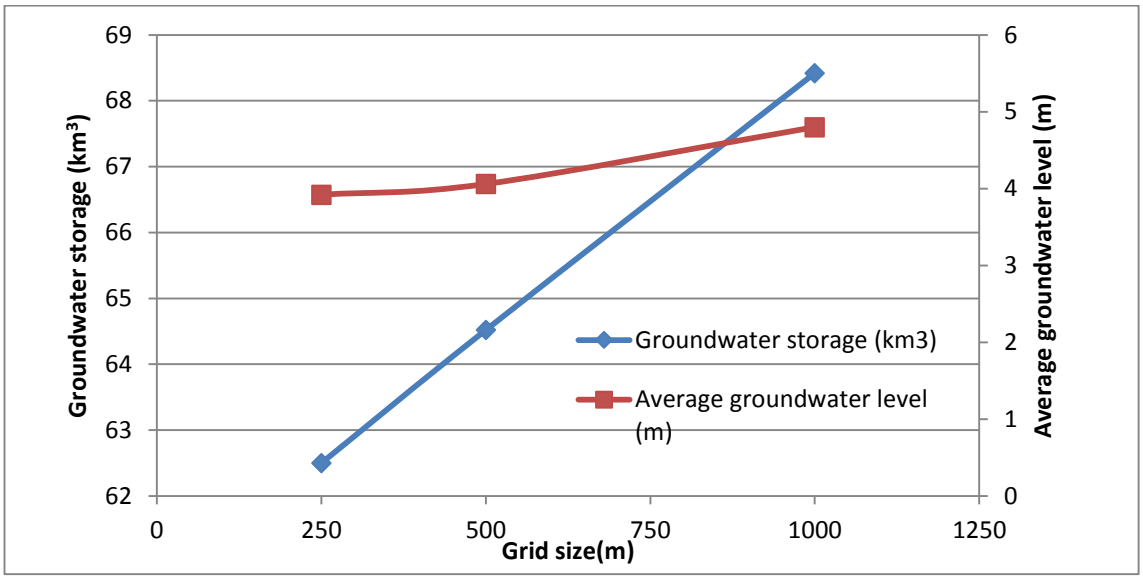

Figure 4.16 Relationship between groundwater storage and average groundwater level with different grid size

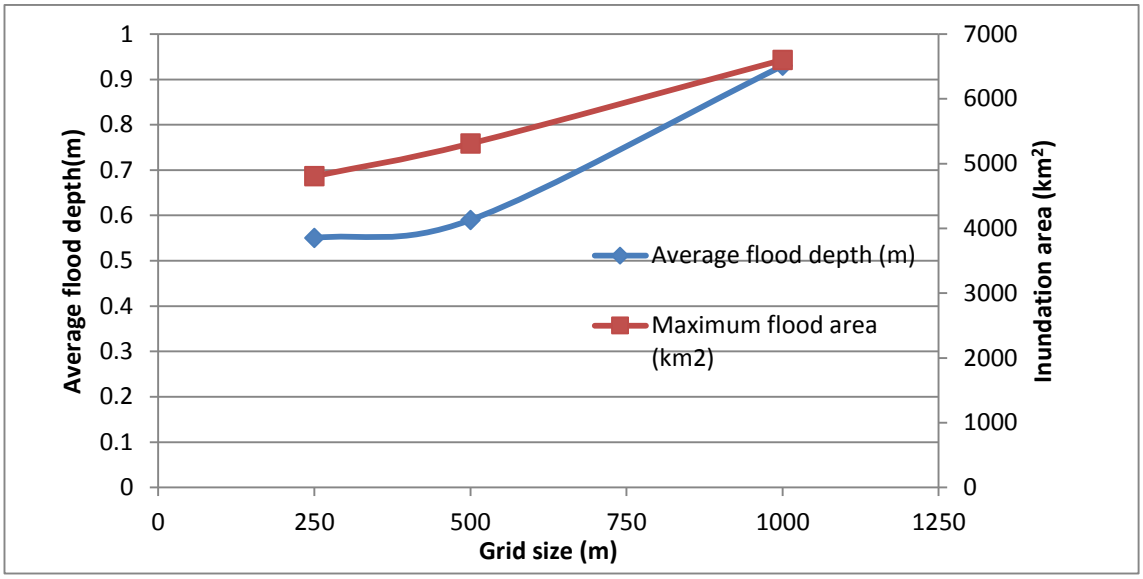

Figure 4.17 Relationship between Inundation area and average flood depth with different grid size

CHAPTER 5 CONCLUSION

Floods and inundation are annual events, which are necessary for agriculture in the Lower Mekong basin. Groundwater resources are influenced by flood water in inundation areas, even though severe floods can destroy these resources. Numerical models based on the behavior of flood flow, over flow, inundation depth and groundwater levels have been used to simulate the influences of change in inundation areas and the distribution of inundation depth caused by effect of grid size in the Mekong river Basin. A study of grid size effects on inundation area and groundwater by the hydrological model was done by resampling the catchment into 250m, 500m and 1000m cell size grid using ArcGIS tools. First of all hydrological models was calibrated based on grid size and applied to other grid size scenarios using the same model. The assessment of model performance was carried out for the model results. Inundation area is very sensitive to the grid size change. The estimated inundation area and groundwater recharge becomes bigger for coarser gird size due to the decrease of cell slope. Calculations from inundation areas have been compared with satellite image outputs from September, 23 2000 and October, 22 2000 and show good agreement between estimated inundation areas and satellite images in three grid size. It concludes that change of grid size that effects in hydrological model on spatial and temporal of groundwater level and inundation area by month and cause different several meters in simulation. Therefore, the effects of grid size on distributed hydrological models will be different for each catchment. Future research is necessary to show if the scaling of the model parameters with respect to grid size resolution can be defined from the catchment physical characteristic.

REFERENCE

Bates, P.D. and De Roo, A.P.J., 2000. "A Simple Raster-Based Model for Floodplain Inundation". **Journal of Hydrology**, Vol. 236, pp. 54-77

Dutta D., Alam J., Umeda K., Hayashi M and Hironaka S., 2007, "A Two-Dimensional Hydrodynamic Model for Flood Inundation Simulation: A Case Study in the Lower Mekong River Basin", **Hydrological processes**, Vol. 21.9, pp. 1223-1237.

Dutta D and Nakayama K., 2009, "Effects of Spatial Grid Resoultion on River Flow and Surface Inundation Simulation by Physically Based Distrubuted Modelling Approach Environment Canterbury, 2000, "Guidelines for the Assessment of Groundwater", **Hydrological process** Vol. 23, pp. 534-545

Abstraction Effects on Stream Flow", **Technical Report Environmental Monitoring Group,** pp.7-8.

Evelyn, G., 2004. "China in the Mekong River basin : the regional security implications of resource development on the Lancang Jiang", **RSIS Working papers**, No. 069.

Hamburg University of Technology, 2010, **Thiessen Polygon Method** [Online], Available: http://daad.wb.tu-harburg.de/fileadmin/BackUsersResources/Hydrology/8-HydrologicalModeling/additional_info/Thiessen_polygon_Method.pdf [2014, April 3].

Hermann, L.C., 2014, "Biophysical Models: Hydrology", **Hydrology models (Hydrology)**, p.1.

Horritt, M.S. and Bates, P.D., 2001b. "Effects of Spatial Resolution on a Raster Based Model of Flood Flow". **Journal of Hydrology**, Vol. 253, pp. 239-249.

Joakim, O., 2000, **Sharing the Good : Modes of Managing Water Resources in the Lower Mekong River Basin**, Doctoral thesis Department of Peace and Development Research University of Gothenburg.

Kazama, S. and Sawamoto, N., 2002. "Relationship between Inundation Area and Irrigation Area on Flood Control in the Lower Mekong." **Proceedings of 13th congress the APD/IAHR**, Vol. 1, pp. 596-601.

Kazama, S., Hagiwara, T., Ranjan, P. and Sawamoto, M., 2007. "Evaluation of Groundwater Resources in Wide Inundation Areas of the Mekong River Basin". **Journal of Hydrology**, Vol. 340, pp. 233– 243.

Liu, S., Lu P., Liu, D., Jin, P. and Wang, W., 2009, "Pinpointing Source and Measuring the Lengths of the Principal Rivers of the World", **International Journal of Digital Earth**, Vol. 2, p. 80-87.

Liu Y.B, Yi, Y, Batelaan O and De Semedt F, "Assesing grid Size Effects on Runoff and Flow Response Using GIS-based Hydrological Model", 2005, **Proceeding of the 13 th International conference on geoinformatics**, pp. 1-8

May, R., Jinno, K. and Tsumi, A., 2010, "Influence of Flooding on Groundwater Flow in Central Cambodia", **Environmental Earth Sciences**, Vol. 63, pp. 151-161.

MRC, 1993–2001. **Lower Mekong Hydrologic Yearbooks.** Mekong River Commission.

Nawarathna, N., Kazama, S., 1999, "Analysis of the Relationship Between Water Balance and Basin Characteristics", **Water Resources Journal**, Vol. 202, pp. 24–38.

Rosalia R, Mark V, Pierre Y.J, M. ASCE, Billy E.J. 2008. "Grid Scale Effects on Watershed Soil Erosion Models". **Journal of hydrologic engineering**, Vol 13, pp. 793-798

Rahman, Mohammad Mahmudur, Naidu, R. and Bhattacharya P., 2009, "Arsenic contrmination in groundwater in the Southeast Asia region", **Environmental geochemistry and health**, Vol. 31, pp. 9-21.

Shah, T., 2006. "Groundwater and Human Development: Challenges and Opportunities in Livelihoods and Environment", **Groundwater research and management: Integrating science into management decisions**, p. 14.

Subramanya, K., 2009, **Engineering Hydrology**, 3rd ed., McGrawHill, Printed in Singapore, p. 13.

Thomas L. P., 2009, "Introduction to Model Validation", **IMAC-XXVII**, 9-12 February 2009, Orlando, Florida, USA, p. 1.

Vazquez, R.F., Feyen, L., Feyen, J., J.C.Refsgarard., 2002.Effect of Grid Size on Effective Parameters and Model Performance of the MIKE-SHE Code. **Hydrological Process 16**, Vol.2, pp. 355-372

Zhao, G.J., Hormann, G., Fohrer, N. and Gao, J.F., 2009, Impact of spatial data resolution on simulated discharge, a case study of Xitiaoxi catchment in South China. **Advances in Geosciences**, Vol. 21, pp.131-137.

Appendix

Water level and observation data in Lower Mekong river basin

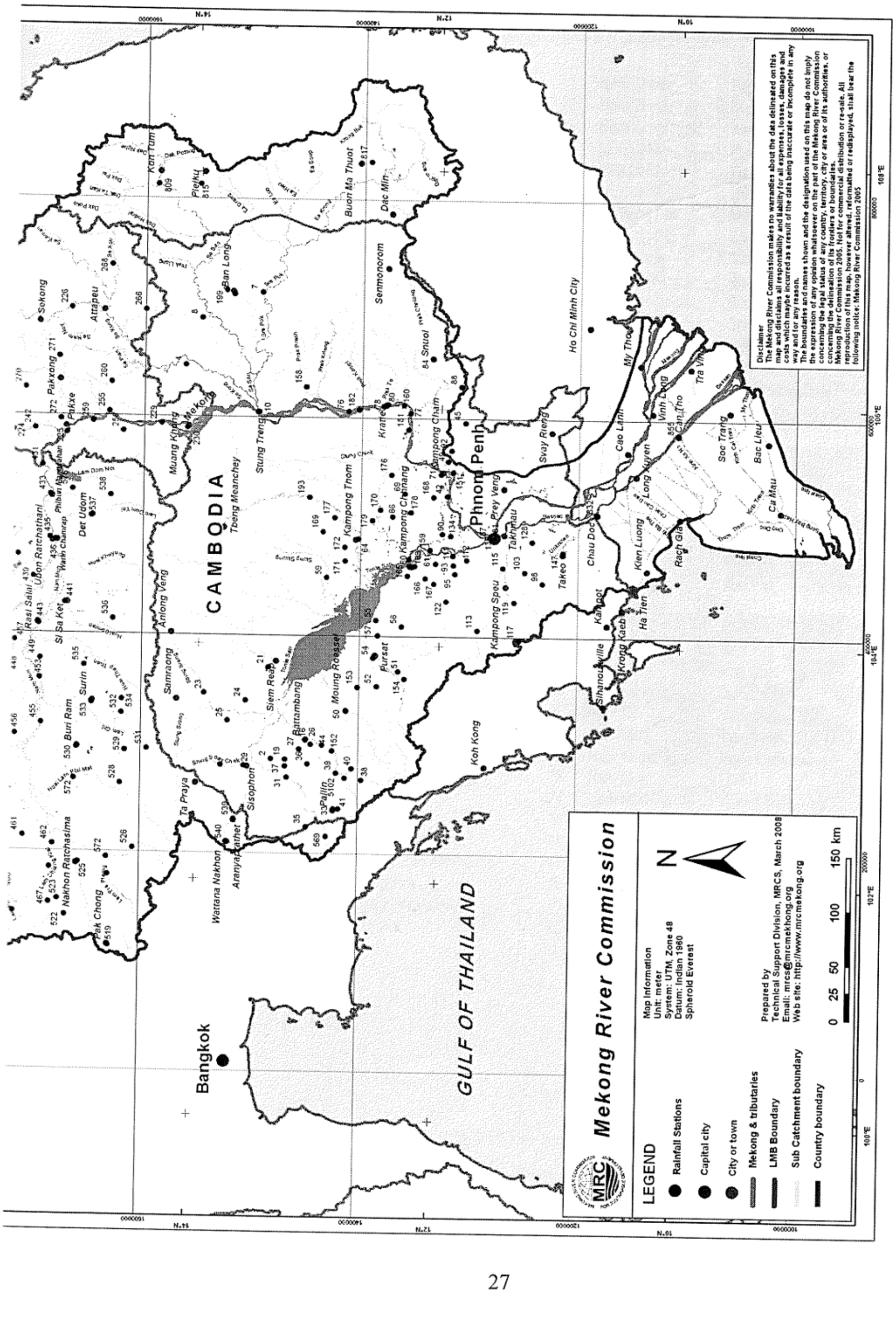

Mekong River Commission
LEGEND
Rainfall Stations
Capital city
City or town
Mekong & tributaries
LMB Boundary
Sub Catchment boundary
Country boundary
Map Information
Unit: meter
System: UTM, Zone 48
Datum: Indian 1960
Spheroid Everest
0 25 50 100 150 km
GULF OF THAILAND
CAMBODIA
Bangkok
Phnom Penh
Ho Chi Minh City
Siem Reap
Battambang
Kampong Thom
Kampong Cham
Stung Treng
Kratie
Pakse
Ubon Ratchathani
Nakhon Ratchasima
Koh Kong
Sihanoukville
Kampot
Takeo
Chau Doc
Can Tho
Ca Mau

MEKONG AT KOMPONG CHAM, CAMBODIA (019802)

Station Description

Location:

Lat. 11° 59.7 N, long. 105° 27.9' E, in front of Service meteorologique climatological station in the town of Kompong Cham and about 410 km from the sea. All discharge measurements made from boat 1,200 m. upstream. This gauge is the auxiliary gauge used to obtain water surface fall for determination of discharge of Mekong at Phnom Penh during period of lakeward flow in Tonle Sap. Abandoned in 1974, reopened in 1991 by a slope gauge.

Gauge and Datum:

Bubble gauge and water stage recorder referred to existing T.P. gauge on downstream side of disused concrete loading ramp. Zero of gauge elevation 0.93 m below M.S.L. Hatien datum.

Drainage Area: 660,000 Km2

Records Available:

Low stage: one daily reading at gauge, mean and high stages: two daily readings at gauge. Khmer T.P. stage record: complete or near complete 1927-28, 1930-73; fragmentary record for 1926. Interrupted since 1974, restarted in 1991. Daily record of bubble gauge since 2 June 1961. Daily discharge since 1 January 1964.

Average Discharge:

10 years (1964-73) 13,660 m3/sec.

Extremes:

2000: Maximum gauge height 15.91 m on 18 September; minimum gauge height 2.46 m on 12 April. 1926-28, 1930-73, 1991-2000: Maximum discharge 57,000 m3/sec.from 19 to 20 September 1966 (gauge height 15.44 m; maximum gauge height 16.11 m on 29 September 1996; minimum gauge height 1.56 m on 27 April 1993.

Remarks:

The station rating is affected by the water profile variations between Kompong Cham and Phnom Penh. Daily discharge during low flow period is estimated from Phnom Penh records.

MEAN GAUGE HEIGHT IN METERS, YEAR 2000

DAY	JAN	FEB	MAR	APR	MAY	JUN	JUL	AUG	SEP	OCT	NOV	DEC
1	5.51	3.96	3.23	2.62	3.40	7.78	12.06	14.58	15.06	13.71	10.56	7.49
2	5.47	3.95	3.30	2.55	3.47	7.83	12.09	14.43	15.23	13.63	10.50	7.40
3	5.42	3.90	3.30	2.52	3.58	8.04	11.90	14.28	15.40	13.45	10.41	7.31
4	5.36	3.85	3.28	2.48	3.57	8.45	11.67	14.12	15.62	13.25	10.29	7.20
5	5.27	3.79	3.22	2.48	3.50	8.43	11.47	13.98	15.72	13.10	10.14	7.09
6	5.23	3.76	3.16	2.47	3.61	8.23	11.53	13.84	15.74	12.95	9.97	6.98
7	5.19	3.72	3.10	2.48	3.83	7.81	11.81	13.77	15.68	12.84	9.78	6.90
8	5.16	3.68	3.06	2.49	3.85	7.55	12.09	13.73	15.69	12.73	9.65	6.82
9	5.13	3.66	3.02	2.48	3.77	7.39	12.35	13.70	15.77	12.54	9.52	6.74
10	5.09	3.63	3.00	2.48	3.70	7.32	12.44	13.68	15.83	12.36	9.42	6.66
11	5.04	3.59	2.96	2.48	3.68	7.24	12.48	13.61	15.85	12.40	9.30	6.60
12	4.98	3.56	2.92	2.46	3.75	7.14	12.82	13.54	15.84	12.52	9.22	6.59
13	4.91	3.51	2.87	2.47	3.88	6.99	13.45	13.44	15.82	12.84	9.15	6.59
14	4.86	3.48	2.87	2.49	4.12	6.97	13.85	13.35	15.82	13.18	9.07	6.55
15	4.80	3.46	2.86	2.48	4.42	7.12	14.16	13.22	15.86	13.30	8.96	6.48
16	4.74	3.47	2.86	2.48	4.56	7.55	14.45	13.16	15.88	13.32	8.86	6.44
17	4.66	3.50	2.90	2.62	4.80	8.26	14.75	13.09	15.90	13.29	8.79	6.38
18	4.61	3.54	2.94	2.87	5.11	9.75	15.00	13.04	15.91	13.24	8.68	6.33
19	4.56	3.58	3.02	3.06	5.42	10.56	15.18	13.03	15.86	13.17	8.58	6.26
20	4.51	3.59	3.05	3.20	5.49	11.00	15.31	13.07	15.76	13.03	8.56	6.18
21	4.47	3.59	3.05	3.26	5.58	11.10	15.41	13.18	15.67	12.80	8.62	6.12
22	4.43	3.58	3.02	3.22	5.73	10.99	15.45	13.18	15.56	12.48	8.57	6.05
23	4.42	3.54	2.95	3.18	6.12	11.03	15.38	13.14	15.43	12.24	8.40	5.98
24	4.39	3.48	2.81	3.18	7.14	11.02	15.25	13.44	15.22	12.11	8.20	5.92
25	4.36	3.39	2.78	3.17	8.17	11.11	15.10	13.92	15.01	11.96	8.01	5.86
26	4.32	3.31	2.74	3.12	8.58	11.46	14.96	14.92	14.77	11.73	7.93	5.83
27	4.30	3.23	2.75	3.09	8.45	11.84	14.90	14.56	14.54	11.40	7.82	5.82
28	4.25	3.18	2.76	3.14	8.32	12.10	14.85	14.78	14.29	11.11	7.72	5.76
29	4.21	3.15	2.76	3.24	8.13	12.11	14.82	14.93	14.08	10.88	7.66	5.68
30	4.16		2.72	3.31	7.96	12.00	14.80	14.98	13.87	10.68	7.58	5.60
31	4.12		2.68		7.83		14.70	14.99		10.59		5.51
Mean	4.77	3.57	2.97	2.79	5.27	9.21	13.76	13.83	15.42	12.54	9.00	6.42
Maximum	5.51	3.96	3.30	3.31	8.58	12.11	15.45	14.99	15.91	13.71	10.56	7.49
Minimum	4.12	3.15	2.68	2.46	3.40	6.97	11.47	13.03	13.87	10.59	7.58	5.51

TONLE SAP AT PREK KDAM, CAMBODIA (020102)

Station Description

Location:
Lat.11° 48.7' N, long. 104° 48.1' E, in Prek Kdam, 150 m northwest from vertical ferry terminal and about 32 km from the Mekong. Discharge measurements made from boat 1,400 m southwest of Wat Prek Chhik. Gauge on Tonle Sap at Phnom Penh Port used as auxiliary gauge for slope determination.

Gauge and Datum:
Bubble gauge and water stage recorder referred to inclined staff gauge with concrete stairway. Zero of gauge elevation 0.08 m above M.S.L. Hatien datum.

Drainage Area: 84,400 km2

Records Available:
Low stage: one daily reading, mean and high stages: two daily readings. Daily record of staff gauge and daily discharge was since 11 February 1960. Bubble gauge record since 4 August 1960. Observations discontinued since 16 July 1973. Operation restarted in 1992.

Extremes:
2000: Maximum gauge height 10.26 m from 23 to 25 September; minimum gauge height 1.02 m on 16 April.
1960-72; 1992-2000: Maximum discharge 11,400 m3/sec towards lake on 30 August 1961 (gauge height 8.80 m); towards sea 12,500 m3/sec on 15 November 1961 (gauge height 8.14 m) ; maximum gauge height 10.26 m from 23 to 25 September 2000, minimum gauge height 0.35 m from 17 to 18 May 1970.

Remarks:
Records for 2000, fair.

MEAN GAUGE HEIGHT IN METERS, YEAR 2000

DAY	JAN	FEB	MAR	APR	MAY	JUN	JUL	AUG	SEP	OCT	NOV	DEC
1	4.97	3.20	1.95	1.20	1.40	3.73	6.16	8.68	9.27	10.10	9.24	6.94
2	4.90	3.15	1.98	1.13	1.41	3.74	6.22	8.58	9.32	10.08	9.16	6.88
3	4.82	3.12	1.93	1.09	1.49	3.69	6.23	8.54	9.40	10.01	9.08	6.78
4	4.75	3.06	1.95	1.09	1.56	3.91	6.18	8.52	9.50	9.96	9.02	6.72
5	4.68	3.02	1.91	1.04	1.68	4.08	6.12	8.51	9.58	9.91	8.90	6.63
6	4.64	2.96	1.86	1.09	1.58	4.07	6.13	8.52	9.64	9.88	8.82	6.56
7	4.56	2.90	1.80	1.09	1.70	4.02	6.22	8.51	9.71	9.82	8.74	6.51
8	4.52	2.86	1.78	1.13	1.74	3.86	6.32	8.53	9.75	9.80	8.66	6.43
9	4.48	2.84	1.72	1.17	1.72	3.77	6.45	8.54	9.79	9.75	8.59	6.34
10	4.44	2.79	1.70	1.19	1.69	3.71	6.53	8.57	9.82	9.76	8.50	6.26
11	4.39	2.74	1.71	1.19	1.60	3.68	6.59	8.55	9.87	9.80	8.43	6.21
12	4.32	2.68	1.67	1.15	1.61	3.69	6.68	8.56	9.94	9.86	8.38	6.18
13	4.27	2.62	1.64	1.10	1.59	3.66	6.89	8.56	9.99	9.90	8.31	6.12
14	4.21	2.56	1.49	1.09	1.61	3.62	7.10	8.58	10.03	9.92	8.24	6.06
15	4.13	2.49	1.51	1.04	1.74	3.62	7.26	8.60	10.05	9.93	8.16	5.99
16	4.07	2.45	1.49	1.02	1.82	3.68	7.42	8.58	10.06	9.94	8.08	5.91
17	4.01	2.43	1.48	1.08	1.92	3.92	7.56	8.58	10.09	9.96	8.03	5.86
18	3.94	2.43	1.46	1.15	2.10	4.39	7.71	8.60	10.15	9.94	7.93	5.81
19	3.90	2.41	1.49	1.30	2.24	4.92	7.84	8.54	10.18	9.92	7.87	5.72
20	3.85	2.41	1.56	1.40	2.38	5.25	7.98	8.54	10.20	9.86	7.80	5.68
21	3.78	2.40	1.55	1.48	2.44	5.43	8.10	8.68	10.22	9.82	7.77	5.60
22	3.74	2.39	1.56	1.56	2.50	5.48	8.22	8.67	10.25	9.78	7.70	5.55
23	3.70	2.33	1.53	1.46	2.40	5.50	8.32	8.67	10.26	9.70	7.61	5.48
24	3.65	2.28	1.48	1.46	2.87	5.52	8.43	8.74	10.26	9.66	7.50	5.42
25	3.62	2.20	1.44	1.42	3.36	5.58	8.48	8.83	10.26	9.64	7.42	5.36
26	3.56	2.16	1.42	1.40	3.79	5.67	8.54	8.90	10.22	9.58	7.34	5.32
27	3.53	2.13	1.40	1.34	3.96	5.87	8.56	9.04	10.19	9.52	7.26	5.26
28	3.47	2.09	1.41	1.34	3.92	6.02	8.57	9.11	10.16	9.44	7.18	5.19
29	3.39	2.00	1.40	1.32	3.86	6.12	8.56	9.15	10.12	9.36	7.11	5.12
30	3.31		1.33	1.36	3.81	6.13	8.50	9.21	10.09	9.30	7.02	5.06
31	3.26		1.30		3.76		8.60	9.21		9.28		5.00
Mean	4.09	2.59	1.61	1.23	2.30	4.54	7.37	8.69	9.95	9.78	8.13	5.93
Maximum	4.97	3.20	1.98	1.56	3.96	6.13	8.60	9.21	10.26	10.10	9.24	6.94
Minimum	3.26	2.00	1.30	1.02	1.40	3.62	6.12	8.51	9.27	9.28	7.02	5.00

MEKONG AT PHNOM PENH, CAMBODIA (019801)

Station Description

Location:
Lat.11° 35' 00" N, long. 104°56' 33" E, in Phnom Penh Chroui Changvar peninsular near the Phnom Penh water supply pumping station, 2,8 km upstream of "Quatre bras " confluence, and 332 km from the sea.

Gauge and Datum:
Bubble gauge and water stage recorder referred to vertical staff gauge fixed on the foot bridge pier of the water supply pumping station. Zero of gauge elevation 1.08 m below M.S.L. Hatien datum.

Drainage Area: 663,000 Km2

Records Available:
Two daily gauge readings for the whole year. Stage recorded by Khmer T.P. at Phnom Penh (Port): complete or near complete 1898-1911, 1913-18, 1921-73; fragmentary 1894-97, 1912, 1919-20. City waterworks stage records 1930-73. Daily record of bubble gauge since 27 June 1973. Daily discharges since 1 January 1960 until 1974, interrupted between 1975 and 1990.

Extremes:
2000: Max. gauge height 11.21 m from 19-21 September; minimum gauge height 2.01 m on 3 April.
1960-73, 1991-2000: Maximum discharge 49,700 m3/sec on 28 August 1961; maximum gauge height 11.21 m from 19 to 21 September 2000; minimum discharge 1,250 m3/sec on 18 April 1960 (gauge height 1.66 m, subject to tidal effect); minimum gauge height 1.22 m on 7 May 1960.

Remarks:
Rating at all stages is affected by backwater conditions created by Tonle Sap. When Tonle Sap is flowing towards sea, station can be rated only by shift analysis. At stages above gauge height 8.00 m, very extensive over-bank flooding commences on the left bank and by-pass flow escapes to the Tonle Sap over the right bank upstream.

MEAN GAUGE HEIGHT IN METERS, YEAR 2000

DAY	JAN	FEB	MAR	APR	MAY	JUN	JUL	AUG	SEP	OCT	NOV	DEC
1	5.19	3.75	2.92	2.26	2.49	4.94	7.53	9.91	10.36	10.80	9.41	6.96
2	5.11	3.71	2.96	2.12	2.53	4.98	7.54	9.86	10.41	10.76	9.34	6.88
3	5.04	3.67	2.94	2.01	2.57	5.12	7.60	9.82	10.48	10.72	9.27	6.77
4	4.98	3.63	2.91	2.06	2.60	5.24	7.60	9.76	10.57	10.63	9.18	6.68
5	4.92	3.59	2.86	2.11	2.64	5.30	7.50	9.71	10.66	10.56	9.09	6.59
6	4.86	3.55	2.80	2.15	2.70	5.30	7.41	9.69	10.73	10.49	8.98	6.50
7	4.80	3.51	2.74	2.19	2.76	5.16	7.37	9.69	10.82	10.43	8.82	6.42
8	4.75	3.48	2.70	2.21	2.83	5.02	7.51	9.68	10.85	10.37	8.70	6.36
9	4.71	3.46	2.68	2.22	2.85	4.94	7.62	9.67	10.89	10.34	8.64	6.28
10	4.67	3.42	2.70	2.23	2.80	4.90	7.79	9.69	10.93	10.33	8.56	6.22
11	4.63	3.36	2.70	2.24	2.74	4.86	7.89	9.70	10.95	10.30	8.48	6.15
12	4.59	3.31	2.67	2.24	2.70	4.82	7.92	9.70	11.00	10.33	8.43	6.12
13	4.54	3.27	2.63	2.20	2.68	4.80	8.50	9.70	11.06	10.40	8.33	6.11
14	4.48	3.24	2.60	2.14	2.72	4.83	8.74	9.70	11.09	10.43	8.28	6.08
15	4.42	3.22	2.58	2.08	2.86	4.90	8.93	9.70	11.13	10.53	8.20	6.02
16	4.36	3.22	2.56	2.06	2.98	5.04	9.85	9.71	11.13	10.52	8.12	5.97
17	4.30	3.24	2.54	2.14	3.06	5.31	9.24	9.70	11.14	10.52	8.04	5.91
18	4.24	3.24	2.52	2.27	3.16	5.95	9.38	9.71	11.16	10.52	7.98	5.87
19	4.20	3.22	2.50	2.48	3.30	6.49	9.48	9.72	11.21	10.50	7.89	5.82
20	4.18	3.20	2.52	2.50	3.54	6.74	9.62	9.74	11.21	10.47	7.85	5.76
21	4.16	3.18	2.54	2.51	3.78	6.94	9.76	9.77	11.21	10.39	7.80	5.71
22	4.13	3.16	2.56	2.52	4.02	6.96	9.86	9.75	11.20	10.30	7.76	5.65
23	4.09	3.14	2.56	2.52	4.26	6.98	9.93	9.76	11.15	10.24	7.68	5.58
24	4.05	3.10	2.54	2.54	4.52	7.00	9.97	9.78	11.16	10.16	7.57	5.48
25	4.01	3.04	2.52	2.52	4.79	7.06	10.00	9.84	11.15	10.15	7.45	5.49
26	3.98	3.00	2.50	2.46	5.07	7.24	10.00	9.92	11.12	10.02	7.35	5.44
27	3.96	2.96	2.49	2.42	5.27	7.42	9.98	9.98	11.03	9.91	7.26	5.42
28	3.93	2.94	2.48	2.44	5.20	7.56	9.96	10.08	10.97	9.80	7.16	5.38
29	3.89	2.92	2.46	2.44	5.13	7.58	9.95	10.19	10.91	9.64	7.08	5.34
30	3.84		2.40	2.46	5.05	7.61	9.94	10.25	10.85	9.54	7.02	5.29
31	3.79		2.34		4.98		9.94	10.29		9.44		5.22
Mean	4.41	3.30	2.63	2.29	3.50	5.90	8.85	9.81	10.95	10.31	8.19	5.98
Maximum	5.19	3.75	2.96	2.54	5.27	7.61	10.00	10.29	11.21	10.80	9.41	6.96
Minimum	3.79	2.92	2.34	2.01	2.49	4.80	7.37	9.67	10.36	9.44	7.02	5.22

MEKONG AT TAN CHAU, VIET NAM (019803)

Station Description

Location:

Lat.10°48.2' N, long. 105°14.6' E, on the right bank of the river, in front of the market in the town of Tan Chau and about 220 km from the sea.

Gauge and Datum:

Floats gauge and water stage recorder referred to vertical staff gauge. Zero of gauge elevation at the M.S.L. Hatien datum. Prior to 1939, Vung Tau datum is related to an assumed datum.

Records Available:

Float gauge records complete or near complete since June 1932.

Extremes:

2000: Maximum gauge height 5.06 m on 23 September; minimum gauge height –0.18 m on 28 and 29 April.

1932-2000: Maximum gauge height 5.30 m on 12 October 1961; minimum gauge height -0.37 m on 11 May 1973.

Remarks:

Records for 2000, fair.

MEAN GAUGE HEIGHT IN METERS, YEAR 2000

DAY	JAN	FEB	MAR	APR	MAY	JUN	JUL	AUG	SEP	OCT	NOV	DEC
1	1.69	1.15	0.89	0.38	0.43	1.44	2.61	4.19	4.28	4.80	4.13	2.70
2	1.69	1.16	0.89	0.40	0.53	1.49	2.67	4.19	4.32	4.76	4.09	2.65
3	1.67	1.13	0.89	0.44	0.63	1.56	2.69	4.18	4.38	4.72	4.03	2.59
4	1.65	1.11	0.87	0.46	0.69	1.62	2.66	4.16	4.43	4.69	3.97	2.52
5	1.61	1.14	0.85	0.49	0.73	1.68	2.64	4.12	4.48	4.64	3.90	2.46
6	1.54	1.12	0.85	0.52	0.75	1.69	2.61	4.10	4.53	4.60	3.84	2.42
7	1.55	1.13	0.84	0.56	0.77	1.62	2.62	4.09	4.58	4.55	3.78	2.38
8	1.55	1.14	0.82	0.57	0.78	1.55	2.64	4.07	4.64	4.51	3.72	2.36
9	1.53	1.14	0.80	0.63	0.74	1.45	2.69	4.05	4.67	4.46	3.66	2.35
10	1.50	1.06	0.79	0.65	0.66	1.38	2.72	4.02	4.69	4.43	3.61	2.34
11	1.47	0.97	0.78	0.63	0.55	1.33	2.74	4.02	4.72	4.39	3.57	2.32
12	1.39	0.94	0.72	0.57	0.48	1.27	2.79	4.00	4.78	4.37	3.53	2.29
13	1.34	0.90	0.67	0.46	0.42	1.23	2.92	4.00	4.81	4.38	3.50	2.29
14	1.31	0.87	0.67	0.40	0.52	1.21	3.04	4.00	4.83	4.40	3.47	2.27
15	1.27	0.90	0.63	0.41	0.63	1.22	3.13	4.00	4.86	4.41	3.42	2.26
16	1.27	0.98	0.57	0.42	0.71	1.26	3.23	4.00	4.91	4.42	3.38	2.23
17	1.32	0.99	0.59	0.47	0.77	1.41	3.31	3.97	4.94	4.42	3.31	2.18
18	1.38	1.01	0.69	0.58	0.81	1.63	3.40	3.97	4.96	4.44	3.29	2.13
19	1.46	1.00	0.72	0.65	0.87	1.92	3.48	3.98	4.99	4.46	3.24	2.11
20	1.47	1.01	0.76	0.69	0.94	2.09	3.57	3.99	5.02	4.46	3.20	2.07
21	1.43	1.01	0.78	0.72	0.97	2.17	3.67	4.00	5.02	4.46	3.20	2.05
22	1.39	0.97	0.78	0.71	1.00	2.18	3.79	3.98	5.03	4.44	3.15	2.04
23	1.37	0.92	0.74	0.64	1.02	2.18	3.89	4.00	5.04	4.42	3.09	2.03
24	1.38	0.87	0.75	0.55	1.10	2.18	3.98	4.03	5.04	4.38	3.05	2.03
25	1.36	0.84	0.78	0.49	1.28	2.19	4.03	4.06	5.00	4.40	3.00	2.01
26	1.32	0.88	0.75	0.42	1.45	2.23	4.06	4.08	4.98	4.40	2.96	1.97
27	1.25	0.89	0.73	0.38	1.48	2.31	4.08	4.11	4.94	4.34	2.92	1.94
28	1.18	0.80	0.74	0.34	1.45	2.42	4.09	4.15	4.91	4.26	2.86	1.93
29	1.18	0.86	0.66	0.33	1.42	2.52	4.12	4.16	4.87	4.22	2.80	1.94
30	1.16		0.62	0.38	1.41	2.58	4.14	4.18	4.83	4.18	2.76	1.91
31	1.13		0.49		1.43		4.16	4.23		4.14		1.89
Mean	1.41	1.00	0.75	0.51	0.88	1.77	3.30	4.07	4.78	4.45	3.41	2.21
Maximum	1.69	1.16	0.89	0.72	1.48	2.58	4.16	4.23	5.04	4.80	4.13	2.70
Minimum	1.13	0.80	0.49	0.33	0.42	1.21	2.61	3.97	4.28	4.14	2.76	1.89

BASSAC AT CHAU DOC, VIET NAM (039801)

Station Description

Location:

Lat.10°42.4' N, long 105°08.0' E, on the right bank of the river about 400 m downstream of the market and about 200 m from the sea. Discharge measurements made from boat at ferry crossing, about 800 m downstream of gauge. A bubble gauge was once located at the south end of the perk in the town of Chau Doc.

Gauge and Datum:

Floats gauge and water stage recorder referred to vertical staff gauge. Zero of gauge elevation 0.000 m below M.S.L. Hatien datum T.P. bubble gauge. Zero of gauge elevation 1.66 m below M.S.L. Hatien datum.

Records Available:

Maximum daily gauge since 29 June 1960. Maximum daily gauge height since 1 January 1962. Mean daily gauge height from 29 June 1960 to 31 December 1961. Bubble gauge records from 29 January 1960 to 3 July 1970. T.P., float gauge recorders 1909-44, 1946-75. Daily gauges height 1971-74 and 1977-91.

Extremes:

2000: Maximum gauge height 4.90 m on 23 September; minimum gauge height –0.28 m on 28 April.
1909-44, 1946-2000: Maximum gauge height 4.97 m on 29 September 1937 and on 15 October 1961; minimum gauge height -0.60 m on 8 May 1987.

Remarks:

Records for 2000, fair.

MEAN GAUGE HEIGHT IN METERS, YEAR 2000

DAY	JAN	FEB	MAR	APR	MAY	JUN	JUL	AUG	SEP	OCT	NOV	DEC
1	1.53	1.06	0.82	0.34	0.40	1.20	2.14	3.77	3.97	4.68	4.05	2.59
2	1.52	1.06	0.83	0.38	0.52	1.25	2.19	3.79	4.00	4.64	4.02	2.54
3	1.50	1.04	0.83	0.42	0.60	1.33	2.22	3.80	4.05	4.60	3.96	2.48
4	1.48	1.03	0.82	0.43	0.66	1.37	2.25	3.79	4.10	4.55	3.89	2.42
5	1.45	1.07	0.81	0.46	0.70	1.42	2.24	3.78	4.14	4.52	3.82	2.36
6	1.42	1.06	0.81	0.50	0.72	1.43	2.23	3.78	4.19	4.48	3.75	2.31
7	1.42	1.06	0.80	0.55	0.74	1.38	2.24	3.78	4.26	4.43	3.69	2.26
8	1.41	1.07	0.78	0.57	0.73	1.32	2.24	3.76	4.30	4.38	3.63	2.22
9	1.38	1.08	0.76	0.62	0.67	1.24	2.26	3.76	4.34	4.34	3.57	2.22
10	1.35	1.01	0.76	0.63	0.60	1.18	2.28	3.76	4.37	4.31	3.51	2.20
11	1.32	0.92	0.74	0.62	0.48	1.13	2.31	3.75	4.40	4.27	3.46	2.18
12	1.25	0.88	0.66	0.57	0.42	1.06	2.34	3.72	4.49	4.28	3.42	2.16
13	1.19	0.84	0.61	0.45	0.36	1.02	2.43	3.72	4.55	4.27	3.38	2.16
14	1.17	0.81	0.62	0.40	0.45	1.00	2.52	3.72	4.60	4.29	3.35	2.16
15	1.14	0.83	0.58	0.42	0.54	1.00	2.60	3.72	4.64	4.30	3.31	2.14
16	1.15	0.91	0.54	0.42	0.62	1.04	2.68	3.71	4.69	4.30	3.28	2.12
17	1.20	0.92	0.55	0.46	0.70	1.15	2.76	3.70	4.72	4.31	3.23	2.07
18	1.26	0.94	0.65	0.57	0.73	1.31	2.81	3.70	4.75	4.32	3.18	2.02
19	1.34	0.93	0.67	0.64	0.76	1.51	2.89	3.71	4.80	4.34	3.13	2.00
20	1.36	0.94	0.70	0.68	0.82	1.63	2.97	3.73	4.83	4.33	3.08	1.96
21	1.33	0.93	0.74	0.70	0.85	1.70	3.06	3.73	4.84	4.32	3.06	1.94
22	1.30	0.91	0.74	0.68	0.87	1.73	3.17	3.72	4.86	4.31	3.02	1.93
23	1.28	0.86	0.71	0.61	0.88	1.73	3.26	3.75	4.89	4.30	2.96	1.91
24	1.29	0.79	0.70	0.53	0.92	1.73	3.35	3.80	4.88	4.27	2.92	1.89
25	1.26	0.77	0.74	0.47	1.02	1.74	3.44	3.81	4.87	4.24	2.87	1.85
26	1.23	0.82	0.71	0.38	1.14	1.76	3.52	3.81	4.85	4.22	2.83	1.82
27	1.15	0.83	0.72	0.33	1.18	1.82	3.57	3.83	4.82	4.18	2.80	1.80
28	1.09	0.75	0.72	0.28	1.16	1.91	3.61	3.85	4.79	4.14	2.75	1.78
29	1.09	0.82	0.64	0.28	1.15	2.01	3.66	3.87	4.76	4.12	2.70	1.77
30	1.07		0.59	0.32	1.16	2.09	3.70	3.90	4.72	4.08	2.65	1.74
31	1.06		0.46		1.18		3.74	3.93		4.05		1.72
Mean	1.29	0.93	0.70	0.49	0.77	1.44	2.80	3.77	4.55	4.33	3.31	2.09
Maximum	1.53	1.08	0.83	0.70	1.18	2.09	3.74	3.93	4.89	4.68	4.05	2.59
Minimum	1.06	0.75	0.46	0.28	0.36	1.00	2.14	3.70	3.97	4.05	2.65	1.72

CURRICULUM VITAE

NAME	Mr. Sutthiwas Chantaluck
DATE OF BIRTH	29 May 1990
EDUCATION RECORD	
HIGH SCHOOL	High school Graduation The Demonstration School of Bansomdejchaopraya Rajabhat University, 2008
BACHELOR'S DEGREE	Bachelor of Engineering (Civil Engineering) with International and Twining Programme King Mongkut's University of Technology Thonburi , 2012
MASTER'S DEGREE	Master of Engineering (Civil Engineering) King Mongkut's University of Technology Thonburi, 2014
SCHOLARSHIP/RESEARCH GRANT	Master Program Partial scholarship Department of Civil Engineering, King Mongkut's University of Technology Thonburi 2013-2014
PUBLICATION	Chantaluck, S., Kazama, S., Ekkawatpanit, C., Amano, A.,Asawapiched, B. (2014), "Assessing Grid Size Effects on Inundation and Groundwater Using Hydrological Model", **Proceeding of JSCE Tohoku conference**, Hachinohe University, Japan